Solid-liquid Separation of Xylene Isomers using Metallocycles

By

Jiajia Ye

Thesis presented in partial fulfilment of the requirements for the degree of Master of Science

Stellenbosch University

Supervisor: Prof. Leonard J. Barbour

Department of Chemistry and Polymer Science

Faculty of Science

April 2022

Declaration

By submitting this thesis electronically, I declare that the entirety of the work contained therein is my own, original work, that I am the sole author thereof (save to the extent explicitly otherwise stated), that reproduction and publication thereof by Stellenbosch University will not infringe any third party rights and that I have not previously in its entirety or in part submitted it for obtaining any qualification.

April 2022

Abstract

Host-guest chemistry is an important concept in supramolecular chemistry. Porous hosts may be able to selectively accommodate guests, making them attractive candidates for potential applications such as sorption, storage, separation, drug delivery, *etc*. In this study, two porous materials were investigated for their solid-liquid xylene separation ability. These materials are the metallocycles **MC1** and **MC2**. Xylenes are an important chemical feedstock to produce consumer products. However, they are always produced as a mixture of isomers and thus their separation is essential.

The first material investigated was **MC1**·2(MeOH). Its phase purity could not be established directly by comparison of the simulated and experimental powder patterns. This is because the MeOH guest readily escapes from the host at ambient temperatures. However, the phase purity can be confirmed after the material is fully activated (**MC1a**). Solvent exchanges of the as-synthesized **MC1**·2(MeOH) with xylenes, as well as liquid sorption of **MC1a** with xylenes were attempted. Both investigations showed that **MC1** is not a suitable material for xylene separation. The host structure remained unchanged after exposure to xylene. Further investigation revealed that the kinetic diameters of the xylenes are too large for these molecules to fit in the host cavity without a phase transformation.

The second material explored was **MC2**·2(DMSO). It can undergo multiple single-crystal to single-crystal transformations upon guest exchange and removal and exhibits solvatochromism. The activation of **MC2** by different methods results in two possible activated forms (open form **3** and collapsed form **4**). In this study, the main obstacle was to obtain phase pure sample of either activated form. The problem was resolved by trialing variations of temperature and time. Vapor and liquid sorption of xylenes were carried out using form **3**. Form **3** is able to separate xylenes in the order of preference of *para*-xylene >> *meta*-xylene > *ortho*-xylene under mild conditions. The pockets within form **3** merge and become channels to accommodate the xylenes, as established by single-crystal X-ray diffraction analysis. The selectivity trend was rationalized as being dependent on the kinetic diameter of the respective xylene isomers. The non-porous form **4** is not suitable for xylene separations even at high temperature. Thus, as the phase purity problem has been solved, porous form **3** with its ability to change pore sizes, is a worthy substrate for xylene purification, and this also has implications for future studies involving gas sorption and storage.

Opsomming

Gasheer-gas-chemie is 'n belangrike konsep in supramolekulêre chemie. Poreuse gashere mag dalk gaste selektief kan akkommodeer, wat hulle aantreklike kandidate maak vir potensiële toepassings soos sorpsie, berging, skeiding, geneesmiddelaflewering ens. In hierdie studie is twee poreuse materiale ondersoek vir hul vastestof-vloeistof xileen skeidingsvermoë. Hierdie materiale is die metallosiklusse **MC1** en **MC2**. Xileen is 'n belangrike chemiese grondstof om verbruikersprodukte te produseer. Hulle word egter altyd geproduseer as 'n mengsel van isomere en dus is hul skeiding noodsaaklik.

Die eerste materiaal wat ondersoek is, was **MC1**·2(MeOH). Die fasesuiwerheid daarvan kon nie direk vasgestel word deur die gesimuleerde en eksperimentele poeierpatrone te vergelyk nie. Dit is omdat die MeOH gas maklik by omgewingstemperature van die gasheer ontsnap. Die fasesuiwerheid kan egter bevestig word nadat die materiaal ten volle geaktiveer is (**MC1a**). Oplosmiddeluitruilings van die soos-gesintetiseerde **MC1**·2(MeOH) met xileen, sowel as vloeistofsorpsie van **MC1a** met xileen, is gepoog. Beide ondersoeke het getoon dat **MC1** nie 'n geskikte materiaal vir xileenskeiding is nie. Die gasheerstruktuur het onveranderd gebly na blootstelling aan xileen. Verdere ondersoek het aan die lig gebring dat die kinetiese diameters van die xileen isomere te groot is vir hierdie molekules om sonder 'n fasetransformasie in die gasheerholte te pas.

Die tweede materiaal wat ondersoek is, was **MC2**·2(DMSO). Dié materiaal kan veelvuldige enkelkristal-tot-enkelkristal-transformasies ondergaan tydens gasuitruiling en -verwydering, en vertoon solvatochromisme. Die aktivering van **MC2** deur verskillende metodes lei tot twee moontlike geaktiveerde vorms (oop vorm **3** en toe vorm **4**). In hierdie studie was die grootste struikelblok om fase-suiwer monsters van beide geaktiveerde vorms te verkry. Die probleem is opgelos deur variasies van temperatuur en tyd te toets. Damp- en vloeistofsorpsie van xileen is uitgevoer op vorm **3**. Vorm **3** toon voorkeur in xileen skeiding in die volgorde van *para*-xileen >> *meta*-xileen > *orto*-xileen onder matige toestande. Die holtes binne vorm **3** smelt saam en word kanale om die xileen te akkommodeer, soos vasgestel deur enkelkristal X-straaldiffraksie-analise. Die selektiwiteitstendens is gerasionaliseer as afhanklik van die kinetiese deursnee van die onderskeie xileen isomere. Die nie-poreuse vorm **4** is nie geskik vir xileenskeidings selfs by hoë temperatuur nie. Dus, omdat die fasesuiwerheidsprobleem opgelos is, is poreuse vorm **3** met sy vermoë om holtegroottes te verander, 'n waardige substraat vir xileensuiwering, en dit het ook implikasies vir toekomstige studies wat gassorpsie en berging behels.

Acknowledgements

First and foremost, I am extremely grateful to my supervisor, Prof. Len Barbour, for giving me the opportunity to be part of this world-class research group. Thank you for providing invaluable advice, guidance and patience throughout this research. It is a great privilege to learn and improve under your guidance.

I would like to say thanks to Dr. Leigh Loots for training on the instruments and help in refining disordered structures. Thanks to Dr. Lisa van Wyk for countless editing of the documents. Thanks to Dr. Marike du Plessis and Dr. Dewald van Heerden. Thank you all for the technical support, patience, advice and assistance at every stage of this work, without which this work would not have been possible.

I would also like to thank Samantha le Roux, who is very enthusiastic and positive, for her praise. I would like to thank Alan Eaby, Banele Motloung, Xueting Wei and all the other members in the Supramolecular Material Research Group for all the kind help and support. It is really pleasant to be part of this group.

My appreciation also goes to my family and friends, thanks for their encouragement and support all throughout my studies.

Lastly, I would like to thank Stellenbosch University for the facilities and the National Research Foundation (NRF) for financial support.

Publications

- J. Ye, M. du Plessis, L, Loots, L. M. van Wyk, L. J. Barbour, *Cryst. Growth Des*., 2022, submitted.

Abbreviations

0D	Zero-dimensional
1D	One-dimensional
2D	Two-dimensional
3D	Three-dimensional
ACN	Acetonitrile
CCDC	Cambridge Crystallographic Data Centre
C_2H_2	Acetylene
CIF	Crystallographic Information File
CO_2	Carbon Dioxide
CS_2	Carbon Disulphide
CSD	Cambridge Structural Database
δ	Chemical Shift (in ppm)
DMSO	Dimethyl Sulfoxide
DSC	Differential Scanning Calorimetry
FT-IR	Fourier Transform Infrared Spectroscopy
G	Guest
GC	Gas Chromatography
H	Host
IUPAC	International Union of Pure and Applied Chemistry
L	Ligand
M	Molecular Mass
MC1	Metallocycle $[Cd_2Cl_4(\mathbf{L1})_2]$
MC2	Metallocycle $[Cu_2Cl_4(\mathbf{L2})_2]$
MeOH	Methanol
MOF	Metal-Organic Framework
mp	Melting Point
NMR	Nuclear Magnetic Resonance
PXRD	Powder X-ray Diffraction
SCD	Single-Crystal X-ray Diffraction
SC-SC	Single-Crystal to Single-Crystal
TGA	Thermogravimetric Analysis

Z	Number of Formula Units in the Unit Cell
α	Angle between the *b* and *c* Axes
β	Angle between the *a* and *c* Axes
γ	Angle between the *a* and *b* Axes
θ	Angle of X-ray Incident Beam or Angle between D–H…A in Hydrogen Bond
px	*para*-Xylene
mx	*meta*-Xylene
ox	*ortho*-Xylene

Atomic color key

Hydrogen

Carbon

Nitrogen

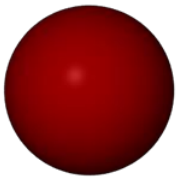

Oxygen

Sulfate

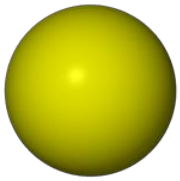

Chlorine

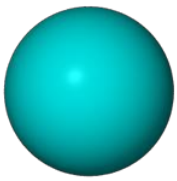

Metal

Table of Contents

Chapter 1

Introduction

1.1 Supramolecular Chemistry

Whereas traditional chemistry is concerned with the covalent bond, supramolecular chemistry, a term coined by Lehn in 1969, concerns *"chemistry beyond the molecule"* or *"the chemistry of molecular assemblies and of the intermolecular bond"*.[1–3] Higher complexity materials could be formed by the self-assembly of molecular subunits that are held together by weak and reversible non-covalent interactions, leading to zero-, one-, two- and three-dimensional (0D-, 1D-, 2D-, 3D-) architectures.[2,3] These *supermolecules* possess features as well defined as those of the constituting molecules themselves, which are *"structurally organized and functionally integrated"*.[2] As supramolecular chemistry continues to develop rapidly, features of molecules can be integrated into designed materials for applications such as catalysis,[4–8] sensing,[9,10] separation,[11–13] sorption,[14–16] storage,[1,17–20] drug delivery,[21] magnetism,[1] electronics,[22,23] etc.

1.2 Crystal Engineering

Crystal engineering is the design and synthesis of desired functional crystalline solids from neutral or ionic building blocks by way of non-covalent intermolecular interactions.[24] The term crystal engineering was first introduced by Pepinsky in 1955,[25] but the modern definition was given by Desiraju as *"the understanding of intermolecular interactions in the context of crystal packing and in the utilisation of such understanding in the design of new solids with desired physical and chemical properties"*.[24] The key concepts required to understand crystal engineering are supramolecular synthons and self-assembly,[24] which will be discussed in greater detail later on. The ultimate ambition of crystal engineering is to design materials with desired properties pertaining to specific applications.[1]

1.2.1 Supramolecular Synthons

Corey defined *synthons* as *"structural units within molecules which can be formed and/or assembled by known or conceivable synthetic operations"*.[26] The term is useful in retrosynthetic analysis. In 1995, Desiraju defined supramolecular synthons as *"spatial arrangements of intermolecular interactions that play the same focusing role in supramolecular synthesis that conventional synthons do in molecular synthesis"* and referred to crystal engineering as the *"new organic synthesis"*.[27,28] Figure 1.1 shows several representative supramolecular synthons.

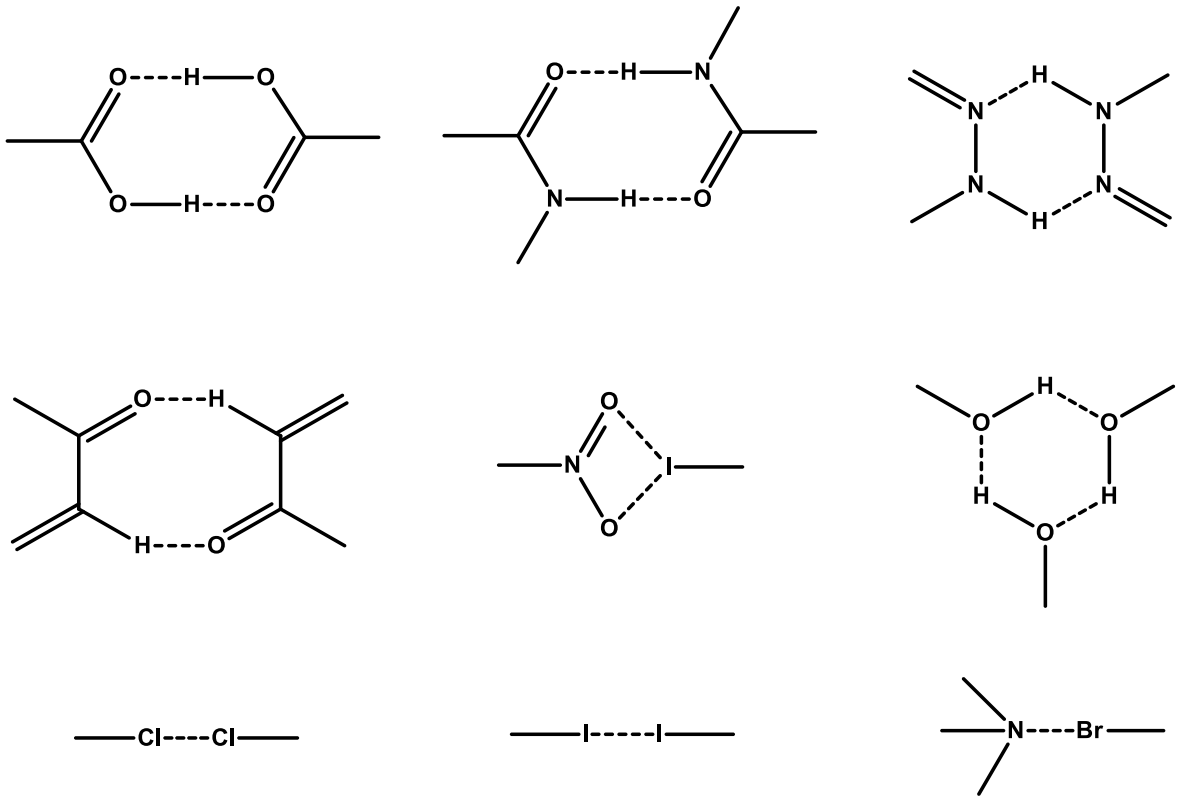

Figure 1.1 Representative supramolecular synthons.[27]

1.2.2 Molecular Recognition and Self-Assembly

Molecular recognition denotes the collective favorable interactions among two or more molecules as a result of non-covalent bonding. Applications such as sensing and separation rely on the selective removal of a specific component from a mixture through molecular recognition to form the most stable host-guest assembly. Molecular recognition is *"binding with a purpose, like receptors are ligands with a purpose"* and

it utilizes molecular complementarity in the same way that the “lock and key” concept is essential to enzymatic function.[1,2]

Molecular self-assembly refers to the spontaneous organization of indeterminate numbers of molecules into larger complex structures by way of reversible, non-covalent intermolecular interactions.[2,29] DNA is a representative example of self-assembly wherein the self-recognition of complementary base-pairs leads to the self-assembly of the double helix through hydrogen bonding.[30] Other examples such as protein folding and phospholipid membranes prove that self-assembly are vital to living organisms.[30]

1.3 Supramolecular Interactions

In supramolecular chemistry, *supermolecules* are molecules held together by non-covalent intermolecular interactions such as hydrogen bonding, dipole-dipole interactions, $\pi \cdots \pi$ interactions and van der Waals interactions.[2,31,32] These intermolecular interactions can be partitioned into medium- and long-range forces.[27] Medium-range forces are isotropic and non-directional and are limited to C···H, C···C and H···H interactions. In general, they delineate the molecular shape and size and govern close-packing.[1,27,33] Long-range forces are electrostatic, anisotropic and directional and involve heteroatomic interactions. These forces regulate intermolecular orientations and functions.[1,27,33]

In 1988 Lehn stated that *“Supermolecules are to molecules and the intermolecular bond what molecules are to atoms and the covalent bond”*.[2] Non-covalent intermolecular forces (2–300 kJ/mol) are considerably weaker in comparison to covalent forces (150–450 kJ/mol).[32] Table 1.1 summarizes some well-known intermolecular forces in supramolecular chemistry.

Table 1.1 Strengths of intermolecular interactions.[32,34]

Interaction type	Intermolecular interaction	Strength (kJ/mol)	Examples
Anisotropic	Coordination bonding	100–300	M–N, M–O
	Hydrogen bonding	4–120	O–H···O, N–H···O
	Dipole-dipole	5–50	Acetone, –C≡N
	$\pi \cdots \pi$	0–50	Ph···Ph, graphite
Isotropic	van der Waals	<5	Inclusion compounds

1.3.1 Coordination Bonding

Coordination bonds are weak covalent interactions between metal ions and organic ligands that are responsible for building up coordination compounds (classified below).[1] The organic molecule acts as a Lewis base and donates its lone pair of electrons to the metal atom, which acts as a Lewis acid. Coordination bonding is relatively the strongest interaction in supramolecular chemistry (Table 1.1) and is directional, anisotropic and contributes to the diversity of supramolecular structures.[34]

1.3.2 Hydrogen Bonding

In addition to the coordination bond, the strongest intermolecular non-covalent force in crystal engineering is hydrogen bonding.[24] It is highly directional and anisotropic[25,34] and is considered the "master key" for molecular recognition.[27] These attributes make it the most important intermolecular interaction in the design of supramolecular architectures. In 2011 the IUPAC defined hydrogen bonding as *"an attractive interaction between a hydrogen atom from a molecule or a molecular fragment, D−H···A in which D is more electronegative than H, and an atom or a group of atoms in the same or different molecule, in which there is evidence of bond formation"*.[25] Hydrogen bonding is a special case of dipole-dipole intermolecular attractions.[33] As shown in Figure 1.2, *D* is the hydrogen bond donor atom to which the hydrogen atom is covalently bound, while *A* is the hydrogen bond acceptor. The strength of a hydrogen bond depends on its geometry as well as the donor and acceptor type. This partitions the hydrogen bond into three categories: strong, moderate and weak as summarized in Table 1.2.[32] Examples of hydrogen bonds found in carboxylic acid dimers and DNA are shown in Figure 1.3.[34]

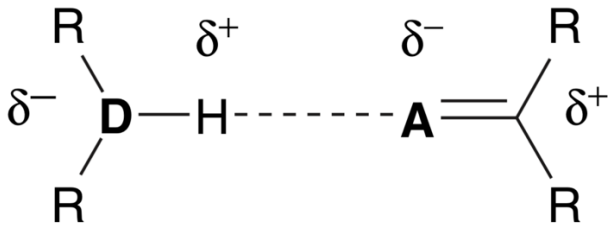

Figure 1.2 Standard way of expressing hydrogen bond donor and acceptor (D, donor atom; A, acceptor atom).[32]

Table 1.2 Interactions and properties of hydrogen bonding. (A: acceptor; D: donor).[32]

Interaction/property	Strong	Moderate	Weak
D–H···A	Mainly covalent	Mainly electrostatic	Electrostatic
Bond energy (kJ/mol)	60–120	16–60	<12
Bond length (Å)			
H···A	1.2–1.5	1.5–2.2	2.2–3.2
D···A	2.2–2.5	2.5–3.2	3.2–4.0
Bond angle (°)	175–180	130–180	90–150
Example	HF complexes	Acids	C–H···A
	$H_5O_2^+$	Alcohols	D–H···π
	—	DNA/RNA	—

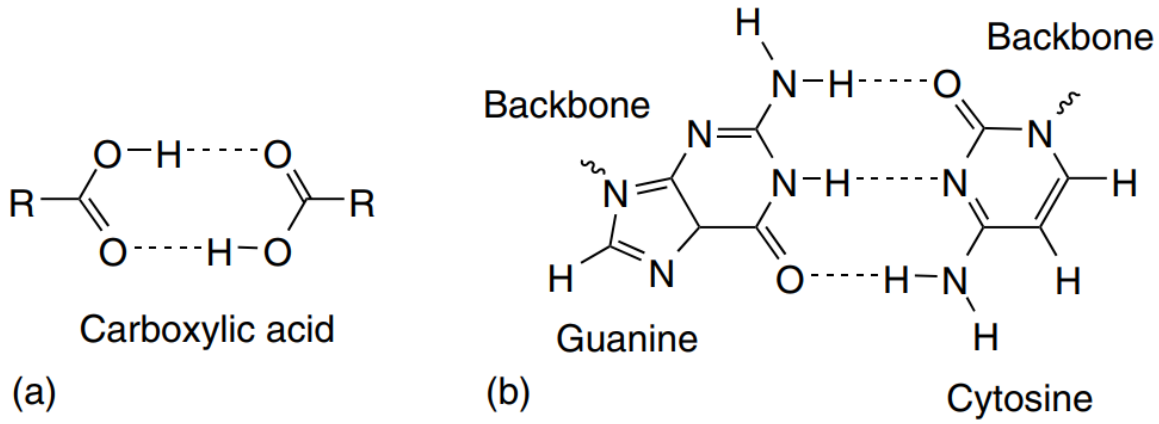

Figure 1.3 Hydrogen bonding present in (a) a carboxylic acid dimer and (b) DNA base pairing.[34]

1.3.3 Dipole-dipole Interactions

Dipole-dipole forces are interactions that result from an electrostatic attraction between opposite partial charges in two molecules.[32,34] They are the weakest directional forces in supramolecular chemistry with a strength of 5-50 kJ/mol.[32] Bulk physical properties such as boiling point, spatial permutation and geometries of interacting molecules are influenced by dipole-dipole interactions.[34] Hydrogen bonding is considered a special case of dipole-dipole interaction.[32,34] Figure 1.4 presents the dipole-dipole interactions in acetone.[32]

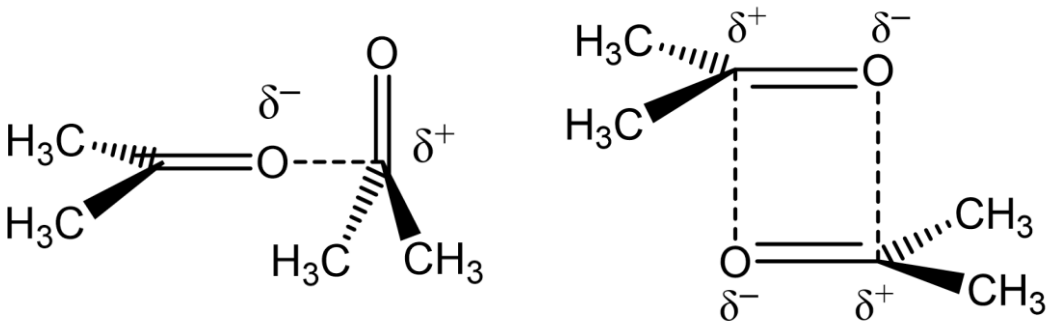

Figure 1.4 Dipole-dipole interaction in acetone.[32]

1.3.4 π···π Interactions/Stacking

Anisotropic, directional π···π interactions refer to non-covalent attractive forces between delocalized electron clouds of aromatic groups.[34,35] In order to minimize the repulsive interaction components, the aromatic rings stack in optimal modes.[36] As presented in Figure 1.5, π···π interactions are divided into three categories: (a) face-to-face (sandwich) (b) offset face-to-face (offset stacked), and (c) edge-to-face (T-shaped).[34,36] Edge-to-face π···π interactions are considered weak C–H···π hydrogen bonds and are stronger than offset stacking, while face-to-face stacking is the weakest π···π interaction.[35,36] An example of π···π interaction is stacking in graphite where the layered structure is held together by weak face-to-face interactions (Figure 1.6).[32]

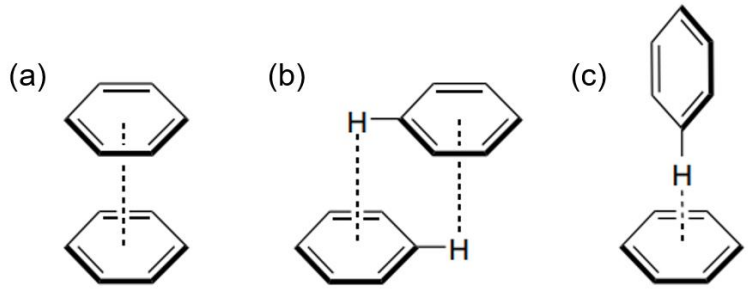

Figure 1.5 Three categories of π···π interactions: (a) face-to-face (sandwich), (b) offset face-to-face and (c) edge-to-face (T-shaped).[34]

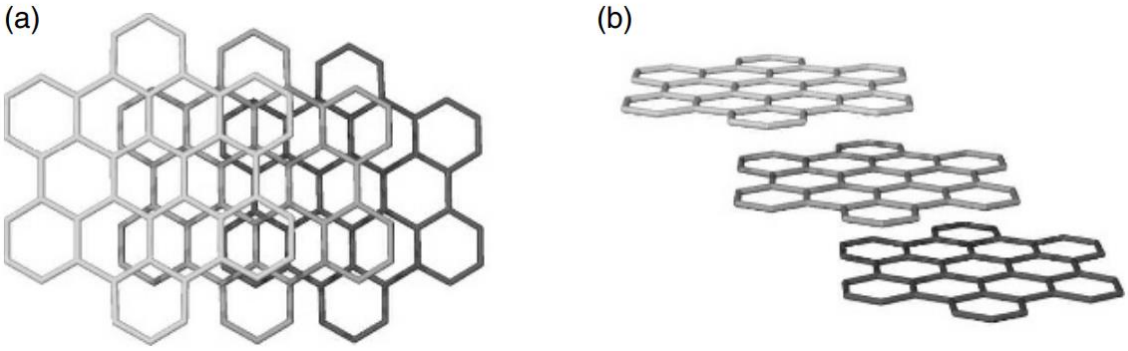

Figure 1.6 (a) Top and (b) side views of the layered structure of graphite, which undergoes face-to-face π···π stacking.[32]

1.3.5 Van der Waals Interactions

Van der Waals forces, also known as London forces, are dispersion effects that take place as a result of fluctuations of electron density of molecules that are in close proximity to one another.[32] Instantaneous dipoles are induced by the correlated fluctuation of the electron clouds of each molecule, giving rise to a short-lived attractive interaction.[32] Van der Waals forces are ubiquitous, non-directional and isotropic,[1] and at less than 5 kJ/mol in strength, they are the weakest intermolecular interactions in crystal engineering.[32] Their strength is determined by the polarizability of the constituent atoms and the distance between the atoms.[32]

1.4 Crystal Packing

A crystal is a macroscopic solid whose internal structure is characterized by patterns composed of atoms, molecules, or ions that repeat periodically in three dimensions.[33] Kitaigorodskii proposed a principle of *close-packing* where molecular crystals pack efficiently to minimize intermolecular voids.[37] Therefore, the 'bumps' on a molecular surface embed into the 'hollows' of another to achieve the highest possible density.[38] Close-packing is delineated by medium-range forces (see Section 1.3).[1,27] The "Horsemen" by M. C. Escher is a pictorial representation of a close-packed arrangement (Figure 1.7).[37]

Figure 1.7 "Horsemen" by M. C. Escher is an example of 2-dimensional close packing.[37]

1.5 Host-Guest Chemistry

1.5.1 Inclusion Compounds

Host-Guest Chemistry is defined as *"the study of large 'host' molecules that are capable of enclosing smaller 'guest' molecules via non-covalent interactions"*.[32] An *inclusion compound* is a complex in which one component (the host) forms cavities in which a second species (the guest) can be accommodated without the formation of a covalent bond between them.[39] There are two types of host molecules, as

demonstrated in Figure 1.8. In the first the host is synthesized to be bowl-shaped and the inclusion complex can occur in both the solution and solid states. Examples include calixarenes, cyclodextrins and cyclophanes. In the second type cavities or channels are formed by the inefficient packing of awkwardly-shaped host molecules into a lattice that can accommodate guest molecules. The latter inclusion compounds can only be present in the solid state and such compounds are termed *clathrates*.[32,40]

The formation of an inclusion compound (H·G) can be expressed by Nassimbeni's formula (Equation 1.1):

$$H_{(s,\alpha)} + nG_{(s,\,l\text{ or }g)} \rightleftharpoons H{\cdot}G_{n\,(s,\beta)} \qquad [\mathbf{1.1}]$$

where α and β represent different phases of the host (H), with and without guest (G), respectively, and n represents the guest:host ratio.[40]

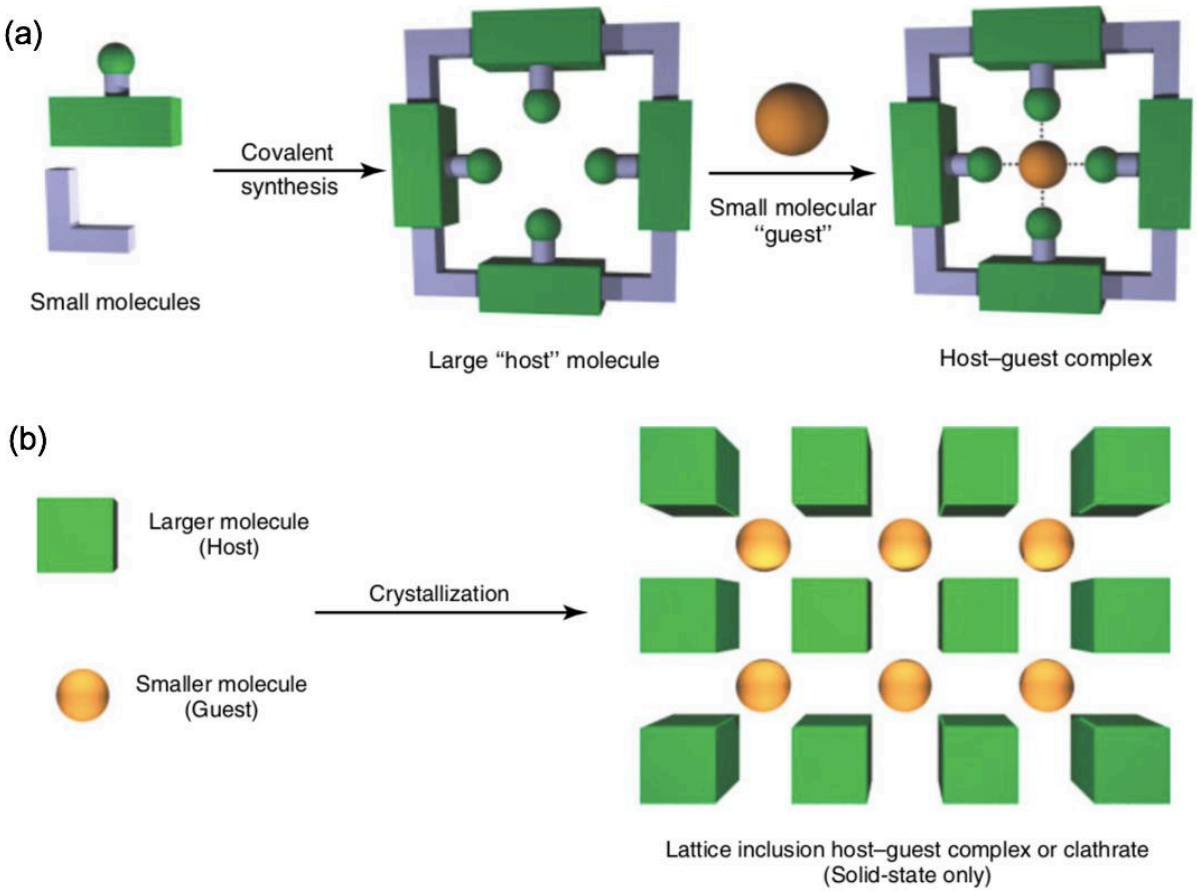

Figure 1.8 Two types of inclusion compounds: (a) host molecules with engineered cavities and (b) lattice inclusion host–guest complexes.[32,41]

When an inclusion compound is immersed in a second guest environment, the original guest may be exchanged for the new guest:

$$H{\cdot}X_{n\,(s,\beta)} \quad + \quad Y_{(s,\,l\text{ or }g,\,excess)} \quad \rightarrow \quad H{\cdot}Y_{m\,(s,\beta)} \quad + \quad nX \qquad [\mathbf{1.2}]$$

where X and Y represent the old and new guest species with guest:host ratios of *n* and *m*, respectively.[42] This can take place in a single-crystal to single-crystal fashion if the structure of the host retains its integrity and does not dissolve and recrystallize around the new guest.[43]

1.5.2 Selectivity

In host-guest chemistry the host usually exhibits some preference for a specific guest.[32] This *selectivity* depends on physico-chemical factors such as intermolecular interactions, size, shape, conformation and complementarity of the host and guest.[40] As a consequence, host-guest systems have the potential to be utilized in molecular separations.

For binary mixtures, selectivity curves can take on distinct shapes as shown in Figure 1.9. X_A and Z_A represent the mole fraction of guest A in the liquid mixture and entrapped in the crystal structure, respectively.[40] $K_{A:B}$ is the selectivity coefficient and is expressed as follows:[40]

$$K_{A:B} = (K_{B:A})^{-1} = \frac{Z_A}{Z_B} \times \frac{X_B}{X_A} \qquad [\mathbf{1.3}]$$

where $(X_A + X_B) = 1$.

The diagonal lines represent zero selectivity with $K_{A:B} = 1$. Curves (a) and (b) represent preference for A over B with modest and high selectivity, respectively. Curve (c) represents concentration-dependent selectivity.[40]

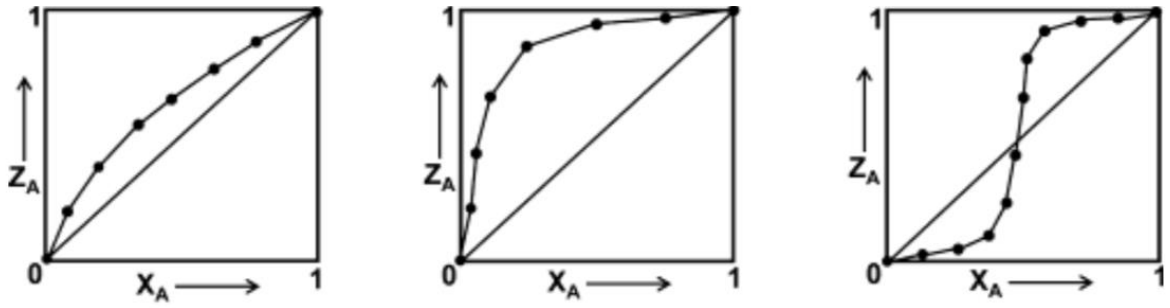

Figure 1.9 The three kinds of selectivity curves obtained from competition experiments.[40]

1.6 Porosity

Porosity in supramolecular chemistry refers to the presence of guest-accessible space in a material, where the host material should maintain its supramolecular architecture upon guest uptake and removal.[44]

Barbour categorized "porosity" into three subgroups, namely: *conventional* porosity, porosity "without pores" (or *transient* porosity) and *virtual* porosity.[33,44] Conventional porosity refers to materials that have permanent permeability while the host framework is not affected when guests are removed or exchanged.[44] Materials that are seemingly nonporous in that the host structure contains pockets but no channels connecting them can show porosity "without pores".[44] This occurs when the crystal is exposed to a guest environment and undergoes a single-crystal to single-crystal transformation to allow permeability and yield an inclusion compound.[44] Virtual porosity is wrongfully assumed when guest molecules or counterions are deleted to generate packing diagrams with large empty voids.[44]

Based on the different spatial dimensions, the porous structure of a crystal structure can be classified into four types as shown in Figure 1.10.[45] They are (a) zero-dimensional (0D) pockets that are closed off by host molecules; (b) 1D channels, (c) 2D layers and (d) 3D intersecting channels.[45]

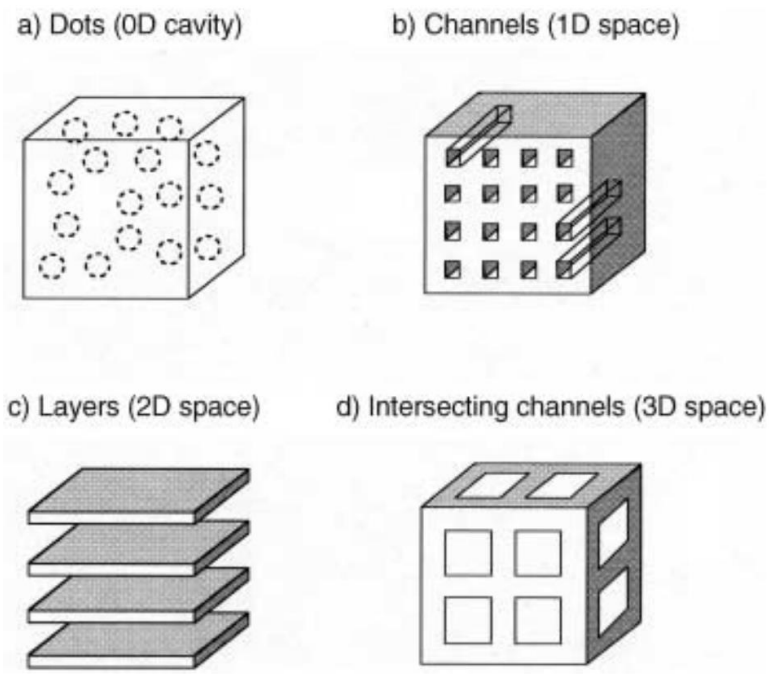

Figure 1.10 The four types of porous structures based on spatial dimensions.[45]

1.7 Sorption

Sorption refers to the process in which a liquid or gaseous guest substance is taken up by a solid material.[33] The terms *sorbate* and *sorbent* refer to the guest and solid host, respectively.[33] Sorption encompasses both *absorption* and *adsorption*; whereas absorption denotes *"penetration of the sorbate beyond the sorbent surface,"* adsorption describes *"surface sorption"*.[33] There are two modes of sorption (Figure 1.11): *chemisorption* involves the formation of a bond between the host and the guest and *physisorption* takes place when the guest is held in place by only weak intermolecular interactions.[33] The term *desorption* is used to describe the reverse of sorption.[33]

Figure 1.12 displays three distinct sorption isotherms. Type I (dash-dot line) represents filling of a microporous material with cavities on the order of 5-20 Å.[45–47] Type II (dashed line) is a result of surface adsorption. S-shaped isotherm profiles (solid line) are obtained when a sorbent undergoes a structural transformation from a nonporous (closed) phase to a porous (open) phase. The points A and B indicate the start and end of the structural transformation, respectively.[45] Point A is also referred to as the onset or "gate-opening" pressure.

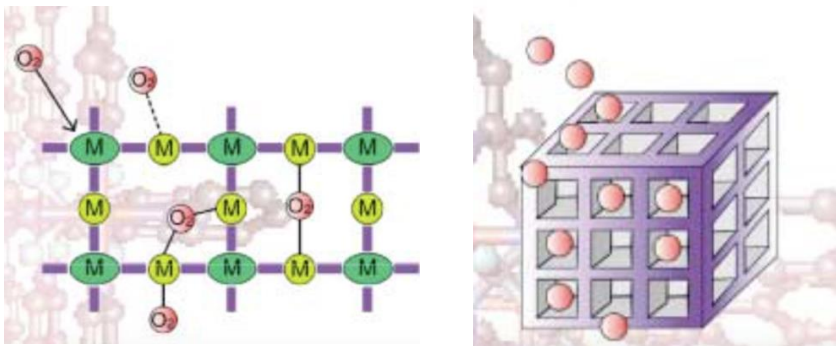

Figure 1.11 Two modes of sorption. Left: chemisorption; right: physisorption.[45]

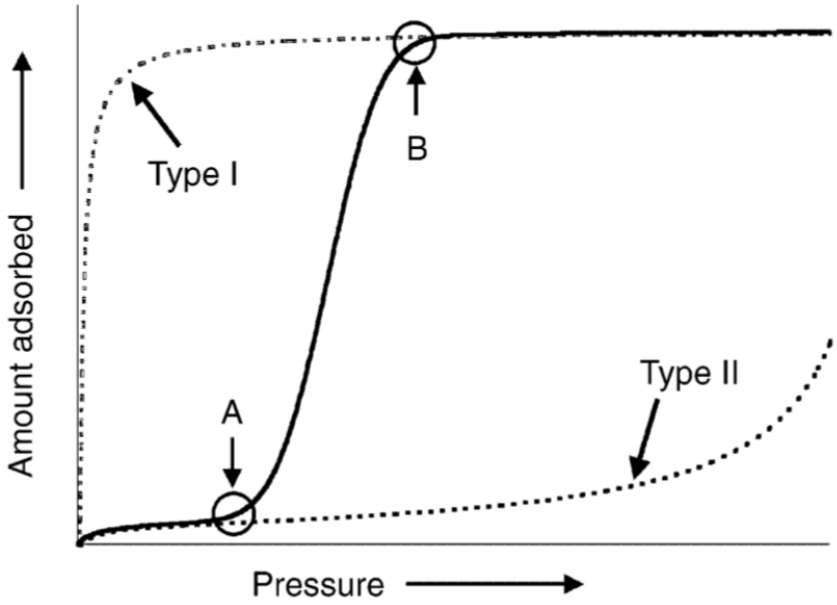

Figure 1.12 Three types of the sorption isotherms.[45]

1.8 Coordination Polymers, Metallocycles, and Metal-Organic Frameworks (MOFs)

A coordination compound comprises a central atom such as a metal ion that is bound to organic ligands, which can be atoms or molecules.[48] The self-assembly of coordination compounds can result in *coordination polymers* or discrete 0D compounds depending on the choice of ligand and crystallization conditions (Figures 1.13 and 1.14).[36,48] Coordination polymers can be further sub-categorized into 1D chains and 2D or 3D nets that are also referred to as metal-organic frameworks (MOFs).[36,48] Metallocycles are examples of discrete coordination compounds.

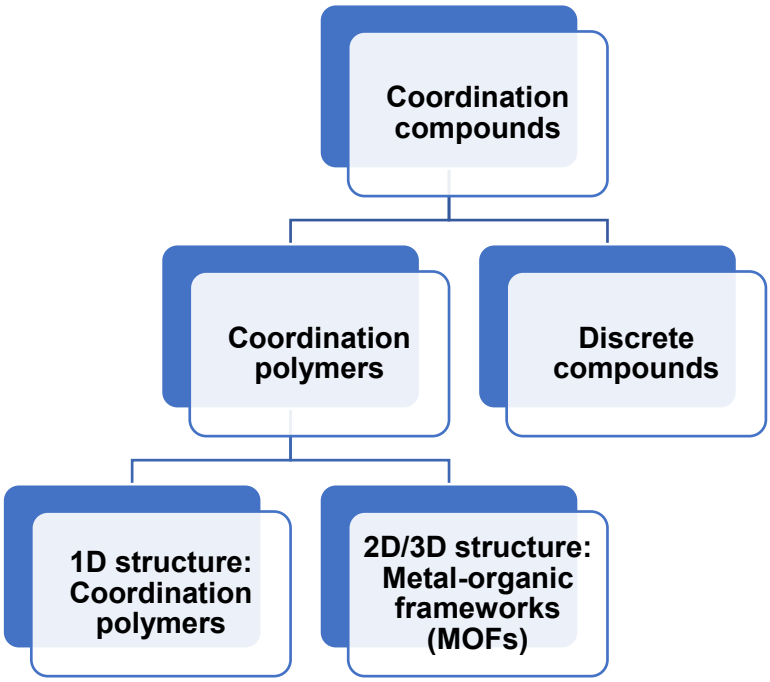

Figure 1.13 A tentative hierarchy of coordination compounds, adapted from Batten *et al.*[48]

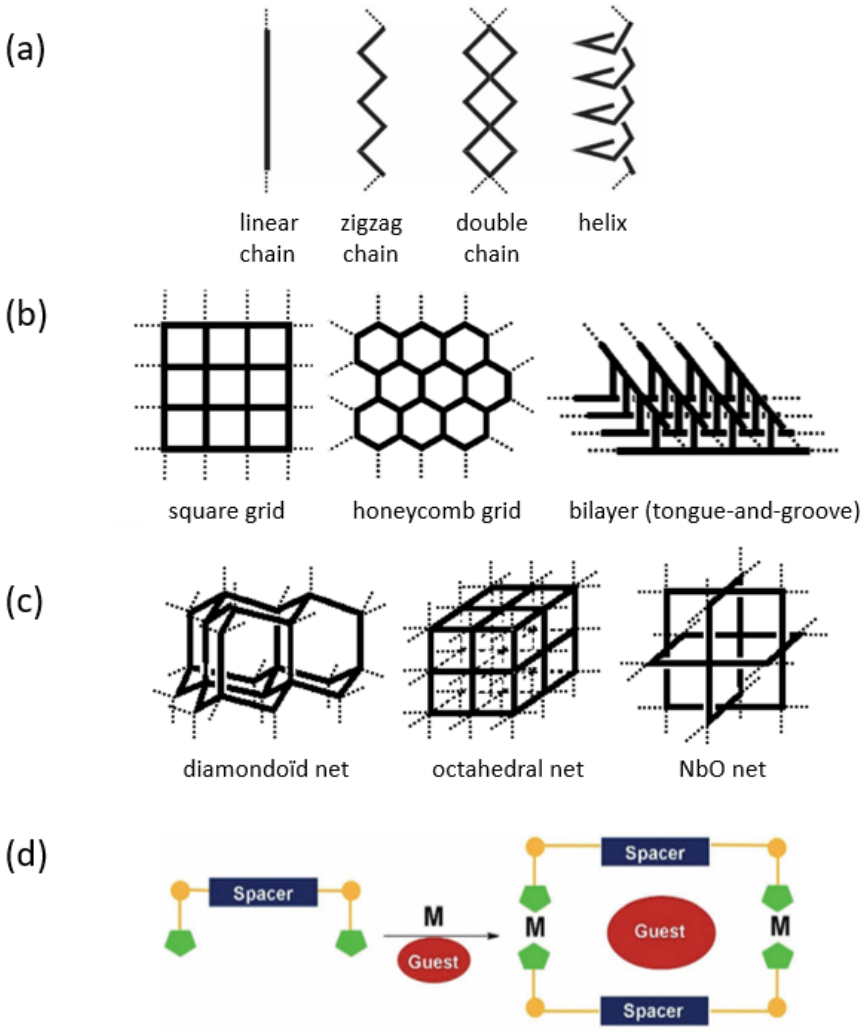

Figure 1.14 Common motifs in coordination compounds: (a) 1D chains; (b) 2D layers; (c) 3D nets; (d) 0D metallocycles.[36,49]

Porosity is an important property of metallocycles and MOFs, making these materials suitable candidates for separation and storage applications. Kitagawa classified porous materials into three generations according to the framework response to guest removal (Figure 1.15).[50,51] First generation materials collapse irreversibly upon guest removal and are no longer porous.[36] Second generation materials have rigid frameworks that maintain their structure upon guest uptake and release.[36] Third generation materials have flexible structures that reversibly transform from one phase to another upon guest uptake and release. Third generation, or soft materials, exhibit sensitivity to external stimuli such as light, heat, pressure, magnetic fields, etc.[14,36] Both second and third generation materials retain their crystallinity after activation, which is the process of removing the guest molecules from the framework.[36]

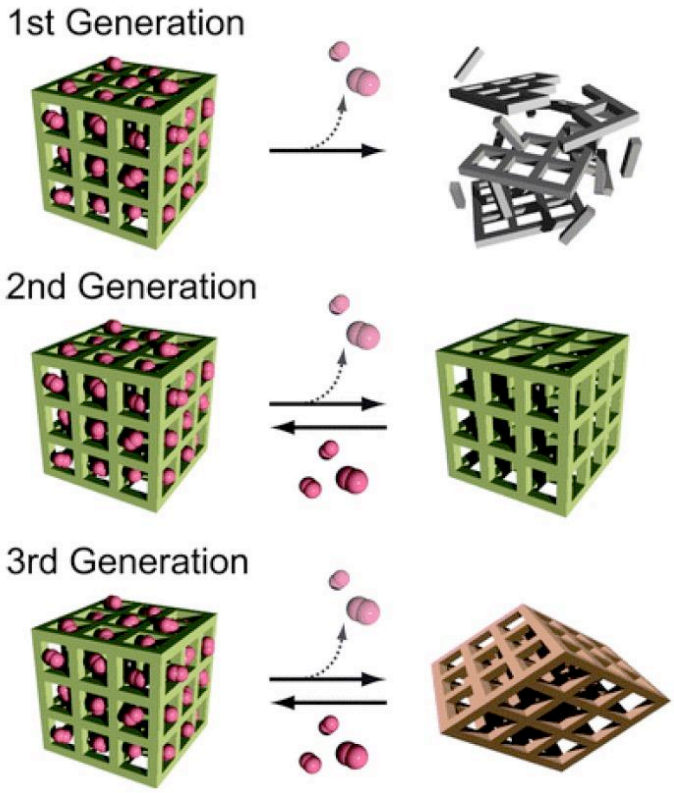

Figure 1.15 Three types of porous materials classified via their softness, rigidity and regularity.[51]

1.9 Aims/Objective of this study

Xylenes are an essential chemical feedstock for petrochemical and pharmaceutical processes.[52] They are widely used for the production of plastics, polymer fibers, rubbers, fuels, solvents and drug intermediates, etc.[9,11,52] Each xylene isomer is a valuable chemical intermediate and the global demand for pure xylene is rising annually. Approximately 42.5 million tons of xylene were consumed in 2010.[52] Generally, xylenes are generated from the refinement of crude oil to yield a mixture of the *para*- (*px*), *meta*- (*mx*) and *ortho*-xylene (*ox*) isomers. Due to their identical molecular weights, and similar densities and boiling points, the separation of xylene isomers is difficult, energy intensive and costly.[9] Industrial separation by distillation accounts for 10-15% of energy consumption worldwide.[11,53] To date, separation of xylenes at scale with a simple, efficient and low-cost method is still an open challenge.[9,52]

Molecular shape, the most distinct feature of the xylene isomers, is due to the relative position of the methyl groups. The Barbour group recently reported a metallocycle that exhibits very good selectivity for *px* over the other two isomers.[11] Therefore, the aim of the current study is to develop an improved understanding of metallocycles and to find other metallocycles that can efficiently separate xylene isomers. We endeavor to find metallocycles that show preference for *mx* or *ox* over *px*. Figure 1.16 shows two metallocycles that have previously been prepared in the Barbour group and that exhibit porosity and large cavities.[54,55] The ability of these two metallocycles to selectively absorb xylenes has been investigated as part of the present study. Techniques such as single-crystal X-ray diffraction (SCD), powder X-ray diffraction (PXRD), thermogravimetric analysis (TGA), solvent exchanges, activation, Fourier transform infrared spectroscopy (FT-IR), vapor sorption, gas chromatography (GC) and nuclear magnetic resonance spectroscopy (NMR) will be elaborated on.

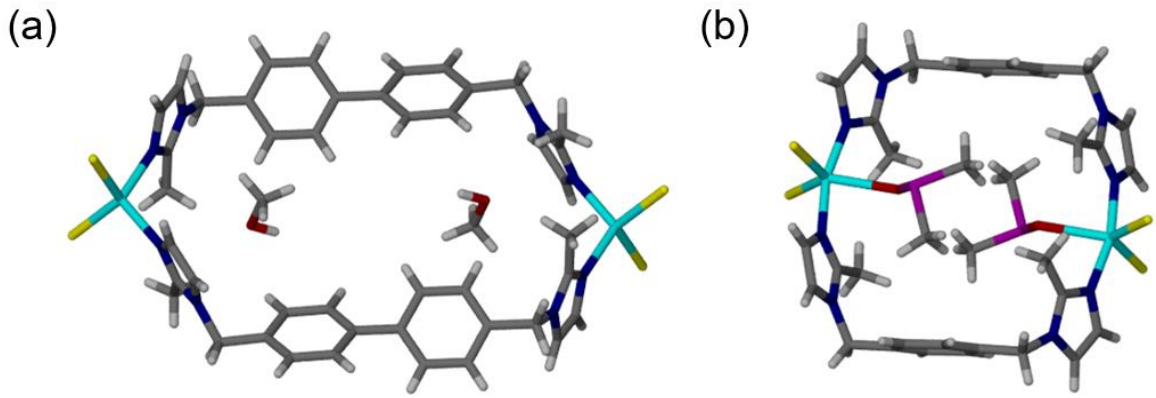

Figure 1.16 Metallocycles reported by the Barbour group.[54,55]

1.10 Thesis Outline

The thesis is structured as follows. Experimental techniques, analytical methods and instruments used in this study are described in **Chapter 2**. **Chapter 3** reports the ability of a Cd-metallocycle (**MC1**) to take up xylenes. **Chapter 4** describes the application of a Cu-metallocycle (**MC2**) for the separation of binary xylene mixtures. **Chapter 5** provides a brief summary and conclusions, and also proposes potential future work.

1.11 References

1 G. R. Desiraju, *Nature*, 2001, **412**, 397–400.

2 J. M. Lehn, *Angew. Chem. Int. Ed. Eng.*, 1988, **27**, 89–112.

3 J. M. Lehn, *Science*, 1993, **260**, 1762–1763.

4 J. Liu, L. Chen, H. Cui, J. Zhang and L. Zhang, *Chem. Soc. Rev.*, 2014, **43**, 6011–6061.

5 W. X. Gao, H. N. Zhang and G. X. Jin, *Coord. Chem. Rev.*, 2019, **386**, 69–84.

6 M. Raynal, P. Ballester, A. Vidal-Ferran and P. W. N. M. Van Leeuwen, *Chem. Soc. Rev.*, 2014, **43**, 1660–1733.

7 M. Raynal, P. Ballester, A. Vidal-Ferran and P. W. N. M. Van Leeuwen, *Chem. Soc. Rev.*, 2014, **43**, 1734–1787.

8 J. M. Lehn, *Science*, 1985, **227**, 849–856.

9 W. Qi, X. Wang, Z. Liu, K. Liu, Y. Long, W. Zhi, C. Ma, Y. Yan and J. Huang, *J. Colloid Interface Sci.*, 2021, **597**, 325–333.

10 D. Wang, D. Jana and Y. Zhao, *Acc. Chem. Res.*, 2020, **53**, 1389–1400.

11 M. du Plessis, V. I. Nikolayenko and L. J. Barbour, *J. Am. Chem. Soc.*, 2020, **142**, 4529–4533.

12 L. Liu, H. Y. Zhang, H. J. Wang, S. Chen, J. H. Wang and J. W. Sun, *Eur. J. Inorg. Chem.*, 2019, **2019**, 1839–1846.

13 G. B. Li, B. Q. Song, S. Q. Wang, L. M. Pei, S. G. Liu, J. L. Song and Q. Y. Yang, *ACS Omega*, 2019, **4**, 1995–2000.

14 A. J. Fletcher, K. M. Thomas and M. J. Rosseinsky, *J. Solid State Chem.*, 2005, **178**, 2491–2510.

15 J. Canivet, J. Bonnefoy, C. Daniel, A. Legrand, B. Coasne and D. Farrusseng, *New J. Chem.*, 2014, **38**, 3102–3111.

16 P. Lama, H. Aggarwal, C. X. Bezuidenhout and L. J. Barbour, *Angew. Chem., Int. Ed.*, 2016, **55**, 13271–13275.

17 K. Sumida, D. L. Rogow, J. A. Mason, T. M. McDonald, E. D. Bloch, Z. R. Herm, T. H. Bae and J. R. Long, *Chem. Rev.*, 2012, **112**, 724–781.

18 L. Jiao, J. Y. R. Seow, W. S. Skinner, Z. U. Wang and H. L. Jiang, *Mater. Today*, 2019, **27**, 43–68.

19 J. A. Mason, M. Veenstra and J. R. Long, *Chem. Sci.*, 2014, **5**, 32–51.

20 J. L. Atwood, L. J. Barbour and A. Jerga, *Science*, 2002, **296**, 2367–2369.

21 G. Mahata, S. Dey and J. Chanda, *Am. J. Drug Discov.*, 2014, **1**, 1–9.

22 E. W. Meijer and and A. P. H. J. Schenning, *Nature*, 2002, **419**, 353–354.

23 A. P. H. J. Schenning and E. W. Meijer, *Chem. Commun.*, 2005, 3245–3258.

24 G. R. Desiraju, *Angew. Chem., Int. Ed.*, 2007, **46**, 8342–8356.

25 G. R. Desiraju, *J. Am. Chem. Soc.*, 2013, **135**, 9952–9967.

26 E. J. Corey, *Pure Appl. Chem.*, 1967, **14**, 19–38.

27 G. R. Desiraju, *Angew. Chem. Int. Ed. Eng.*, 1995, 34, 2311–2327.

28 D. Shekhar Reddy, Y. E. Ovchinnikov, O. V. Shishkin, Y. T. Struchkov and G. R. Desiraju, *J. Am. Chem. Soc.*, 1996, **118**, 4085–4089.

29 G. M. Whitesides, J. P. Mathias and C. T. Seto, *Science*, 1991, **254**, 1312–1319.

30 G. Yu, K. Jie and F. Huang, *Chem. Rev.*, 2015, **115**, 7240–7303.

31 A. Nangia, *J. Chem. Sci.*, 2010, **122**, 295–310.

32 J. W. Steed, D. R. Turner and K. J. Wallace, *Core Concepts in Supramolecular Chemistry and Nanochemistry*, John Wiley & Sons, Ltd., 2007.

33 L. J. Barbour, D. Das, T. Jacobs, G. O. Lloyd and V. J. Smith, in *Supramolecular Chemistry: From Molecules to Nanomaterials*, John Wiley & Sons, Ltd., 2012.

34 D. B. Varshey, J. R. G. Sander, T. Friščić and L. R. MacGillivray, in *Supramolecular Chemistry: From Molecules to Nanomaterials*, John Wiley & Sons, Ltd., 2012.

35 W. R. Zhuang, Y. Wang, P. F. Cui, L. Xing, J. Lee, D. Kim, H. L. Jiang and Y. K. Oh, *J. Control. Release*, 2019, **294**, 311–326.

36 A. Y. Robin and K. M. Fromm, *Coord. Chem. Rev.*, 2006, **250**, 2127–2157.

37 G. R. Desiraju, J. J. Vittal and A. Ramanan, in *Crystal Engineering: A*

Textbook, 2011.

38 W. D. S. Motherwell, *CrystEngComm*, 2017, **19**, 6869–6882.

39 J. L. Atwood and J. W. Steed, *Encyclopedia of Supramolecular Chemistry*, Marcel Dekker. Inc., 2004.

40 L. R. Nassimbeni, *Acc. Chem. Res.*, 2003, **36**, 631–637.

41 J. W. Steed, J. L. Atwood and P. A. Gale, in *Supramolecular Chemistry: From Molecules to Nanomaterials*, John Wiley & Sons, Ltd, 2012.

42 M. R. Caira, L. R. Nassimbeni, F. Toda and D. Vujovic, *J. Chem. Soc. Perkin Trans. 2*, 2001, **2**, 2119–2124.

43 L. J. Barbour, *Aust. J. Chem.*, 2006, **59**, 595–596.

44 L. J. Barbour, *Chem. Commun.*, 2006, 1163–1168.

45 S. Kitagawa, R. Kitaura and S. I. Noro, *Angew. Chem., Int. Ed.*, 2004, **43**, 2334–2375.

46 K. S. W. Sing, D. H. Everett, R. A. W. Haul, J. Rouquerol and T. Siemieniewska, *Pure Appl. Chem.*, 1985, **57**, 603–619.

47 Q. Y. Yang, P. Lama, S. Sen, M. Lusi, K. J. Chen, W. Y. Gao, M. Shivanna, T. Pham, N. Hosono, S. Kusaka, J. J. Perry, S. Ma, B. Space, L. J. Barbour, S. Kitagawa and M. J. Zaworotko, *Angew. Chem., Int. Ed.*, 2018, **57**, 5684–5689.

48 S. R. Batten, N. R. Champness, X. M. Chen, J. Garcia-Martinez, S. Kitagawa, L. Öhrström, M. O'Keeffe, M. P. Suh and J. Reedijk, *CrystEngComm*, 2012, **14**, 3001–3004.

49 V. I. Nikolayenko, A. Heyns and L. J. Barbour, *Chem. Commun.*, 2017, **53**, 11306–11309.

50 S. Kitagawa and M. Kondo, *Bull. Chem. Soc. Jpn.*, 1998, 71, 1739–1753.

51 S. Horike, S. Shimomura and S. Kitagawa, *Nat. Chem.*, 2009, **1**, 695–704.

52 G. Zhang, Y. Ding, A. Hashem, A. Fakim and N. M. Khashab, *Cell Reports Phys. Sci.*, 2021, **2**, 100470.

53 D. S. Sholl and R. P. Lively, *Nature*, 2016, **532**, 435–437.

54 T. Jacobs and L. J. Barbour, *New J. Chem.*, 2013, **37**, 71–74.

55 M. du Plessis, V. I. Nikolayenko and L. J. Barbour, *Inorg. Chem.*, 2018, **57**, 12331–12337.

Chapter 2

Experimental Techniques

2.1 Ligand Synthesis

2.1.1 4,4′-Bis(2-methylimidazol-1-ylmethyl)biphenyl (L1)

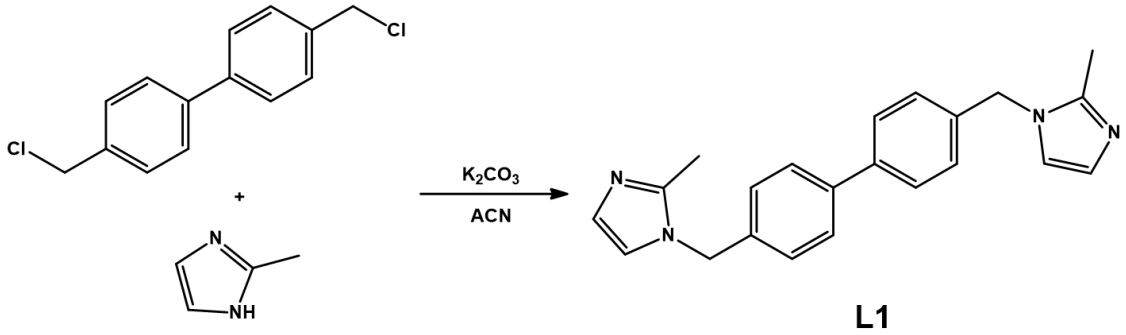

L1

Scheme 2.1 Synthesis of ligand 4,4′-bis(2-methylimidazol-1-ylmethyl)biphenyl (**L1**).

The ligand 4,4′-bis(2-methylimidazol-1-ylmethyl)biphenyl (**L1**) was synthesized using the method reported by Jacobs *et al*.[1] 4,4′-Bis(chloromethyl)-1,1′-biphenyl (7.03 mmol, 1.76 g) and 2-methylimidazole (16.8 mmol, 1.38 g) and potassium carbonate (45.5 mmol, 6.30 g) were measured and added to 60 mL acetonitrile to form a suspension. The mixture was stirred under reflux for 10-15 hours, resulting in an orange reaction mixture and beige precipitate. The precipitate was filtered off and the excess solvent was removed using a rotary evaporator. A honey-colored oil was obtained, dissolved in chloroform (60 mL) and then extracted with water (3 x 100 mL). The organic extract was subsequently dried over $MgSO_4$ and filtered. The filtrate was collected and the excess solvent was removed with a rotary evaporator. A yellow-orange oil was obtained. The product was precipitated out with diethyl ether. The mixture was then placed in a refrigerator overnight for further precipitation. The light orange solid was filtered, washed with ethyl acetate, and then dried in a glass oven overnight at 50 ºC and under dynamic vacuum (2 x 10^{-2} mbar).

Yield: 0.413 g, 17.2%; M.P. 169.6 – 171.5 °C.

^{1}H NMR (600MHz, $CDCl_3$): δ 2.35 (s, 6H); 5.09 (s, 4H); 6.87 (s, 2H); 6.97 (s, 2H); 7.12 (d, J = 8.4 Hz, 4H); 7.53 (d, J = 7.8 Hz, 4H).

^{1}C NMR (600MHz, $CDCl_3$): δ 13.3, 49.6, 120.0, 127.3, 127.6, 127.7, 135.8, 140.2, 145.1.

2.1.2 1,4-Bis((2-methyl-1H-imidazol-1-yl)methyl)benzene (L2)

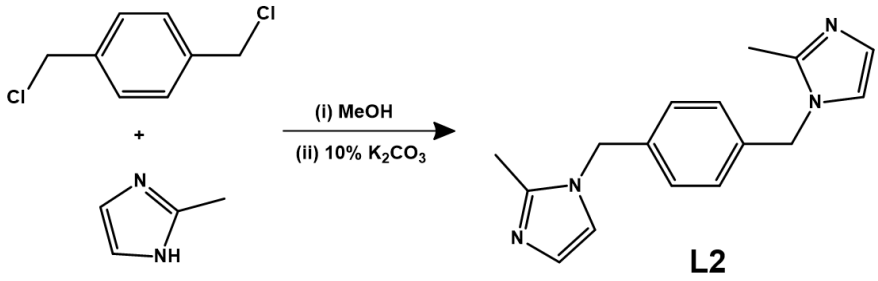

Scheme 2.2 Synthesis of ligand 1,4-bis((2-methyl-1H-imidazol-1-yl)methyl)benzene (**L2**).

Method 1: The ligand 1,4-bis((2-methyl-1H-imidazol-1-yl)methyl)benzene (**L2**) was synthesized via a S_N2 routine, which was reported by Dobrzańska *et al*.[2] The method was modified by du Plessis *et al*.[3] Starting materials *α,α'*-dichloro-*p*-xylene (10 mmol, 1.75 g) and 2-methylimidazole (98 mmol, 6.71 g) were added to 100 mL methanol to form a suspension. The mixture was stirred under reflux at 65 °C for 24 hours, after which it was cooled to room temperature. Excess solvent was removed with a rotary evaporator. A 10% K_2CO_3 aqueous solution was added to the cooled mixture, upon which the mixture became slightly milky. It was then placed in a refrigerator overnight for further precipitation. When K_2CO_3 precipitated first, it was removed by filtration and additional K_2CO_3 aqueous solution was added. White, needle-shaped crystals were formed and were collected by filtration. Products were washed with distilled water to remove any excess K_2CO_3, after which they were washed with ethyl acetate and dried on filter paper overnight.

Yield: 1.3737 g, 51.51%; M.P. 83.3 – 85.6 °C.

^{1}H NMR (300 MHz, DMSO-d_6): δ 2.19 (s, 6H); 5.09 (s, 4H); 6.74 (d, J = 0.9 Hz, 2H); 7.09 (d, J = 1.2 Hz, 2H); 7.11 (s, 4H).

^{1}C NMR (300 MHz, DMSO-d_6): δ 12.8, 48.6, 120.7, 126.5, 127.8, 137.0, 144.4.

Method 2: An alternative method was modified from that reported by Nikolayenko *et al.*[4] and du Plessis[5]: 2-methylimidazole (10 mmol, 0.82 g), ground potassium hydroxide (41 mmol, 2.30 g) and dimethyl sulfoxide (15 mL) were added to a round bottom flask and the mixture was stirred for ca. 2 hours. A yellow-brown suspension

was obtained and *α,α′*-dichloro-*p*-xylene (5 mmol, 0.88 g) was added. The reaction was allowed to stir overnight. Undissolved KOH and brown residue were filtered off. A brown solution was obtained. Distilled water was added to the residue to dissolve the KOH on the filter paper, allowing it to drop into the filtrate to precipitate the product. A yellowish product was collected by filtration, washed with ethyl acetate and dried on filter paper overnight.

Yield: 0.8479 g, 63.44%

Both methods worked well. Method 1 uses larger scale. Excess 2-methylimidazole was used to deprotonate itself. Method 2 uses equimolar amounts of the starting materials and KOH was used to deprotonate the 2-methylimidazole. Method 1 works under reflux at 65 °C, while method 2 works at ambient temperature, without reflux. Although both methods provide pure product in good yield, method 2 was preferred because when using method 1, K_2CO_3 sometimes precipitated first.

2.2 Preparation of Metallocycles

2.2.1 **MC1**·2(MeOH)

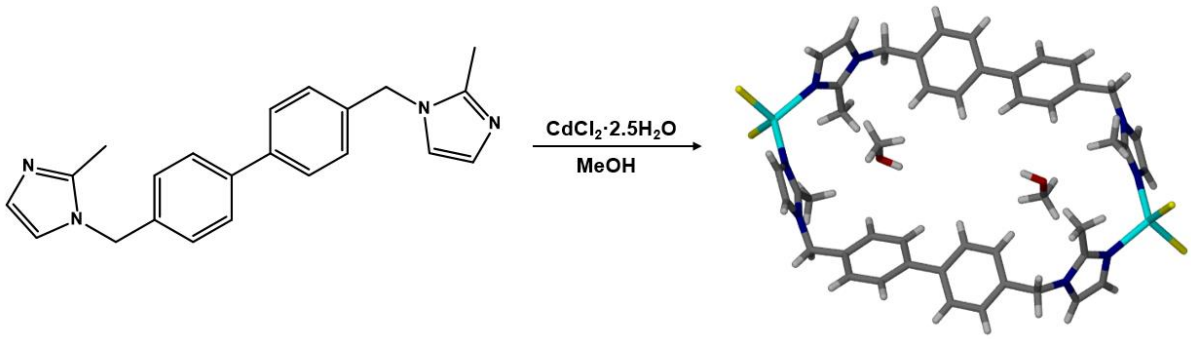

Scheme 2.3 Preparation of the metallocycle $[Cd_2Cl_4(\mathbf{L1})_2]\cdot 2CH_3OH$ (**MC1**·2(MeOH)) by a layering method.

Colorless rectangular block-shaped crystals of **MC1**·2(MeOH) were synthesized by layering a solution of $CdCl_2\cdot 2.5H_2O$ (0.05 mmol, 11.4 mg) in methanol (MeOH, 2 mL) on top of a solution of **L1** (0.05 mmol, 17.1 mg) in chloroform (2 mL).[1] Crystals were obtained by slow diffusion within 3 days.

2.2.2 **MC2**·2(DMSO)

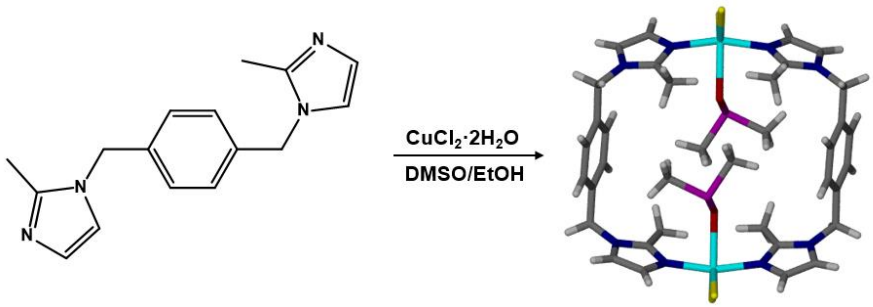

Scheme 2.4 Preparation of $[Cu_2Cl_4(\mathbf{L2})_2]\cdot 2(CH_3)_2SO$ (**MC2**·2(DMSO)) by a layering method.

Green block-shaped crystals of **MC2**·2(DMSO) were prepared by layering a solution of $CuCl_2\cdot 2H_2O$ (0.05 mmol) in ethanol (EtOH, 2 mL) on top of a solution of **L2** (0.05 mmol) in dimethyl sulfoxide (DMSO, 2 mL).[4] Crystals were obtained within 3–7 days. An alternative preparation method was also employed in which the metal salt and **L2** are both dissolved separately in acetone and added to the same glass vial without further mixing. A precipitate was formed when the two solutions were combined. The vial was then covered with parafilm and a few holes poked in the film. Orange blocks of **MC2**·2(acetone) were obtained by slow evaporation after a few days.[2] The layering method was used more often since it was more reproducible. The slow evaporation procedure did not always result in crystals if the solvent evaporated too fast.

2.3 Analytical Techniques and Instrumentation

2.3.1 Single Crystal X-Ray Diffraction (SCD)

Single crystal X-ray diffraction (SCD) is a useful analytical tool that is used to elucidate the structure of crystalline materials. The packing and arrangement of the molecules in a crystal can be visualized and therefore the atomic coordination, bond lengths, bond distances and intermolecular interactions can be evaluated.

The temperature of the system was controlled with an Oxford Cryosystems 700+ cryostat supplied with liquid nitrogen. Then, a good quality single crystal was selected based on its size and ability to extinguish plane polarised light. It was placed on a MiTiGen™ mount with the aid of the Paratone®N oil (Figure 2.1) using a

microscope. The mounted crystal was attached to the goniometer. A Bruker 3-circle DUO Apex II X-ray diffractometer equipped with an Incoatec IμS HB microfocus source (MoKα radiation λ = 0.71073 Å), with a multilayer monochromator, was used. A CCD (charge-coupled device) area detector was used to capture the single crystal X-ray intensity data. Data collection and reduction were achieved using the Bruker APEX-3 software employing standard procedures.[6] Structures were solved and refined using SHELX-2016[7–9] with X-Seed as a graphical interface.[10,11] Riding models were employed to place hydrogen atoms in calculated positions. Surfaces of guest-accessible volumes were mapped with a probe radius of 1.5 Å using MSRoll.[12–14] Structural diagrams were generated using POV-Ray.[15]

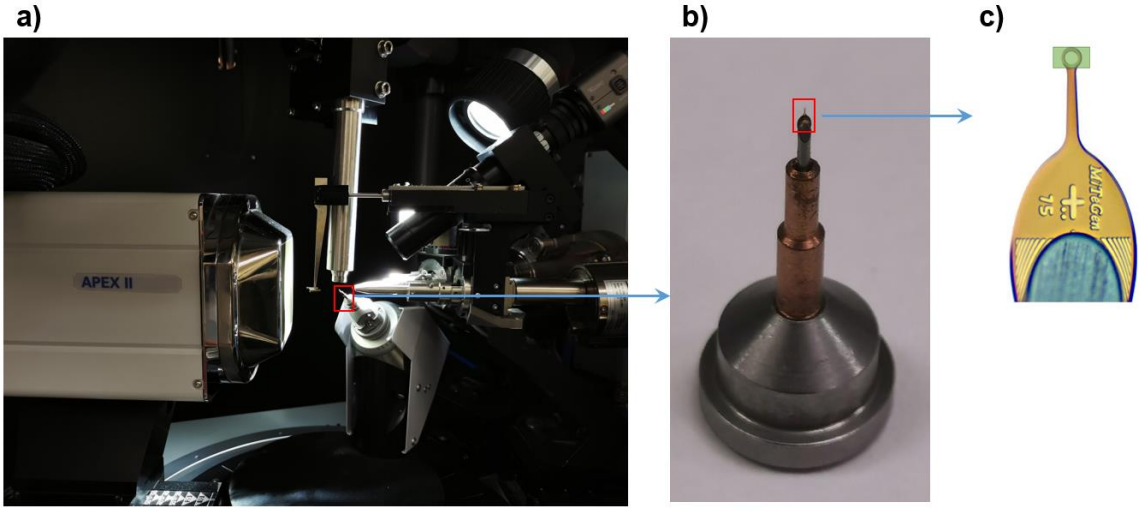

Figure 2.1 (a) The Bruker Apex II DUO diffractometer interior. (b) and (c) Illustrations of a single crystal mounted on a MiTeGen[16] foil.

2.3.2 Powder X-Ray Diffraction (PXRD)

Powder X-ray diffraction is a non-destructive technique utilized for the confirmation of phase purity of a bulk sample. A Bruker D2 Phaser benchtop powder diffractometer utilizing Bragg−Brentano geometry and equipped with a Lynxeye detector and Cu Kα radiation (λ = 1.5418 Å) was employed. Surface solvent was removed by drying on filter paper. Then crystals were ground into powders and transferred and distributed evenly onto a zero-background sample holder. Intensity data for most samples were captured with 2θ scans in the range 5–50°. The step size was set at 0.02° and exposure time was 0.50 seconds per step (PXRD experiments for activated Cu-based crystals were performed in range 10–25°, with step size set to 0.16° and exposure

time 0.75 seconds). The sample stage was rotated at 30 rpm. The experiments were carried out at ambient temperature and pressure. The X'Pert HighScore Plus software package was used to analyze the powder patterns and the results were compared to the powder patterns calculated from single crystal structures using Mercury.[17–21] Thus, the phase purities of the crystallizations could be determined.

2.3.3 Thermogravimetric Analysis (TGA)

Thermogravimetric analysis (TGA) records a thermogram of weight loss with increasing temperature. It provides an approximate indication of the activation temperature, implied from the temperature range over which the guest is lost. TGA was performed using a TA Instruments Q500 system. The experiments were carried out with a balance purge flow rate at 60 mL/min and sample purge flow rate at 40 mL/min. Nitrogen was used as the purge gas. Surface solvent was removed by drying on filter paper. Approximately 1–5 mg of sample was added to an aluminium sample pan and heated from room temperature to 600 °C (xylene inclusion compounds were heated to 300 °C), with a ramp rate of 10 °C/min. The thermograms were analyzed using the Universal Analysis 2000 software (TA Instruments).

2.3.4 Nuclear Magnetic Resonance Spectroscopy (NMR)

The synthesized ligands, **L1** and **L2,** were dissolved in deuterated chloroform ($CDCl_3$) and deuterated dimethyl sulfoxide (DMSO-d_6), respectively. ^{1}H and ^{13}C NMR spectra were recorded using either a 300 or a 600 MHz Varian Unity Inova NMR spectrometer. MestReNova[22] was used to analyze the spectra.

2.3.5 Fourier Transform Infrared (FT-IR) Spectroscopy

Fourier Transform Infrared (FT-IR) spectroscopy was used to confirm the identity of the guest molecules in the molecular host. Solvent exchange can be monitored by FT-IR analysis. IR transmission spectra at room temperature were recorded with a Bruker Alpha P ATR-IR spectrometer. The experiments were carried out using the Bruker OPUS software. A background scan was carried out before each sample scan. KnowItAll®[23] software was used for IR spectral analysis.

2.3.6 Glass Oven

The glass oven is equipped with a vacuum pump operating at a pressure of 2×10^{-2} mbar. It can heat samples from room temperature to 300 °C under vacuum. The oven was used to dry the synthesized ligands and to activate crystals.

2.3.7 Vapor Sorption

Sorption experiments were carried out in a controlled atmosphere using a modified version of a vapor balance that was reported by Barbour and co-workers.[24] The apparatus measures the weight change of a sample as a function of time. The device is enclosed in a wooden cabinet. Edison bulbs and built-in fans are used for temperature regulation. A vacuum pump (0.1 mbar) and a pressure sensor are attached to the system. Pre-weighed samples (ca. 30 mg) were loaded into an aluminium basket, which was then attached to a thin steel wire connected to a microelectronic balance. The balance is monitored by a computer program that provides a real-time plot of weight change as a function of time. After the sample was loaded, the system was evacuated and allowed to equilibrate for approximately 1–2 minutes under reduced pressure. The vapor control valve was opened once the mass of sample was stabilized (this represents time zero). The temperature of the apparatus was maintained at 25 °C. The balance was zeroed before the experiment started and the sorption was carried out until the sample reached an equilibrium state (no longer than 24 hours). Figure 2.2 shows the vapor sorption apparatus.

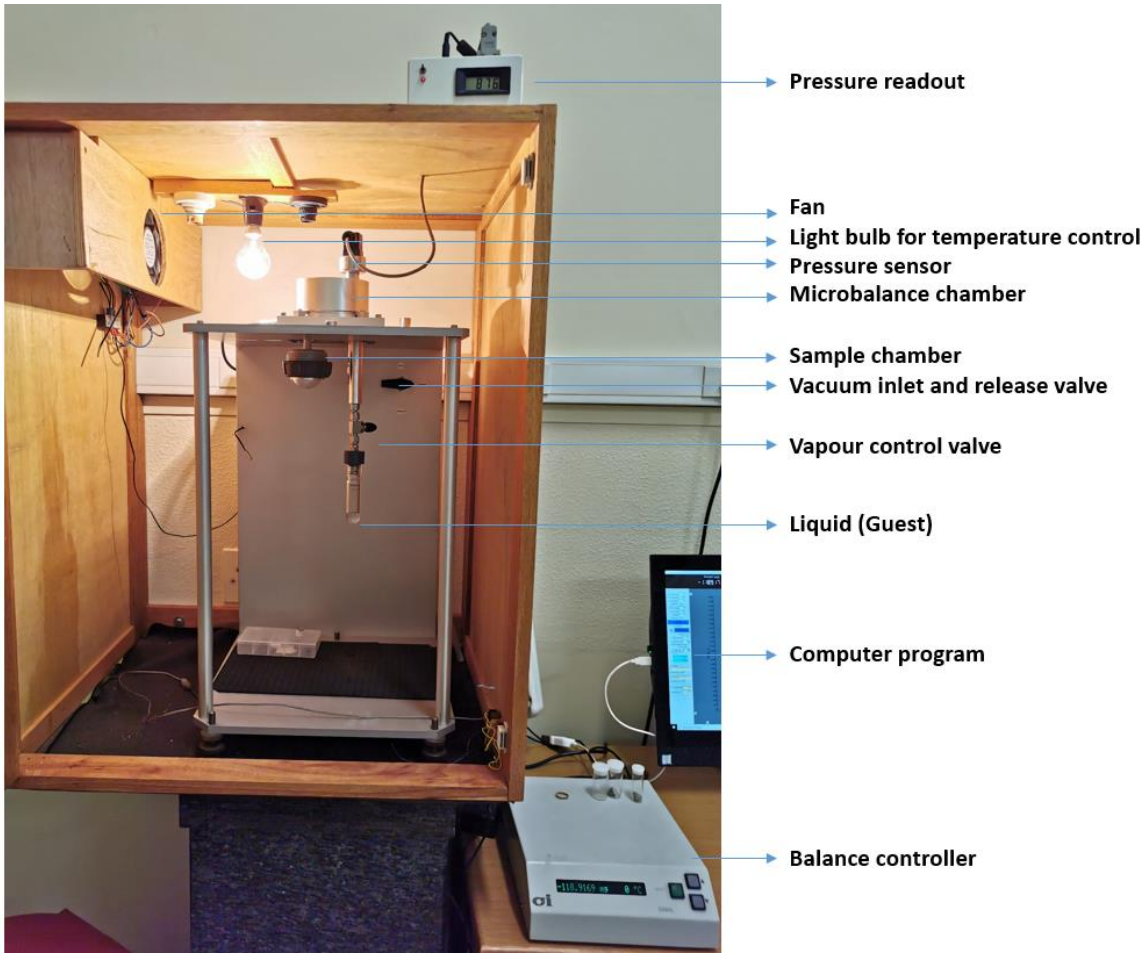

Figure 2.2 The vapor sorption apparatus.

2.3.8 Gas Chromatography (GC)

Gas chromatography (GC) is a quantitative and qualitative analytical tool. It was used in this project to determine the fractions of the xylenes in mixtures used for selectivity experiments. The apohost of **MC2** was immersed in xylenes for at least 24 hours, then was dried on filter paper for ca. 30 minutes, followed by soaking in acetonitrile (ACN) at 45 °C for 24–48 hours. The xylene molecules were replaced by ACN. Then the crystals of **MC2** were removed from the ACN by filtering through syringe filters with polytetrafluoroethylene (PTFE) membranes of pore size 0.45 µm. The filtrate was used for GC analysis to determine the composition of the xylene isomers. A Varian 3900 gas chromatograph equipped with a flame ionization detector (FID) was used to analyze the filtrate. An HP INNOWAX (crosslinked polyethylene glycol) column with dimensions 30 m x 0.25 mm and a film thickness of 0.5 µm was used. The experiments were carried out at an initial temperature of 40 °C maintained for two minutes then

ramped at 10 °C/min to 180 °C. The injector and detector were kept at 220 °C. The carrier gas used was helium, with a flow rate of 1 mL/min. 1 µL of each sample was injected through the GC inlet with a split ratio of 1:100. The split vent flow rate was 143 mL/min. The software CompassCDS[25] was used for system operation and data acquisition.

2.4 Software

2.4.1 Cambridge Structural Database (CSD)

The Cambridge Structural Database (CSD)[26] is maintained and distributed by the Cambridge Crystallographic Data Centre (CCDC). It is a powerful tool used to search published single-crystal structures as it contains complete records such as molecular formula, structure, unit cell, defined geometry, intermolecular interactions, authors, *etc*. The database has been in existence for more than 50 years and Figure 2.3 shows the growth of the CSD since 1972 until the beginning of 2016.[26]

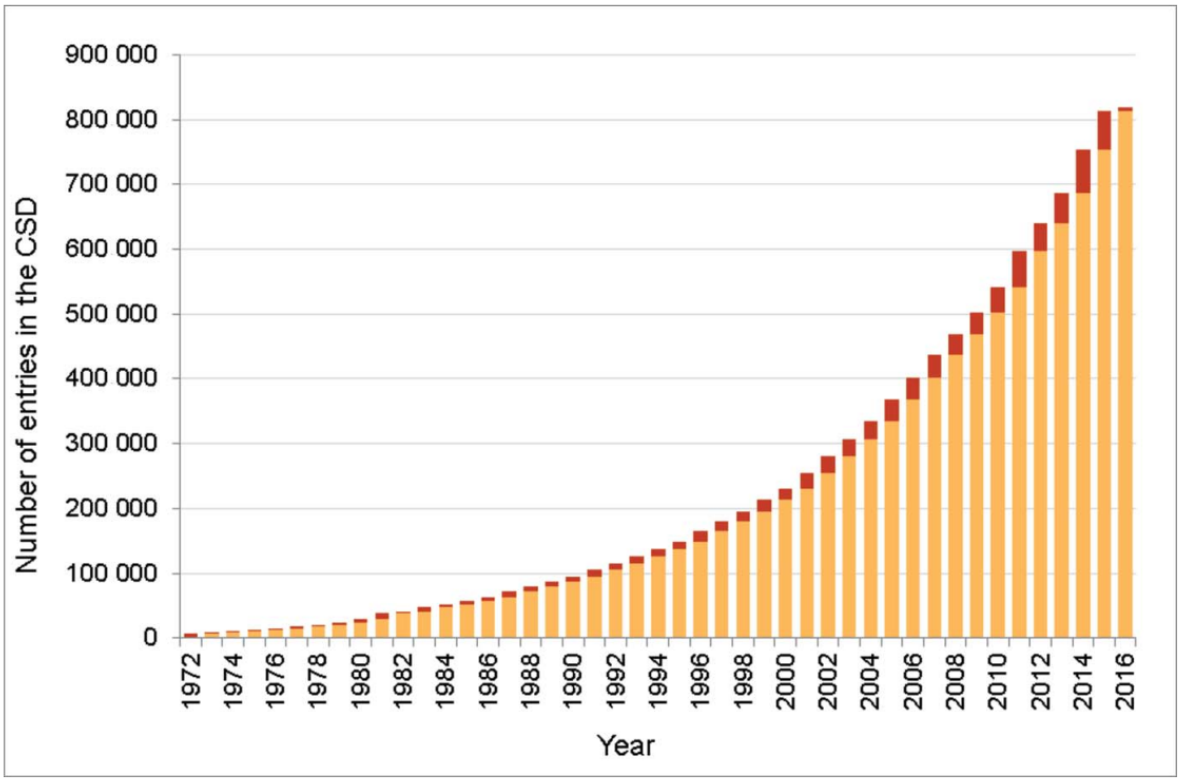

Figure 2.3 Growth of the CSD since 1972 with the red bars representing the structures added annually.[26]

2.4.2 X-Seed

X-Seed[10,11] is a crystallographic software tool that serves as a graphical interface to SHELX,[6] MSRoll[12–14] and POV-Ray.[15] SHELX is used to solve and refine the structures, MSRoll is used to generate surfaces of guest-accessible volume and POV-Ray is used to generate structural diagrams. MSRoll calculates the guest-accessible volume present in the molecular host. It will create an output file .cav which can be imported into X-Seed and incorporated into POV-Ray to generate a host structure with the guest-accessible space mapped. When using MSRoll, the contact surface type and 1.5 Å probe radius type were chosen. These guest-accessible volumes are defined as probe-accessible volumes by van Heerden and Barbour.[27] Figure 2.4 represents a probe-accessible surface (blue line) and a probe-traversable surface (dashed contour) mapped out by the surface and center of a spherical probe, respectively, as it is rolled over the van der Waals surface of a host.[27]

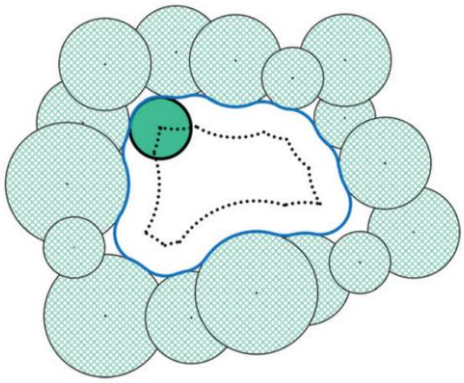

Figure 2.4 Blue: the probe-accessible surface; dashed line: the probe-traversable surface.[27]

2.4.3 Mercury

Mercury[17–21] is part of the CSD software suite. It can be utilized for the visualization of crystal structures and intermolecular interactions, to determine powder patterns from single-crystal structures, and to calculate probe-accessible volumes within the molecular host. In this study, a 1.5 Å probe radius and 0.2 Å grid spacing were applied.

2.4.4 Platon/SQUEEZE

Platon[28]/SQUEEZE[29,30] is a software tool that can sum the number of unmodelled electrons in the voids of a single crystal. From the comparison of the electron counts per metallocycle to the known numbers of electrons in the guest, the number of guest molecules trapped per metallocycle may be deduced.

2.4.5 Olex2

Olex2[31] is program that can be utilized to analyze crystal structures. In this study, it was used to generate the electron density maps at a 2 $e^{-}/Å^3$ level when the guest molecules could not be modelled. Positive electron densities are indicated as green surfaces. Close contacts due to intermolecular interactions were also determined using Olex2.

2.5 References

1 T. Jacobs, G. O. Lloyd, J. A. Gertenbach, K. K. Müller-Nedebock, C. Esterhuysen and L. J. Barbour, *Angew. Chem., Int. Ed.*, 2012, **51**, 4913–4916.

2 L. Dobrzańska, G. O. Lloyd, C. Esterhuysen and L. J. Barbour, *Angew. Chem., Int. Ed.*, 2006, **45**, 5856–5859.

3 M. du Plessis, V. I. Nikolayenko and L. J. Barbour, *Inorg. Chem.*, 2018, **57**, 12331–12337.

4 V. I. Nikolayenko, L. M. Van Wyk, O. Q. Munro and L. J. Barbour, *Chem. Commun.*, 2018, **54**, 6975–6978.

5 M. du Plessis, MSc Thesis, Stellenbosch University, 2012.

6 *APEX3, SAINT, and SADABS*; Bruker AXS Inc.: Madison, WI, 2016.

7 G. M. Sheldrick, *Acta Crystallogr.*, 2008, **A64**, 112–122.

8 G. M. Sheldrick, *Acta Crystallogr.*, 2015, **C71**, 3–8.

9 G. M. Sheldrick, *Acta Crystallogr.*, 2015, **A71**, 3–8.

10 J. L. Atwood and L. J. Barbour, *Cryst. Growth Des.*, 2003, **3**, 3–8.

11 L. J. Barbour, *J. Appl. Crystallogr.*, 2020, **53**, 1141–1146.

12 M. L. Connolly, *J. Appl. Crystallogr.*, 1983, **16**, 548–558.

13 M. L. Connolly, *Science*, 1983, **221**, 709–713.

14 M. L. Connolly, *J. Mol. Graph.*, 1993, **11**, 139–141.

15 *POV-Ray for Windows*, version 3.6.1a.icl8.win32; Persistence of Vision Pty. Ltd., 2003.

16 MiTeGen, MicroLoops LD™, https://www.mitegen.com/learn/technotes/microloopsld/, (accessed 20 January 2022)

17 R. Taylor and C. F. Macrae, *Acta Crystallogr. Sect. B Struct. Sci.*, 2001, **B57**, 815–827.

18 I. J. Bruno, J. C. Cole, P. R. Edgington, M. Kessler, C. F. Macrae, P. McCabe, J. Pearson and R. Taylor, *Acta Crystallogr. Sect. B Struct. Sci.*, 2002, **B58**, 389–397.

19 C. F. Macrae, P. R. Edgington, P. McCabe, E. Pidcock, G. P. Shields, R. Taylor, M. Towler and J. Van De Streek, *J. Appl. Crystallogr.*, 2006, **39**, 453–457.

20 C. F. Macrae, I. J. Bruno, J. A. Chisholm, P. R. Edgington, P. McCabe, E. Pidcock, L. Rodriguez-Monge, R. Taylor, J. Van De Streek and P. A. Wood, *J. Appl. Crystallogr.*, 2008, **41**, 466–470.

21 C. F. MacRae, I. Sovago, S. J. Cottrell, P. T. A. Galek, P. McCabe, E. Pidcock, M. Platings, G. P. Shields, J. S. Stevens, M. Towler and P. A. Wood, *J. Appl. Crystallogr.*, 2020, **53**, 226–235.

22 MestReNova, https://mestrelab.com/, (accessed 21 January 2022).

23 KnowItAll® Informatic system 2018, Bio-Rad Laboratories, Inc.

24 L. J. Barbour, K. Achleitner and J. R. Greene, *Thermochim. Acta*, 1992, **205**, 171–177.

25 CompassCDS, https://scioninstruments.com/products/compass-cds/, (accessed 20 January).

26 C. R. Groom, I. J. Bruno, M. P. Lightfoot and S. C. Ward, *Acta Crystallogr. Sect. B Struct. Sci. Cryst. Eng. Mater.*, 2016, **B72**, 171–179.

27 D. P. van Heerden and L. J. Barbour, *Chem. Soc. Rev.*, 2021, **50**, 735–749.

28 A. L. Spek, *Acta Crystallogr. Sect. D Biol. Crystallogr.*, 2009, **65**, 148–155.

29 P. van der Sluis and A. L. Spek, *Acta Crystallogr. Sect. A*, 1990, **46**, 194–201.

30 A. L. Spek, *Acta Crystallogr. Sect. C Struct. Chem.*, 2015, **71**, 9–18.

31 O. V. Dolomanov, L. J. Bourhis, R. J. Gildea, J. A. K. Howard and H. Puschmann, *J. Appl. Crystallogr.*, 2009, **42**, 339–341.

Chapter 3

Separation of Xylene Isomers using a Cd-based Metallocycle

3.1 Introduction

Jacobs *et al.* prepared the metallocycle $[Cd_2Cl_4(\mathbf{L1})_2]\cdot 2(CH_3OH)$ (**MC1**·2(MeOH)) by layering a methanol solution of $CdCl_2\cdot 2.5(H_2O)$ over a chloroform solution of the ligand 4,4′-bis(2-methylimidazol-1-ylmethyl)biphenyl (**L1**).[1] The synthetic approach is presented in Scheme 3.1 and shows that after crystallization two MeOH molecules are located in each discrete metallocycle.[1] The packing diagram is shown in Figure 3.1(a). The metallocycles stack along the *c* axis and a pocket is formed between adjacent metallocycles. The MeOH molecules are positioned at the two opposite ends of the pocket. These semi-transparent surfaces indicate the presence of potentially guest-accessible space.[1]

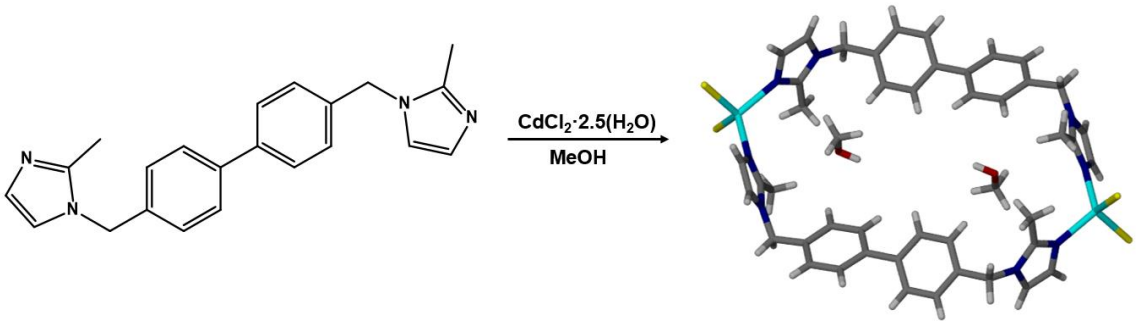

Scheme 3.1 Formation of the solvated metallocycle $[Cd_2Cl_4(\mathbf{L1})_2]\cdot 2(CH_3OH)$ (**MC1**·2(MeOH)).[1]

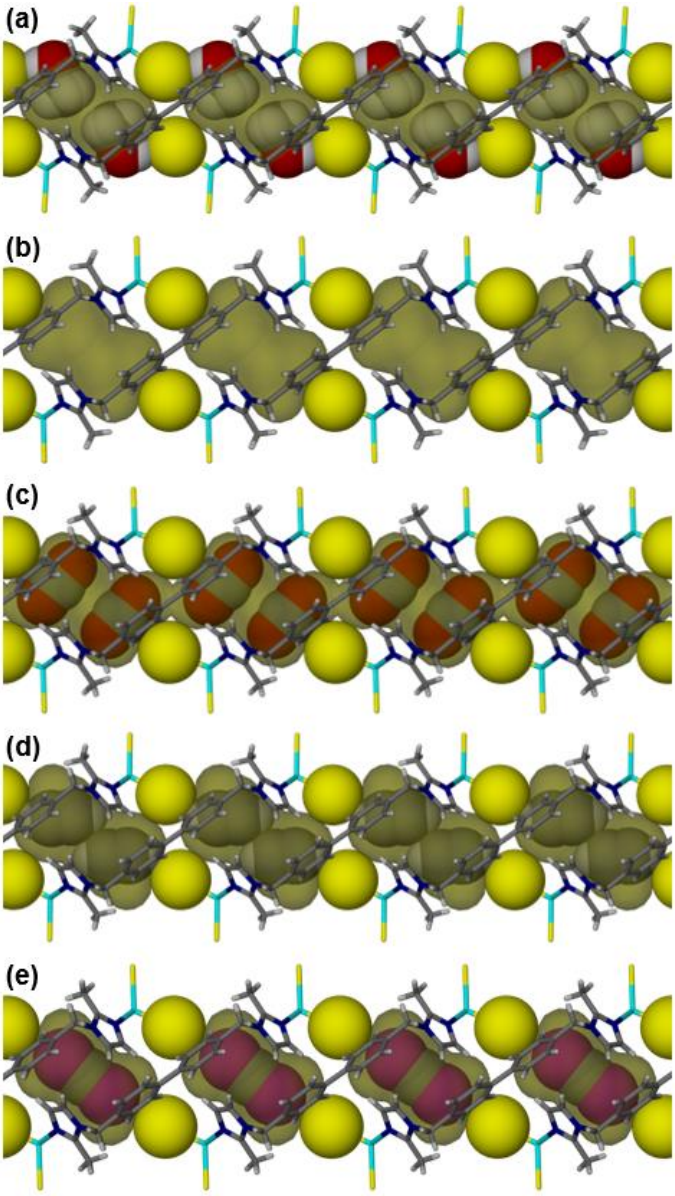

Figure 3.1 The **MC1** metallocycles stack along [001] and a cavity is formed between two adjacent metallocycles. (a) Each cavity is occupied by a pair of methanol molecules (**MC1**·2(MeOH)); (b) Packing diagram of apohost (**MC1a**); (c) Each cavity is occupied by a pair of carbon dioxide molecules (**MC1**·2(CO_2)); (d) Each cavity is occupied by a pair of acetylene molecules (**MC1**·2(C_2H_2)); (e) Crystal packing of **MC1**·CS_2, one CS_2 molecule lies along the length of the cavity. All the packing diagrams are viewed down [010]. The guest-accessible surface was mapped with r_{probe} = 1.5 Å.[1] The host molecules are shown in capped-stick representation, and the coordinating chloride ions are represented as yellow capped-sticks or van der Waals spheres. Guest molecules are shown in space filling representation. Guest-accessible space is shown as gold Connolly surfaces with 50% transparency. Adapted from Jacobs *et al.*[1,2]

As both CO_2 and C_2H_2 exhibit similar molecular volumes (33.9 Å^3 and 33.4 Å^3, respectively) to MeOH, Jacobs *et al.*[1] investigated the sorption ability of the metallocycle **MC1** for CO_2 and C_2H_2. The metallocycle **MC1**·2MeOH was desolvated at room temperature to achieve the activated form (**MC1a**). The crystal structure remained unchanged and shape of the cavity was maintained after activation (Figure 3.1 b).

Variable-pressure single-crystal X-ray diffraction experiments were carried out in environmental gas cells with controlled gas pressure.[1] The sorption of CO_2 reached full occupancy of two molecules per cavity at a pressure of 10 bar and at –40 °C (63.6% occupancy at the same pressure, but 22 °C).[1] The sorption of C_2H_2 reached 91.1% occupancy at 16 bar and 22 °C, also equating to two molecules per cavity.[1] Figures 3.1 (c) and (d) show the crystal structure of **MC1** with CO_2 and C_2H_2 positioned, respectively (**MC1**·2(CO_2) and **MC1**·2(C_2H_2)).[1]

A liquid sorption experiment for **MC1a** and CS_2 (**MC1**·CS_2) was also performed.[2] As shown in the packing diagram Figure 3.1 (e), one CS_2 molecule lies along the length of the cavity that forms between two adjacent metallocycles.[2]

3.2 Results

Based on the previously reported results, we speculated that **MC1** might be permeable to xylenes in the same manner as for CS_2. The ligand of the metallocycle has a long spacer and is flexible. We thus hypothesized that **MC1** might re-arrange its crystal packing to accommodate the xylene molecules. This might, in turn, allow specific selectivity for the xylene isomers. Therefore, liquid sorption ability experiments for **MC1a** were carried out with xylenes.

3.2.1 Synthesis of MC1

Metallocycle **MC1**·2MeOH was synthesized following the published approach.[1] A single crystal of suitable quality was selected and analyzed by single-crystal X-ray diffraction (SCD). As shown in Table 3.1, selected unit-cell parameters of **MC1**·2MeOH are compared to the literature,[1] indicating that the same metallocycle is formed. Powder X-ray diffraction (PXRD) analysis was carried out to confirm the phase purity of bulk samples. Figure 3.2 shows a comparison of the experimental powder patterns and powder patterns simulated from single-crystal structures of **MC1**·2(MeOH) and **MC1a**.

Table 3.1 Selected crystal data for **MC1**·2(MeOH).

Compounds	**MC1**·2(MeOH)	
	Experimental (this work)	Literature[1]
Formula unit*	$[Cd_2Cl_4(\mathbf{L1})_2]\cdot 2(CH_3OH)$	$[Cd_2Cl_4(\mathbf{L1})_2]\cdot 2(CH_3OH)$
Formula weight (g/mol)	1115.6	1115.6
Crystal system	Monoclinic	Monoclinic
Space group	*C2/m*	*C2/m*
Z	2	2
a (Å)	17.1935(14)	17.2080(16)
b (Å)	15.6065(12)	15.5925(15)
c (Å)	9.6863(8)	9.6635(9)
α (˚)	90	90
β (˚)	114.301(1)	114.257(2)
γ (˚)	90	90
Cell volume (Å^3)	2368.84	2363.95

*Per formula unit = per metallocycle.

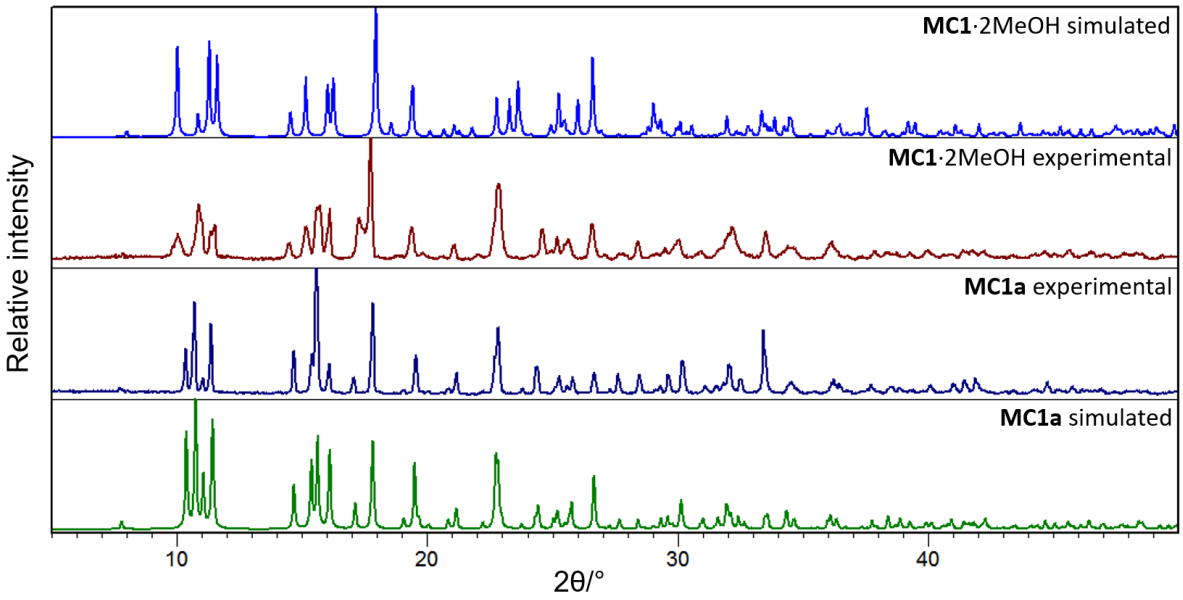

Figure 3.2 Comparison of the experimental and simulated powder patterns of **MC1**·2(MeOH) and **MC1a** in this study.

As shown in Figure 3.2, the experimental powder pattern of as-synthesized **MC1**·2(MeOH) did not provide a good comparison to the simulated powder pattern. Therefore, the phase purity is questionable. However, the experimental and simulated powder patterns of apohost do match well and phase purity is therefore confirmed. The thermogram of the as-synthesized **MC1**·2(MeOH) (Figure 3.3) indicates that the MeOH starts to escape from the **MC1** host at a relatively low temperature (16 °C). Some of the guest might therefore have escaped during preparation of the **MC1**·2(MeOH) sample for PXRD analysis and this might be the reason that the experimental and simulated powder patterns do not match. As shown in Figure 3.2, the experimental powder pattern of **MC1**·2(MeOH) is more similar to the powder pattern of **MC1a** rather than that simulated from the **MC1**·2(MeOH) single-crystal structure. The fully desovated **MC1a** was obtained by placing **MC1**·2(MeOH) under vacuum for 3 hours. Once **MC1**·2(MeOH) is fully activated, the experimental powder pattern matches the simulated powder pattern well and confirms the phase purity.

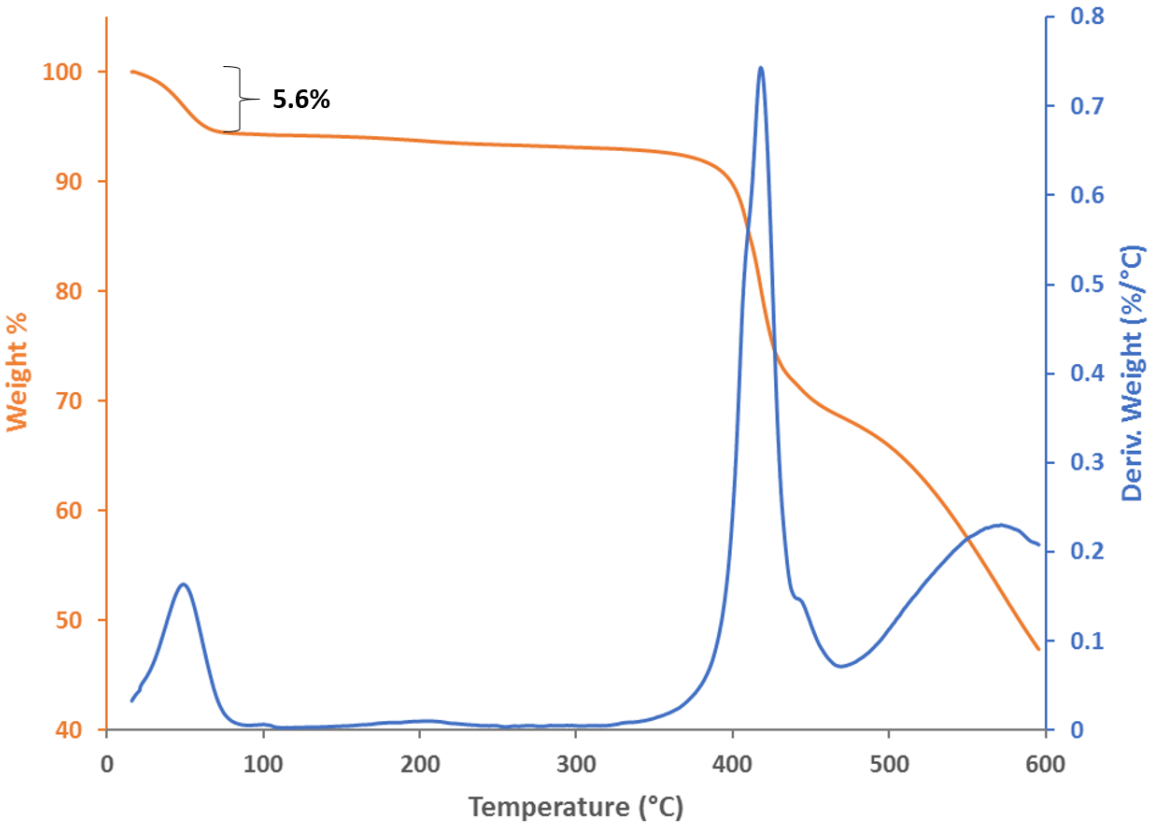

Figure 3.3 TGA thermogram of **MC1**·2(MeOH). The weight loss starts at approximately 16 °C and is completed at approximately 82 °C. The weight loss corresponds to two MeOH molecules per metallocycle (calculated weight loss 5.7%).

3.2.2 Solvent Exchange

Once the purity of the crystal bulk sample was confirmed, solvent exchange experiments were performed for **MC1**. Crystals of the as-synthesized **MC1**·2(MeOH) were immersed in equimolar mixtures of *para*-, *meta*- and *ortho*-xylene (*px*, *mx*, *ox*) and the solvent refreshed at least three times. This process was carried out over 2–3 days. The resulting crystals were analyzed by SCD. Figure 3.4 presents the structure of the metallocycle after solvent exchange. There is some electron density in the metallocycle but no appropriate model of the guest could be formulated. The Platon[3]/SQUEEZE[4,5] routine was used to sum the unmodelled electrons in the crystal structure. Table 3.2 shows the results of the SQUEEZE analysis. Each xylene isomer has 58 electrons per molecule and each MeOH molecule has 18 electrons. In the as-synthesized crystal structure, there are two MeOH molecules per metallocycle. As

shown in Table 3.2, after solvent exchange the electron count seems to be equivalent to one MeOH molecule per metallocycle. Figure 3.5 shows the thermogram of **MC1**·2(MeOH) after solvent exchange with *px*. There is a weight loss up to approximately 250 °C, indicating that there is likely some guest present in the metallocycle. It is difficult to determine the identity of the guest from the electron counts and the thermogram, even though the electron count is very close to that of one MeOH molecule, but it is also possible that the guest is xylene at less than full occupancy. Figure 3.6 shows a comparison of difference electron density maps generated in Olex2,[6] where (a) is the difference electron density map for **MC1**·2(MeOH) and (b) is that after solvent exchange with *px*. Both electron density maps are generated at a level of 2 $e^{-}/Å^{3}$ and are notably different. The guest present in the metallocycle is perhaps a mixture of MeOH and xylenes (inferred from the thermogravimetry and the electron density maps). However, the sorption efficiency is clearly very low; our aim was to find a material that can sorb xylenes more efficiently and therefore separate the xylene isomers.

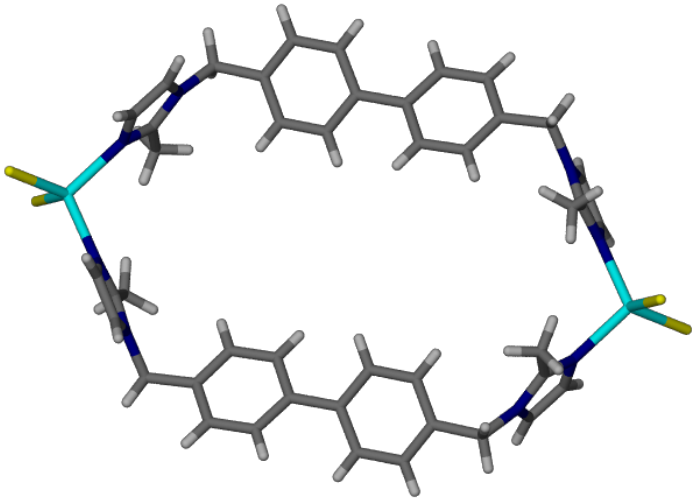

Figure 3.4 Structure of **MC1** after solvent exchange, the guest in the cavity could not be modelled.

Table 3.2 Results from SQUEEZE analysis.

Material	Electrons per unit cell	Electrons per formula unit (Z = 2)	Guest per formula unit (Z = 2)
MC1·2(MeOH)	66	33	~ 2
MC1_se*_1	30	15	-
MC1_se*_2	26	13	-

*se: solvent exchanges; 1: solvent exchange from MeOH to equimolar xylene mixtures; 2: solvent exchanges from MeOH to pure *px*.

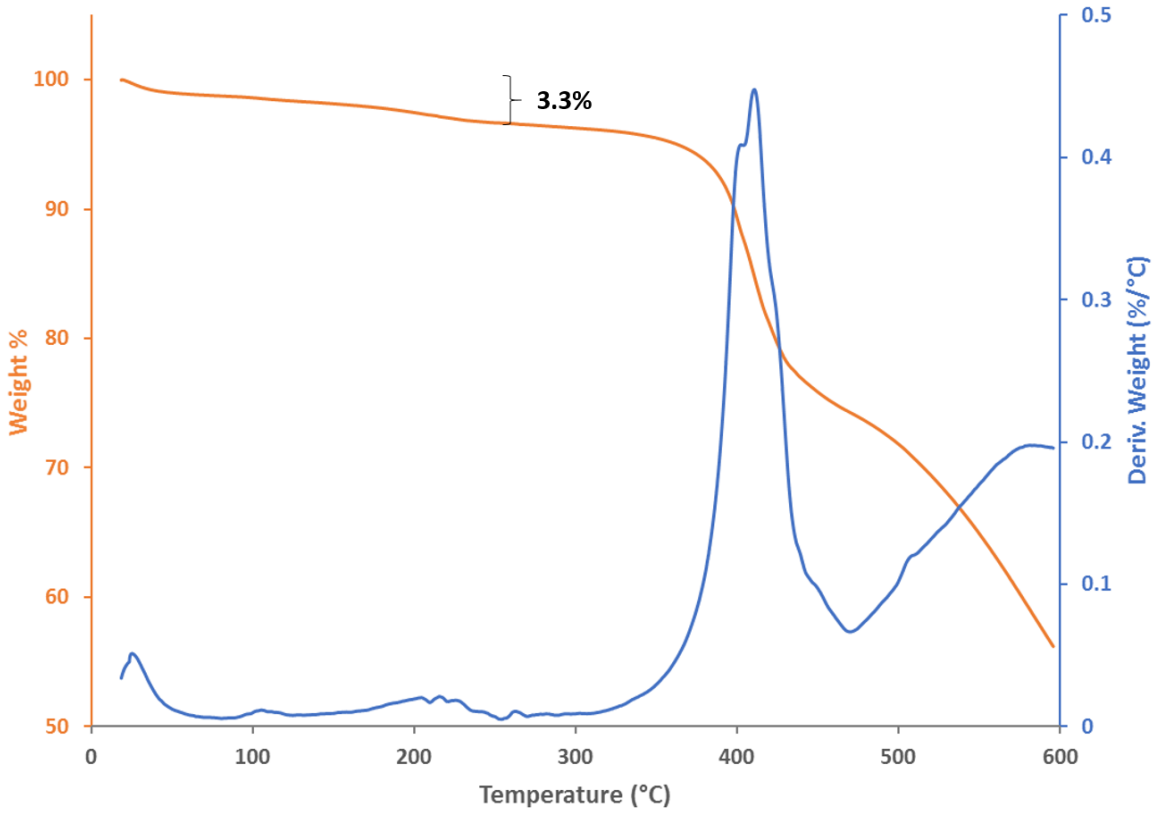

Figure 3.5 Thermogram of **MC1**·2(MeOH) after solvent exchange with *px*. Approximately 3.3% weight loss by around 250 °C. The theoretical weight loss of one MeOH per metallocycle is 3.0% and of one xylene molecule per metallocycle is 9.2%.

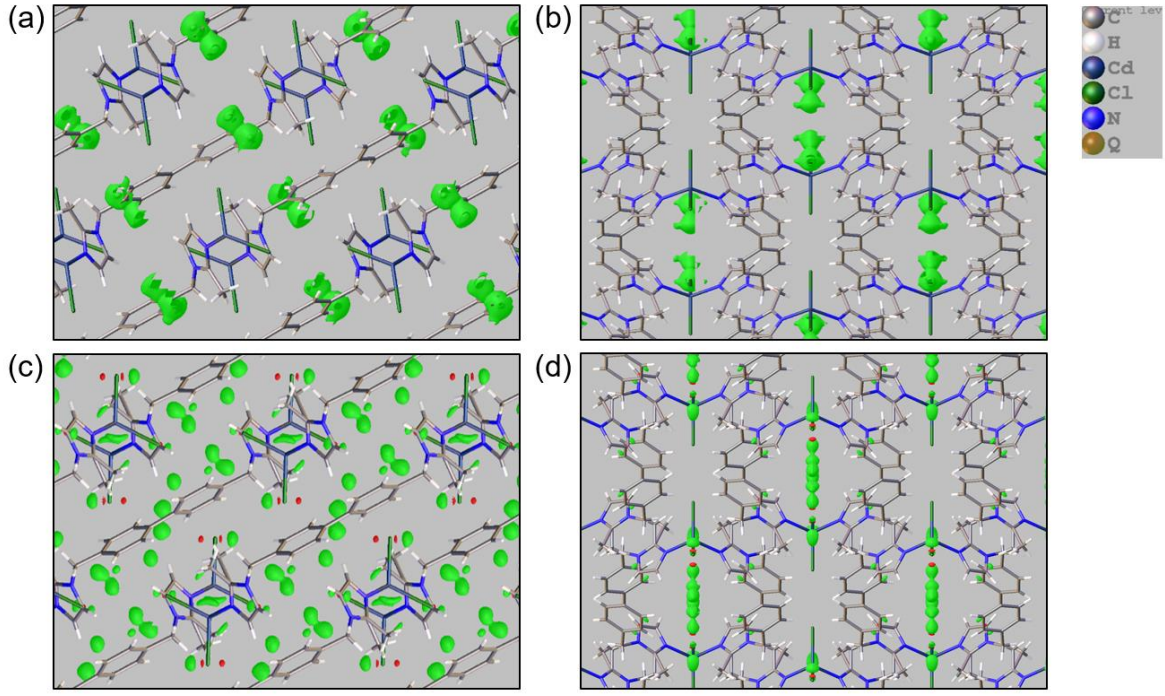

Figure 3.6 Difference electron density maps of **MC1**·2(MeOH) ((a) and (b)) and **MC1**·2(MeOH) ((c) and (d)) after solvent exchange with *px*. (a) and (c) viewed along [010] and (b) and (d) viewed down [001]; maps were generated at the 2 $e^{-}/Å^3$ level.

3.2.3 Liquid Xylene Sorption of MC1

It appears that MeOH guest molecules in **MC1**·2(MeOH) cannot be easily exchanged for xylenes by means of solvent exchange. However, liquid sorption by the apohost material may be governed by a different mechanism. Therefore, liquid xylene sorption by **MC1a** was carried out by immersing **MC1a** in liquid xylene (Sigma-Aldrich, ≥75.0%) for more than 24 hours. Figure 3.7 presents the thermograms of **MC1a** exposed to *px* and a xylene mixture (24 hours) at different temperatures. After **MC1a** was immersed in xylenes at 25 °C for 24 hours, TGA was carried out to determine if xylene was sorbed. Similar to the apohost, the thermogram showed almost no weight loss up to approximately 350 °C. This indicated that no xylene was absorbed.

The pocket of the **MC1a** is approximately rectangular in shape, as shown in Figure 3.1(b). Figure 3.1(e) shows how one CS_2 molecule lies along the length of the pocket.[2] Therefore, if **MC1** shows selectivity to xylenes, *px* would have the greatest potential to be absorbed, because it might lie along the length of the pocket, as does CS_2. Since sorption might be aided by heat, with thermal expansion providing a larger

cavity to fit the *px*,[7] **MC1a** was immersed in *px* at 80 and 100 °C for more than 24 hours (TGA results are also shown in Figure 3.7). Once again the thermograms were similar to that of the apohost. Thus **MC1** does not appear to absorb xylenes under the conditions investigated and it is not suitable for xylene separation. Therefore, **MC1** was not investigated any further for its xylene sorption capabilities.

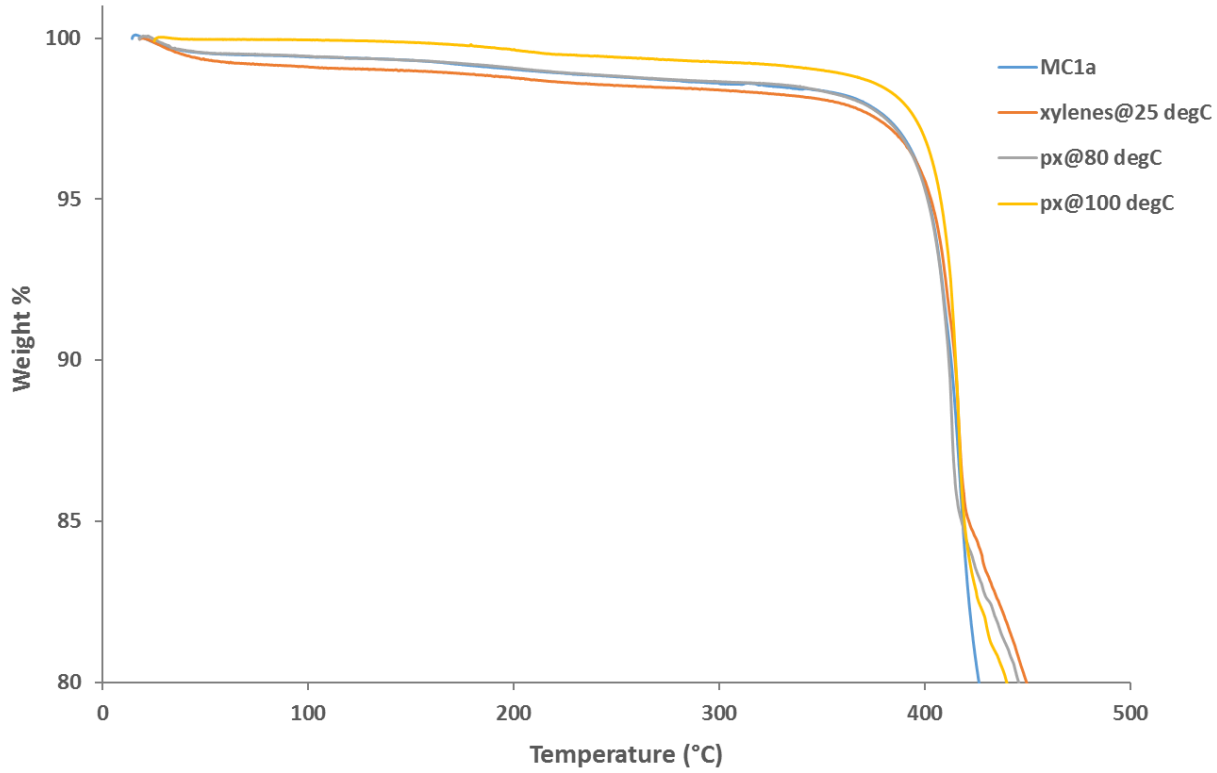

Figure 3.7 Thermograms for **MC1a** exposed to a xylene mixture (≥75.0%) at room temperature and *px* at different temperatures for 24 hours. Within 100 °C, weight loss is less than 1%. All thermograms show little guest lost, with decomposition at approximately 350 °C, similar to the apohost.

3.2.4 Polarity and Kinetic Diameter

Immersion of **MC1a** in a liquid xylene mixture at 25 °C or higher for more than 24 hours showed no notable uptake of xylenes into **MC1**, as confirmed by TGA. **MC1** is permeable to MeOH, CO_2, C_2H_2 as well as CS_2. Only MeOH is polar, while CO_2, C_2H_2 and CS_2 are non-polar. Therefore, polarity is not considered to be the determining factor that prevents xylenes from entering the metallocycle.

As shown in Table 3.3, the kinetic diameter of *px* is 5.8 Å, while *mx* and *ox* have kinetic diameters of 6.4 and 6.5 Å, respectively. The kinetic diameters of xylenes are much larger than those of the guests previously introduced into **MC1**. Xylenes are likely prevented from passing between pockets due to steric hindrance by the chloride ions in the host (shown as yellow spheres in Figure 3.1).

Table 3.3 Kinetic diameters for guests to which **MC1** is permeable, and the xylenes.

	Kinetic diameters (Å)	References
MeOH	3.6	8
CO_2	3.3	9
C_2H_2	3.3	9
CS_2	3.6	9
px	5.8	10
mx	6.4	10
ox	6.5	10

3.3 Conclusion

In previous studies of **MC1** by the Barbour group, **MC1** was shown to be permeable to guests such as MeOH, CO_2, C_2H_2 as well as CS_2. We hypothesized that it might also be permeable to xylenes due to its long spacer and the flexible nature of the ligand, which might lead to a larger cavity or channel. Before sorption experiments could be carried out, phase purity of the bulk sample needed to be confirmed. The experimental powder pattern of as-synthesized bulk sample did not provide a good match to the simulated pattern. Consequently, phase purity of the as-synthesized material could not be confirmed. However, powder patterns after activation confirmed the phase purity of the bulk activated sample. Sometimes, if one experiment seems unsuccessful, further experiments might rationalize the “failure” and prove that it was indeed successful.

After the phase purity of the activated material was confirmed, several experiments were performed to test if xylenes can be taken up by **MC1a**. Similar TGA thermograms were obtained to that of **MC1a**, as shown in Figure 3.7, indicating that xylenes are not absorbed and that the apohost remains guest-free. The polarity and

kinetic diameter of the guests to which **MC1** is known to be permeable were compared to those of the xylenes. Polarity is not the factor inhibiting the sorption of xylenes into the metallocycle. Rather, steric effects appear to be the reason as xylenes have much larger kinetic diameters that the guests to which **MC1** is permeable. Xylenes might be blocked from entering the host due to steric hindrance by the chloride ions. Since our aim was to find a material that can sorb and separate xylenes efficiently, **MC1** is clearly not a good choice in this regard.

3.4 References

1 T. Jacobs, G. O. Lloyd, J. A. Gertenbach, K. K. Müller-Nedebock, C. Esterhuysen and L. J. Barbour, *Angew. Chem., Int. Ed.*, 2012, **51**, 4913–4916.

2 T. Jacobs and L. J. Barbour, *CrystEngComm*, 2013, **15**, 1512–1514.

3 A. L. Spek, *Acta Crystallogr. Sect. D Biol. Crystallogr.*, 2009, **65**, 148–155.

4 P. van der Sluis and A. L. Spek, *Acta Crystallogr. Sect. A*, 1990, **46**, 194–201.

5 A. L. Spek, *Acta Crystallogr. Sect. C Struct. Chem.*, 2015, **71**, 9–18.

6 O. V. Dolomanov, L. J. Bourhis, R. J. Gildea, J. A. K. Howard and H. Puschmann, *J. Appl. Crystallogr.*, 2009, **42**, 339–341.

7 D. Das, T. Jacobs and L. J. Barbour, *Nat. Mater.*, 2010, **9**, 36–39.

8 H. Hu, J. Zhu, F. Yang, Z. Chen, M. Deng, L. Weng, Y. Ling and Y. Zhou, *Chem. Commun.*, 2019, **55**, 6495–6498.

9 E. Albrecht, G. Baum, T. Bellunato, A. Bressan, S. Dalla Torre, C. D'Ambrosio, M. Davenport, M. Dragicevic, S. Duarte Pinto, P. Fauland, S. Ilie, G. Lenzen, P. Pagano, D. Piedigrossi, F. Tessarotto and O. Ullaland, *Nucl. Instruments Methods Phys. Res. Sect. A Accel. Spectrometers, Detect. Assoc. Equip.*, 2003, **510**, 262–272.

10 F. Vermoortele, M. Maes, P. Z. Moghadam, M. J. Lennox, F. Ragon, M. Boulhout, S. Biswas, K. G. M. Laurier, I. Beurroies, R. Denoyel, M. Roeffaers, N. Stock, T. Düren, C. Serre and D. E. De Vos, *J. Am. Chem. Soc.*, 2011, **133**, 18526–18529.

Chapter 4
Solid-liquid Separation of Xylene Isomers using a Cu-based Metallocycle

4.1. Introduction

Xylenes are an indispensable chemical feedstock used in the petrochemical and pharmaceutical industries to obtain value-added products.[1,2] For example, *para*-xylene (*px*) can be oxidized to terephthalic acid for subsequent use in the production of polyesters, polyamides, plastics, films, as well as blown beverage bottles.[3] *Meta*-xylene (*mx*) can be oxidized to isophthalic acid, which is a precursor to polyesters, while *ortho*-xylene (*ox*) can be converted to phthalic anhydride, which is a precursor for plasticizers.[2,4] The pure isomers of xylene are generally required for the preparation of consumer products or as chemical solvents and the annual global demand for these compounds is still rising.[1,5] Approximately 42.5 million tons of xylenes were consumed in 2010.[6] Petroleum is the only natural source of xylenes,[2] which are produced during the refinement of crude oil or by methylation of benzene or toluene. Xylene is always obtained as a mixture of the three isomers (*px*, *mx* and *ox*),[1,2] which then need to be separated as pure isomers. Since the isomers are identical in molecular weight and possess similar physical properties such as their densities, boiling points, polarities, etc., their separation is difficult, energy-intensive and costly.[2,5,7] Although the xylenes can still be separated using conventional methods such as distillation, employment of this process on an industrial scale accounts for 10–15% of the worldwide energy consumption.[8] To date, industrial-scale separation of xylenes by means of a simple, efficient and low-cost method remains an unresolved challenge.[1,5] According to recent reviews,[1,9] adsorption by porous materials such as zeolites,[9] metal-organic frameworks (MOFs)[7,9–15] and others[16,17] has been explored and proven to be effective as an alternative strategy for purification of the xylene isomers. Porous materials are

selective and highly efficient, with the potential to save approximately 70−90% of the energy costs associated with separation processes, as compared to thermal distillation.[1,9,18]

The Barbour Group recently reported remarkable selectivity of an intrinsically porous metallocycle for *px*, with the ability to separate all three xylene isomers in a multi-step process.[19] As an extension of that work, this study explores the inclusion and separation of the xylenes by crystals of the similar metallocyclic compound $[Cu_2Cl_4(\mathbf{L2})_2]$ (**MC2**), where **L2** is the ligand 1,4-bis((2-methyl-1H-imidazol-1-yl)methyl)benzene. The structure and properties of **MC2** have already been reported, showing that it undergoes a series of remarkable single-crystal to single-crystal (SC-SC)[20] conformational switches upon guest removal and exchange.[21–24] To date we have identified four interconvertible structure types[25] (**1**–**4**), where each of types **1** and **2** comprises an isoskeletal[26,27] series of inclusion compounds based on the identity of the guest, and types **3** and **4** are two different guest-free forms (Scheme 4.1).

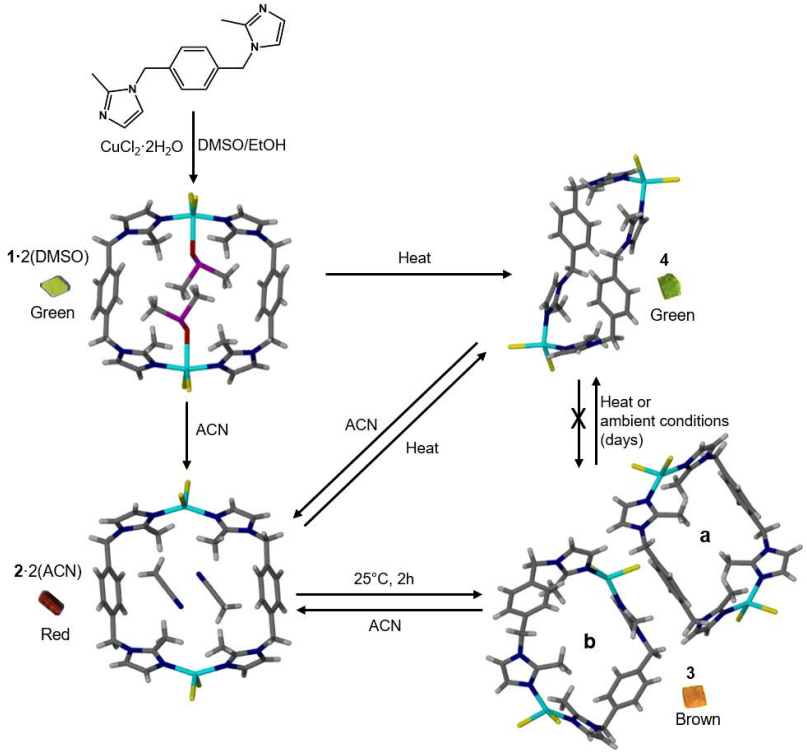

Scheme 4.1 Left: preparation of $[Cu_2Cl_4(\mathbf{L2})_2]$ (**MC2**) by the formation of **1**·2(DMSO), followed by guest exchange with acetonitrile to form **2**·2(ACN). Bottom: removal of ACN under mild conditions to yield the activated form **3**. Top right: the collapsed form **4** is obtained by heating any of the other forms **1**–**3**. Conversion from **3** to **4** is irreversible.

The interconversions between these structure types involve rotation of some of the coordinating imidazolyl groups of **L2**, which alters the shape and volume of intrinsic guest-accessible space. It is useful to describe the conformations of the bridging ligands by referring to their methyl groups as being oriented either up ("U") or down ("D") relative to the plane of the metallocycle, as projected in Figure 4.1. Starting with the upper-left methyl group and proceeding in a clockwise direction, the conformation of **MC2** in host type **1** can thus be described as UUDD. Upon displacement of the dimethyl sulfoxide (DMSO) molecules by acetonitrile (ACN), the host structure changes to type **2**, with **MC2** assuming the UDDU conformation.

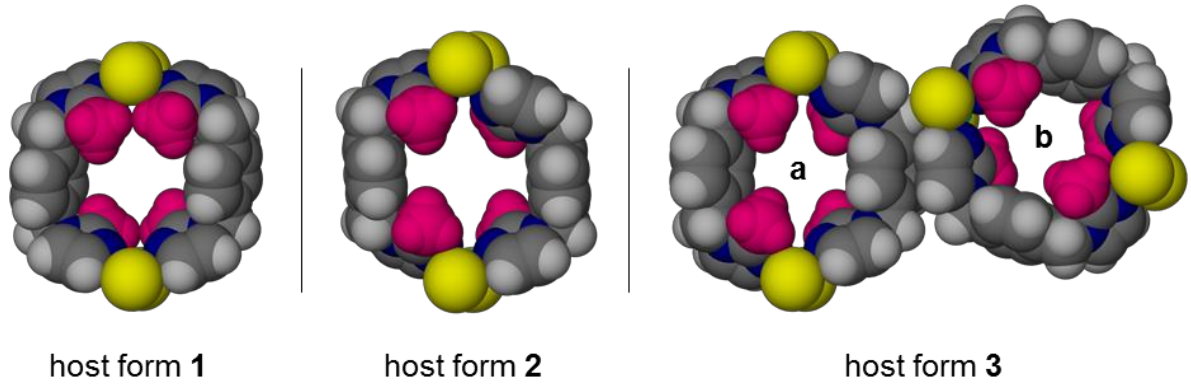

Figure 4.1 Space-filling representations of the metallocycles in the different open conformations encountered in host structure types **1** – **3**. In types **1** and **2**, the guest molecules are omitted for clarity. The methyl groups on the imidazolyl moieties are colored pink to highlight salient conformational differences.

Interestingly, **MC2** can assume one of two different structural types upon activation[21] (Scheme 4.1). Activation at low temperature (25 °C) leads to the 0D porous form **3**, with two crystallographically distinct metallocycles in the asymmetric unit (**3a** and **3b**), assuming conformations UDDU and DUDU, respectively. The non-porous collapsed form **4** is obtained upon activation at higher temperatures (> 80 °C). However, form **4** cannot absorb xylenes efficiently under ambient conditions, and we therefore focused our attention on the use of form **3** for the xylene separation studies.

Crystals of **MC2** also exhibit solvatochromism[23] and the ability to absorb volatile solids[24] by means of SC-SC guest exchange. During previous studies the Barbour Group had established that the most reliable method of forming bulk-pure **MC2** is to grow crystals by layering a solution of $CuCl_2$ in ethanol over of a solution of **L2** in DMSO. This method produces the **1**·2(DMSO) solvate in high yield, with two DMSO

molecules occupying the intrinsic aperture of the metallocycle. Each of the Cu ions of **MC2** is coordinated to one of the DMSO guest molecules.[22–24] Removal of the DMSO guest without collapse of the metallocycle offers a tantalizing route to creating a porous[28] material. Unfortunately, DMSO removal requires heat, which causes the metallocycles to assume the 'imploded' conformation,[21,22] i.e., loss of the guest-templated aperture results in the nonporous crystal form **4**. However, the DMSO molecules can be readily replaced by immersing the crystals in acetonitrile (ACN); this results in a change from structure type **1** to type **2**, yielding the solvate **2**·2(ACN). The ACN molecules can then be removed under mild conditions to produce the porous guest-free form **3**. To date the porosity of **3** has not yet been explored because it has been difficult to obtain as a pure phase. Since form **3** can be converted into form **4** at high temperature, vacuum or over time, and form **4** cannot revert back to form **3**,[21] the guest-free material was often obtained as a mixture of forms **3** and **4** (Figure 4.2). The problem of phase purity has been addressed as part of this study (i.e., avoiding heat and using freshly activated samples), the objective of which was also to investigate the potential of the remarkably flexible compound **MC2** to discriminate between the three isomers of xylene.

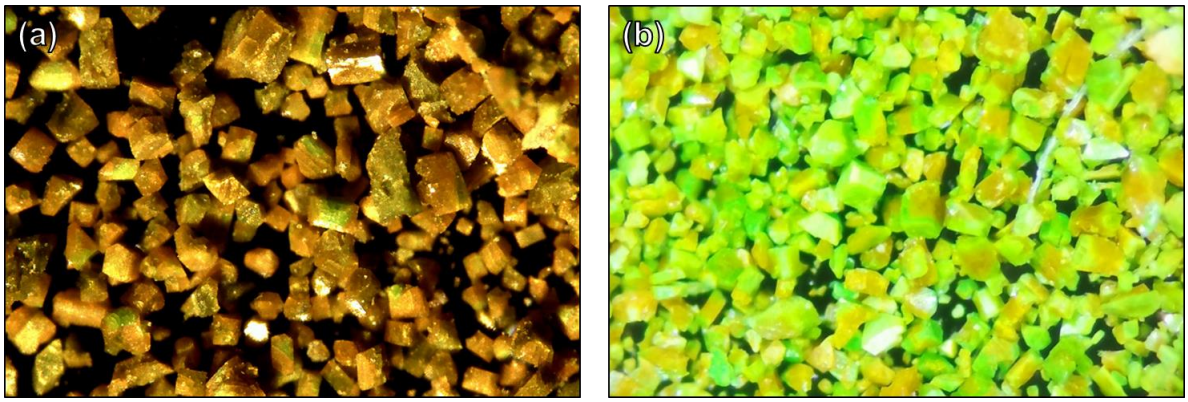

Figure 4.2 Photomicrographs of the activated crystals as a mixture of forms **3** and **4** (a) after form **3** was stored under ambient conditions for several days and (b) resulting from direct heating of **2**·2(ACN) under reduced pressure at 80 °C overnight.

4.2. Preparation and Activation of the Metallocycle MC2

The ligand 1,4-bis((2-methyl-1H-imidazol-1-yl)methyl)benzene (**L2**) was synthesized from *α,α'*-dichloro-*p*-xylene and 2-methylimidazole via an S_N2 route as detailed in Chapter 2.[21,23,24,29] A solution of $CuCl_2 \cdot 2H_2O$ (0.05 mmol) in ethanol (EtOH, 2 ml) was layered over a solution of the ligand (0.05 mmol) in dimethyl sulfoxide (DMSO, 2 ml). Green block-shaped crystals of **1**·2(DMSO) were obtained in 3-7 days. Table 4.1 shows a comparison of the single-crystal X-ray data of the as-synthesized metallocycle to that previously reported, confirming that the correct form of the metallocycle was obtained. Phase purity was confirmed by PXRD (Figure 4.3). Thermogravimetric analysis (TGA) of the as-synthesized material is shown in Figure 4.4.

Table 4.1 Comparison of single-crystal data.

Compounds	**1**·2(DMSO) (experimental)	**1**·2(DMSO) (literature)[23]
Formula unit	$C_{36}H_{48}Cl_4Cu_2N_8O_2S_2$	$C_{36}H_{48}Cl_4Cu_2N_8O_2S_2$
Formula weight (g mol^{-1})	957.86	957.86
Crystal system	Monoclinic	Monoclinic
Space group	$P2_1/c$	$P2_1/c$
Z	2	2
a (Å)	8.8814(23)	8.8724 (19)
b (Å)	13.0664(34)	13.043(3)
c (Å)	17.8120(46)	17.770(4)
α (˚)	90	90
β (˚)	95.494(4)	95.506(3)
γ (˚)	90	90
Cell volume ($Å^3$)	2057.55	2046.90

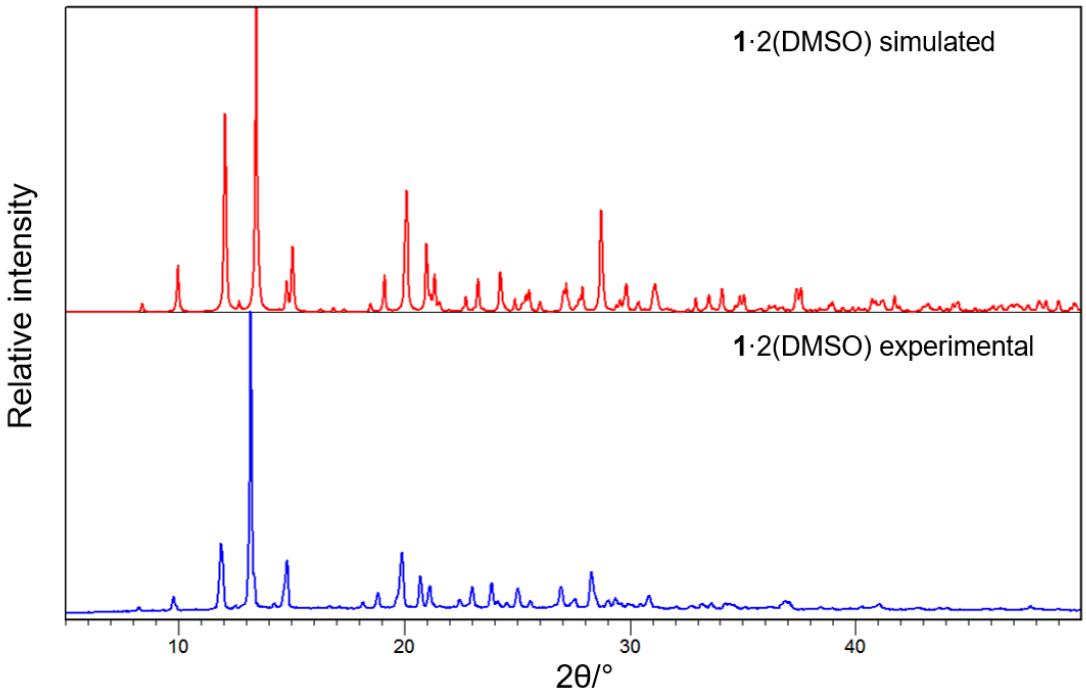

Figure 4.3 Powder pattern simulated from the single-crystal structure of **1**·2(DMSO) (top) and the experimental powder pattern for comparison (bottom).

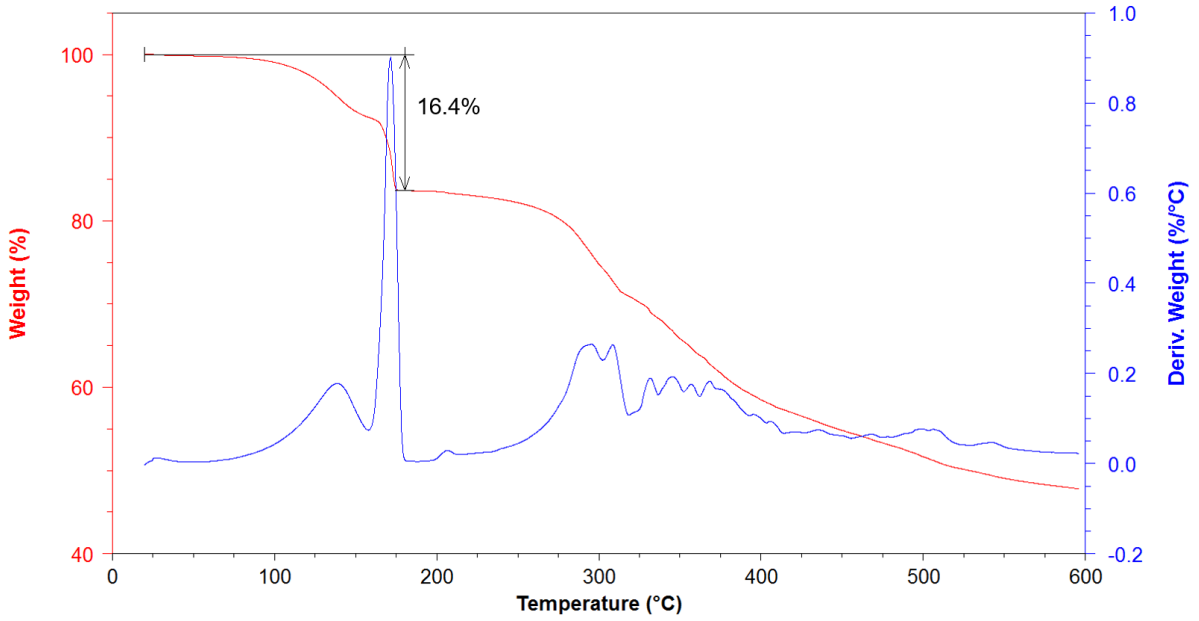

Figure 4.4 TGA thermogram of the as-synthesized material **1**·2(DMSO). The weight loss of 16.4% is equivalent to two DMSO molecules per metallocycle. Theoretical weight loss is 16.4%.

4.2.1. Solvent Exchange

Since DMSO has a high boiling point, and because it is coordinated to the metal in the as-synthesized metallocycle **1**·2(DMSO), it is difficult to remove from the host. Therefore, guest exchange was carried out. The mother liquor was removed from the crystallization vial using a glass pipette. Acetonitrile (ACN) was added to rinse the as-synthesized crystals, followed by replacement with fresh ACN at least three times. A color change from green (**1**·2(DMSO)) to red (**2**·2(ACN)) indicated that the guest-exchange process was completed.[23] The process took about 2–3 days. Figure 4.5 shows the TGA thermogram of phase **2**·2(ACN).

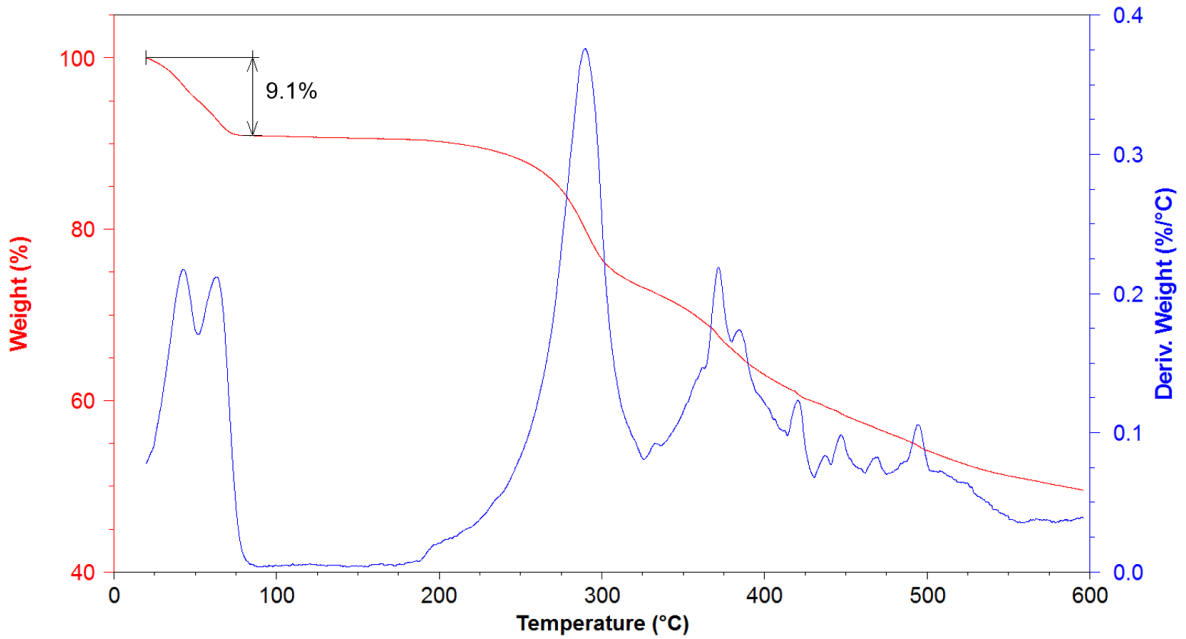

Figure 4.5 Thermogram of **2**·2(ACN). The weight loss of 9.1% is equivalent to two molecules of acetonitrile per metallocycle. Theoretical weight loss is 9.3%.

4.2.2. Activation

Crystals **2**·2(ACN) were activated prior to the vapor and liquid sorption experiments. As shown in Scheme 4.1, depending on the activation method, one of two different apohost phases can be obtained upon activation of structure type **2**. Form **3** is obtained upon activation at 25 °C and form **4** by heating any of types/forms **1**-**3** at temperatures > 80 °C. The open form **3** and closed form **4** can be distinguished visually

by color (form **3** is brown and form **4** is green). The phase purities were confirmed by PXRD (Figure 4.6). TGA confirms that the crystals were successfully activated (Figures 4.7 and 4.8). Figure 4.9 show photomicrographs of the activated crystals in phase purity.

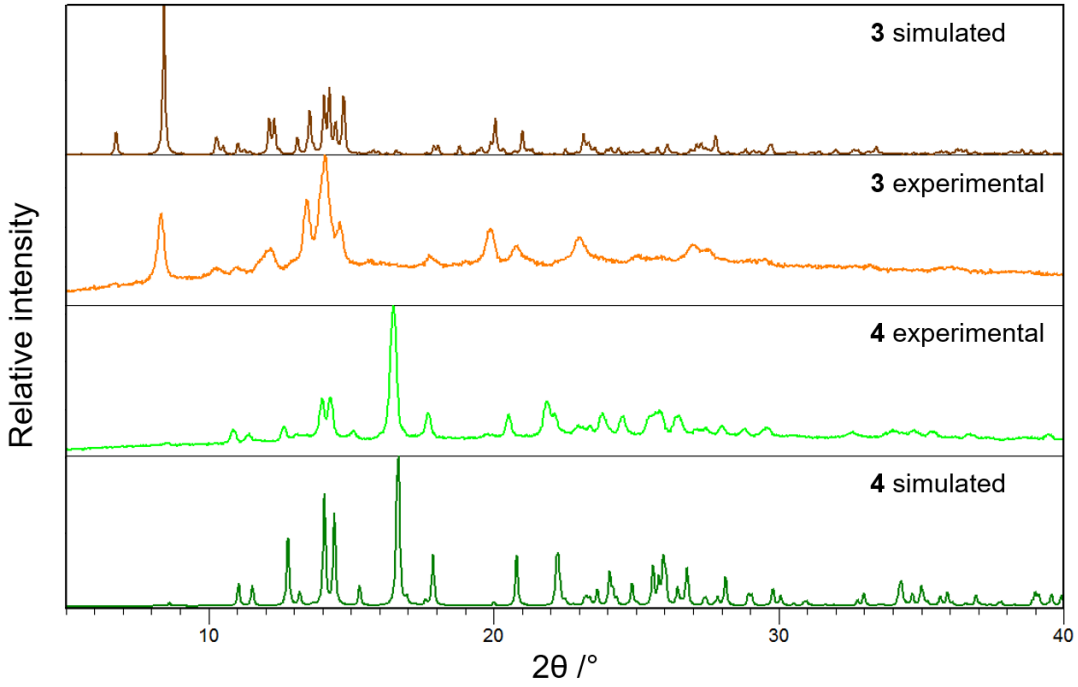

Figure 4.6 Simulated and experimental powder diffractograms of forms **3** and **4**.

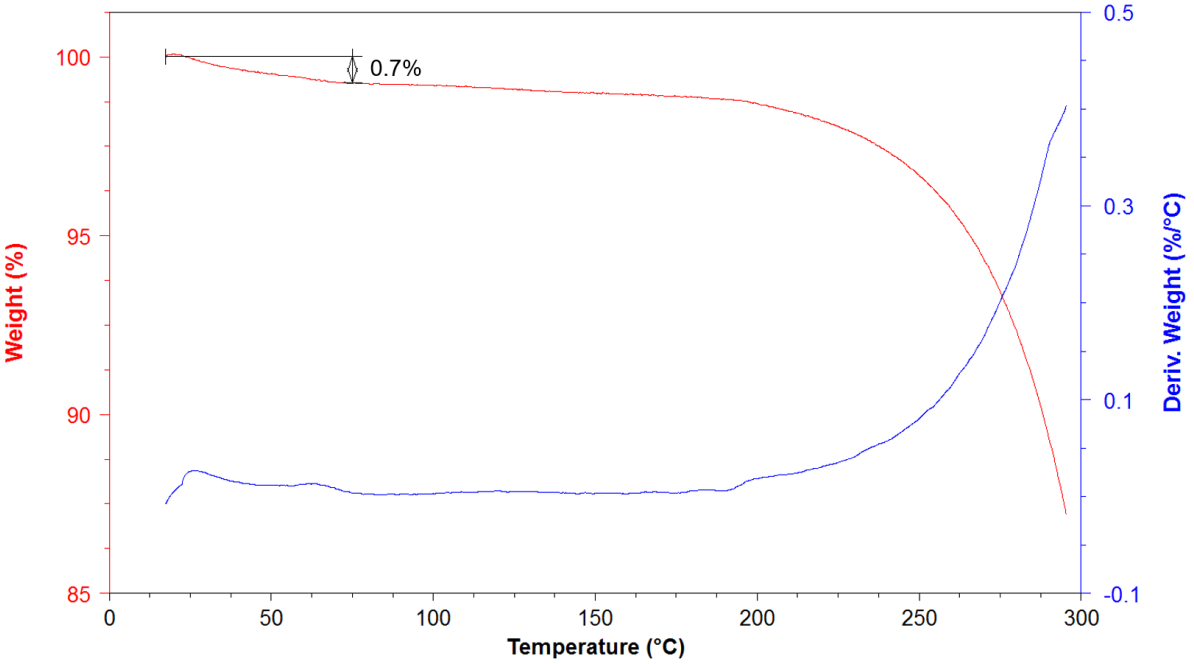

Figure 4.7 TGA thermogram of guest-free form **3**.

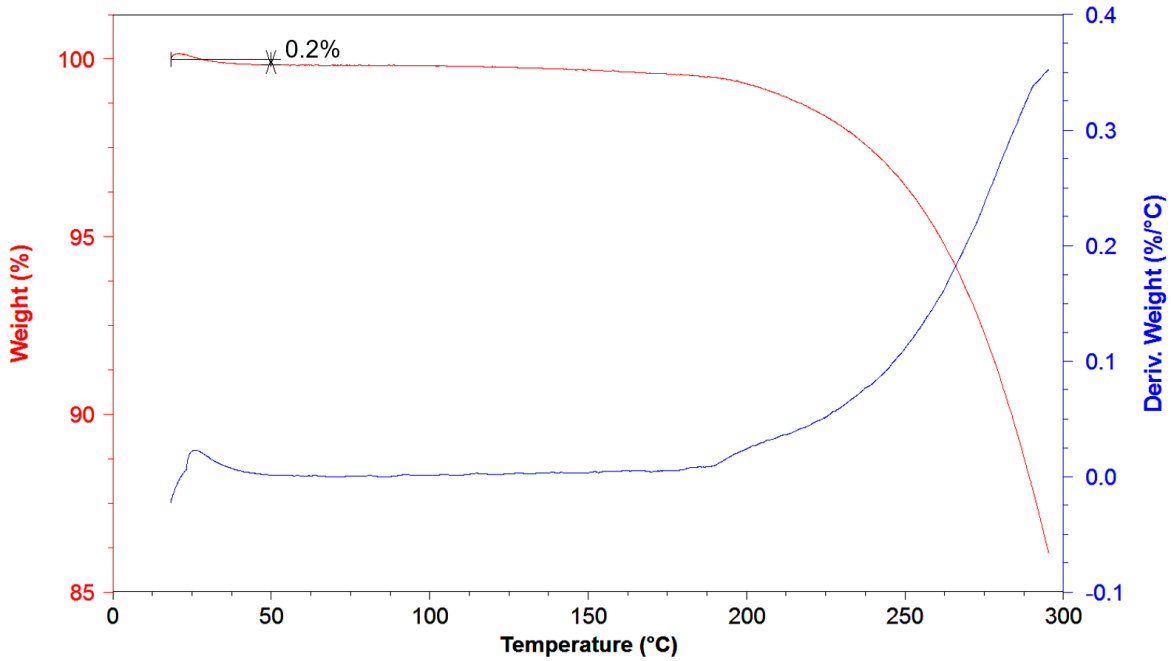

Figure 4.8 TGA thermogram of the collapsed form **4**.

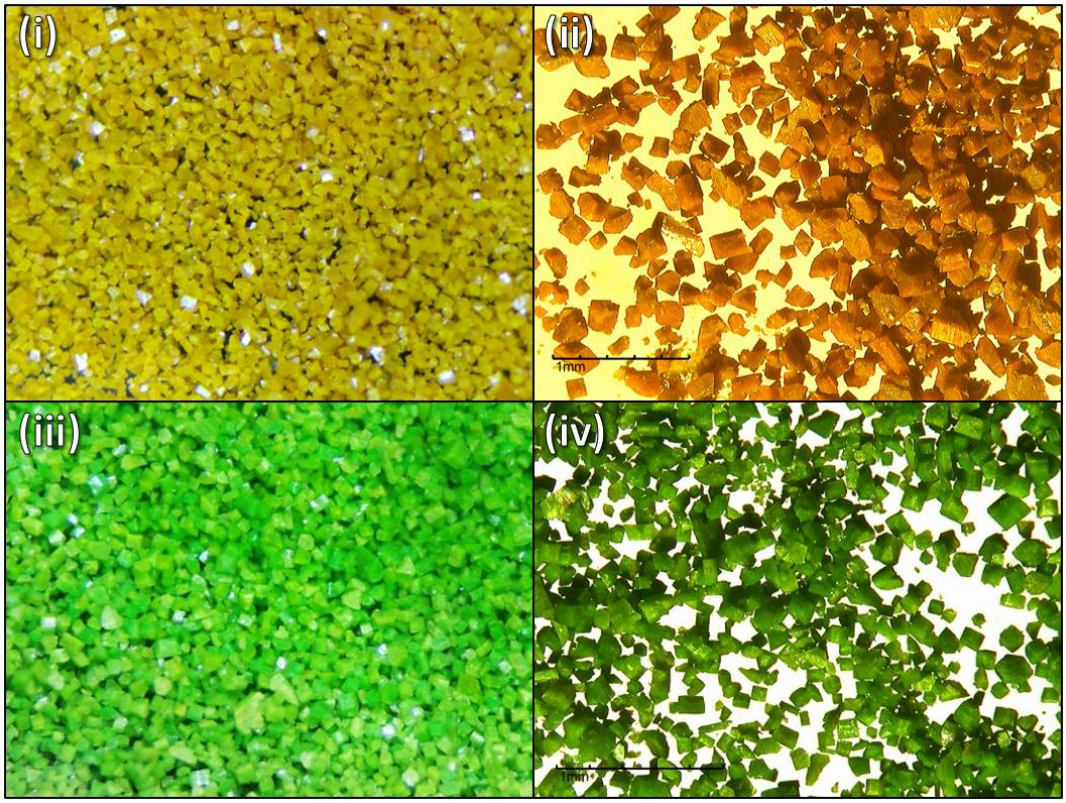

Figure 4.9 Photomicrographs of crystals of forms **3** (top) and **4** (bottom). Images (i) and (iii) were recorded using transillumination with polarized light. Images (ii) and (iv) were recorded without the use of polarized light.

4.3. Liquid Sorption using Form 4

Once pure form **4** was obtained, several liquid sorption experiments were carried out. Crystals of **4** were immersed in equimolar ternary xylene mixtures (*px*/*mx*/*ox* = 1:1:1) at different temperatures for approximately 24 hours, after which TGA thermograms were recorded (Figure 4.10). As the temperature during liquid exposure is increased, more xylene is absorbed by the host. However, even for liquid exposure at 80 °C, the TGA weight loss up to 200 °C was only 3.2%. For a host:guest ratio of 1:1, the theoretical weight loss is 11.7%. Therefore, we deduce that liquid xylene sorption with **4** is not efficient.

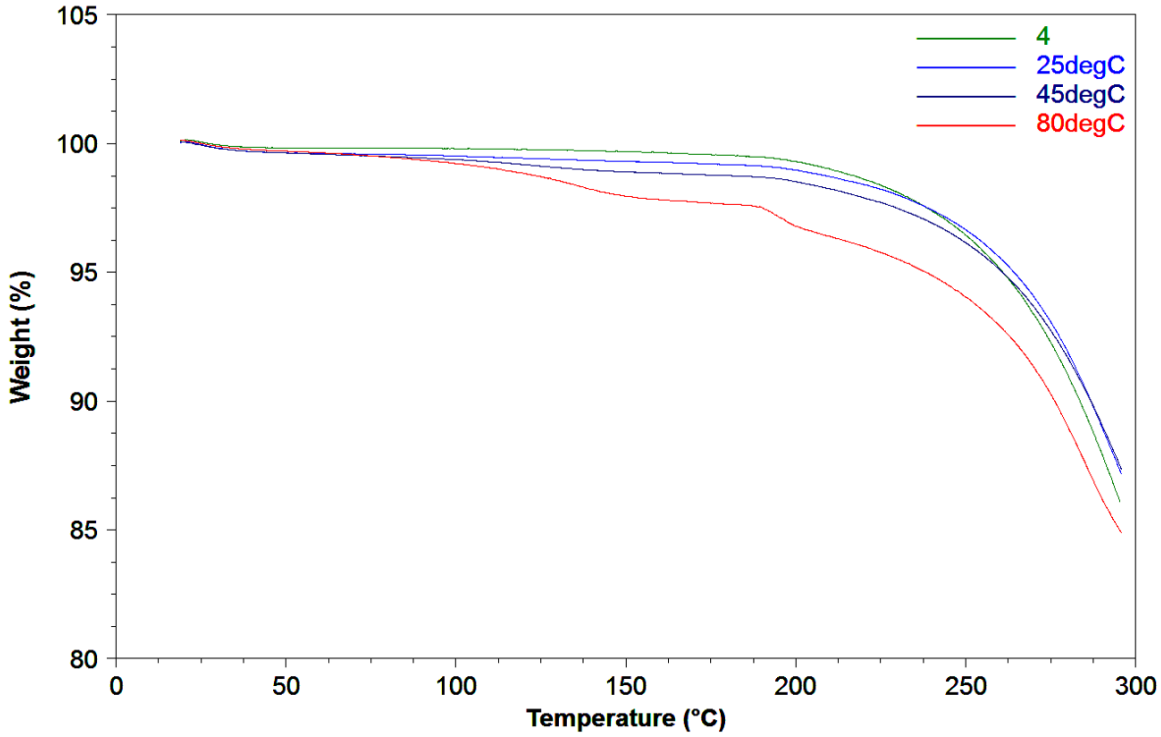

Figure 4.10 Thermograms of **4** before and after immersion in equimolar ternary xylene mixtures for approximately 24 hours at different temperatures.

4.4. Solubility of Host Form 3

Microcrystalline **3** was immersed in commercial mixed xylenes (≥ 75.0%) for approximately 60 hours. Several photomicrographs (Figure 4.11) were taken to show that the material does not dissolve and re-crystallize in liquid xylenes. Therefore, we could proceed with the liquid xylene selectivity experiments.

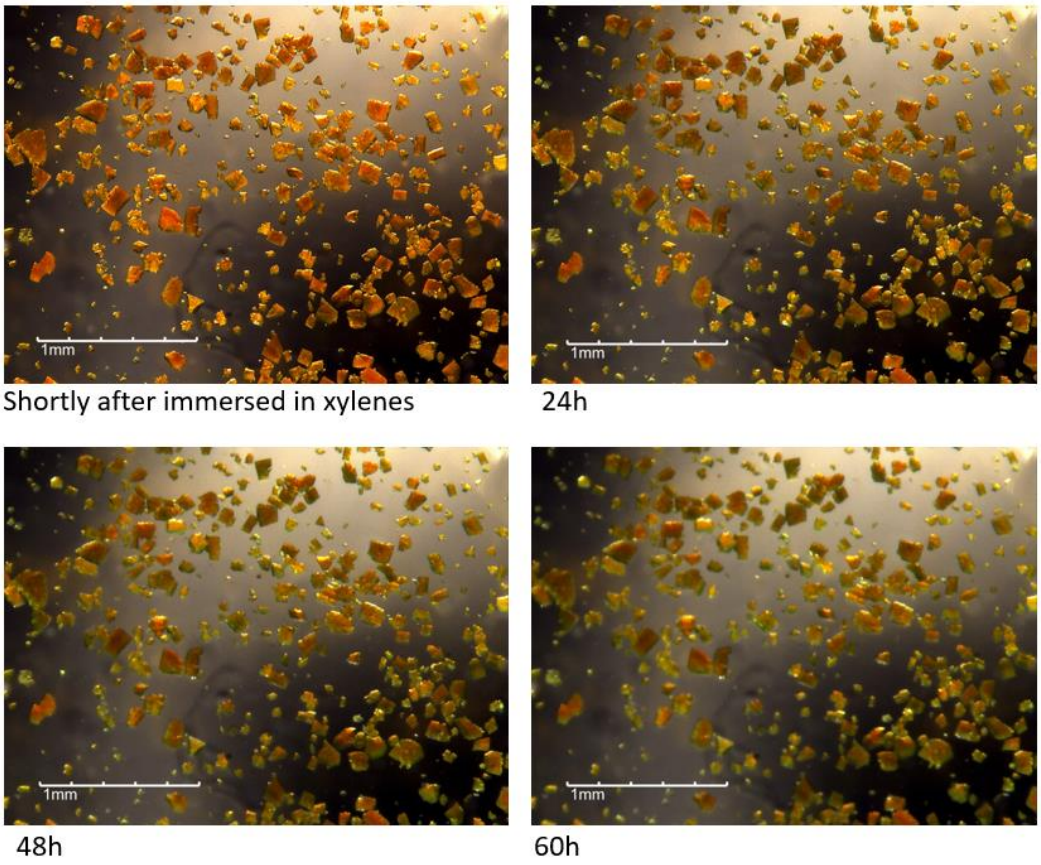

Figure 4.11 Photomicrographs of **MC** in xylenes over a period of 60 hours.

4.5. TGA Thermograms: Liquid Sorption

Thermograms (Figures 4.12–4.14) were recorded for xylene-included forms obtained by liquid sorption with form **3** before and after drying on filter paper at 25 °C for approximately 30 minutes. The plots indicate that xylene does not easily escape from the host at room temperature. Figure 4.15 shows the thermograms of pure- and mixed-xylene inclusion compounds.

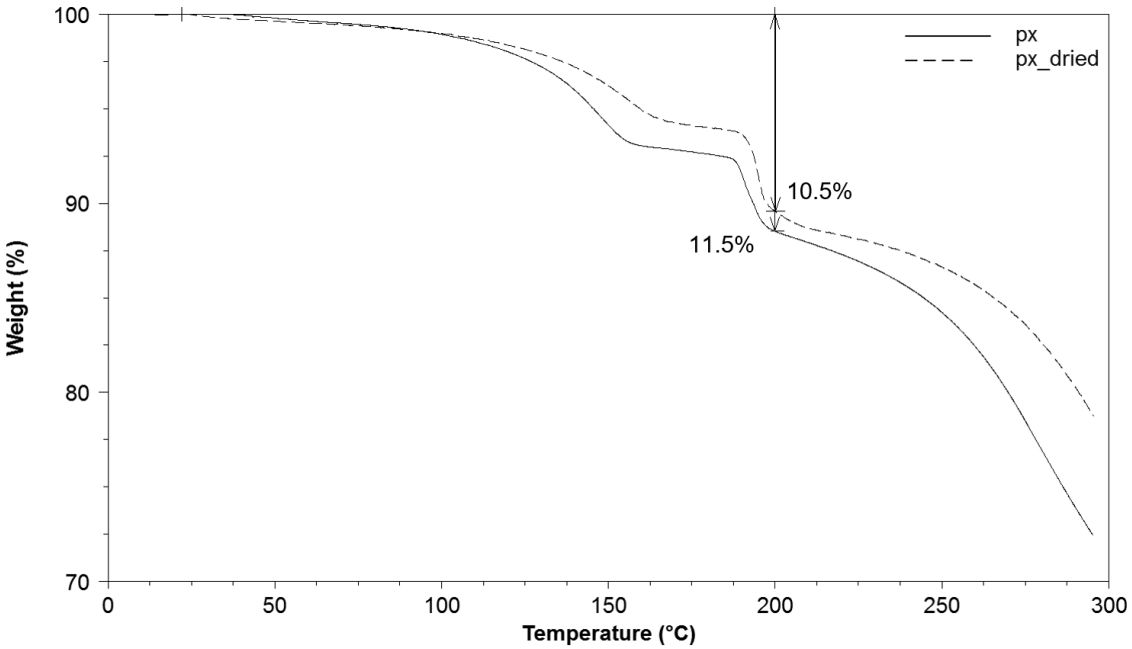

Figure 4.12 Comparison of thermograms after immersing form **3** in liquid *px* for at least 24 hours, before and after drying on filter paper for 30 min, with 11.5% and 10.5% weight loss at 200 °C, respectively. The theoretical weight loss of one xylene molecule per metallocycle is 11.7%.

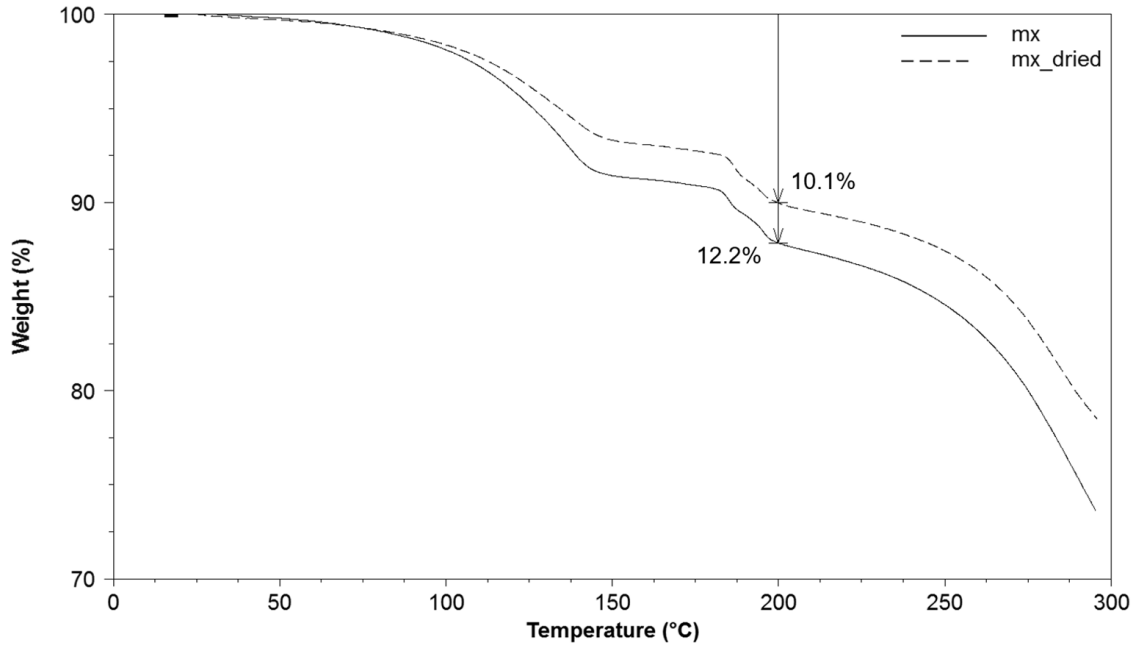

Figure 4.13 Comparison of thermograms after immersing form **3** in liquid *mx* for at least 24 hours, before and after drying on filter paper for 30 min, with 12.2% and 10.1% weight loss at 200 °C, respectively. The theoretical weight loss of one xylene molecule per metallocycle is 11.7%.

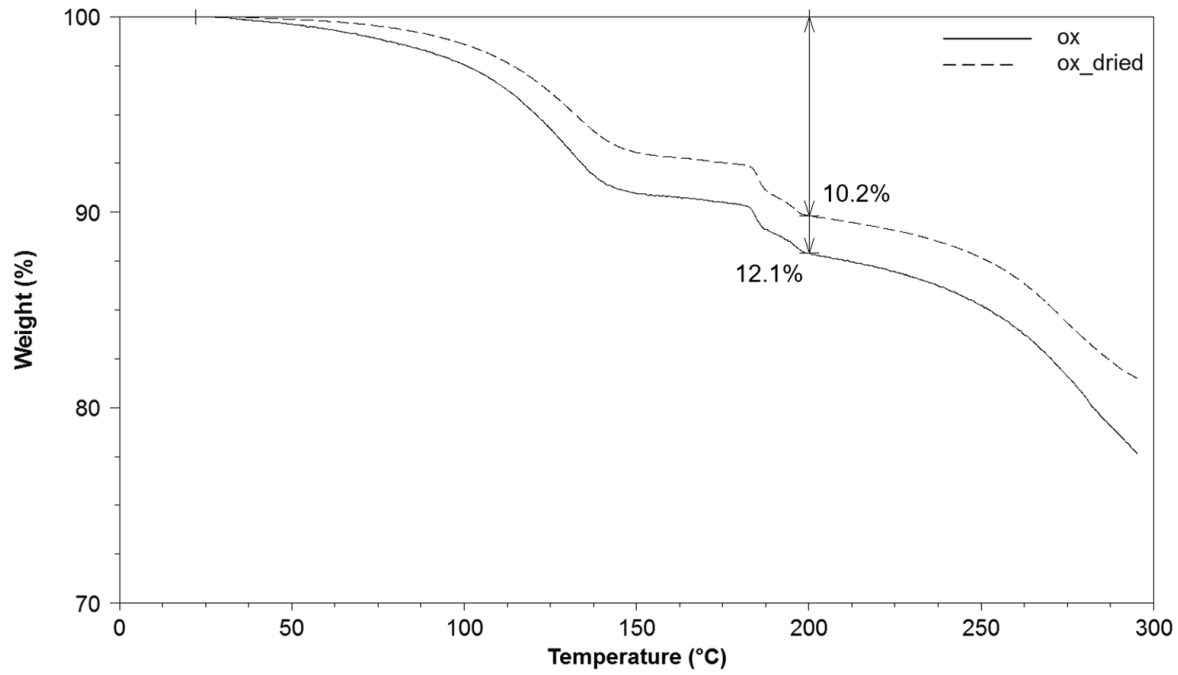

Figure 4.14 Comparison of thermograms after immersing form **3** in liquid *ox* for at least 24 hours, before and after drying on filter paper for 30 min, with 12.1% and 10.2% weight loss at 200 °C, respectively. The theoretical weight loss of one xylene molecule per metallocycle is 11.7%.

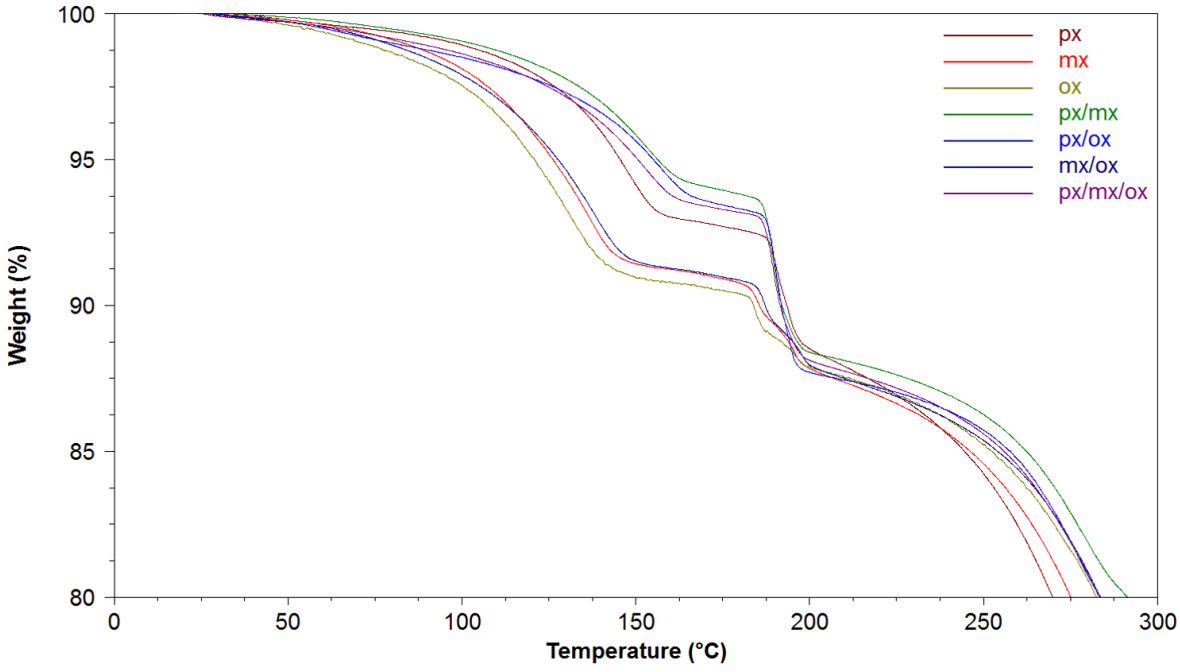

Figure 4.15 Thermograms of pure- and mixed-xylene inclusion compounds.

4.6. Selectivity Experiments

Binary liquid xylene mixtures (*px*/*mx*, *px*/*ox*, *mx*/*ox*) were prepared by weighing the individual components using a Shimadzu AUW220D dual-range semi-micro balance. The ratios (A:B) of the binary mixtures were approximately 10:0, 9:1, 8:2…, 1:9, 0:10 and the liquids were mixed by stirring. In a typical experiment approximately 20 – 25 mg of pre-weighed, freshly activated **3** was immersed in one of the xylene mixtures and stored at 25 °C for at least 24 hours. The sample was then allowed to dry on filter paper for approximately 30 minutes to minimize errors due to the presence of residual surface solvent. TGA was used to confirm that the included xylenes do not escape from the host material during the drying period (Figures 4.12–4.14). The dried sample was then immersed in 2 ml acetonitrile in an oven at 45 °C for 24 – 48 hours to allow for complete replacement of the guest; the color changed from orange to red and acetonitrile uptake was confirmed by TGA (Figure 4.16). Thereafter, the crystals were removed by filtration using an Acrodisc® syringe filter equipped with a 0.45 µm PTFE membrane. The filtrate was collected and analyzed by GC. A similar procedure was followed for the ternary equimolar xylene mixture. The GC chromatographs provide a good approximation of the relative guest isomer content in the crystals. Chromatograms recorded for pure samples of *px*, *mx* and *ox* showed that these compounds are eluted from the column after 8.65, 8.75 and 9.48 minutes, respectively.

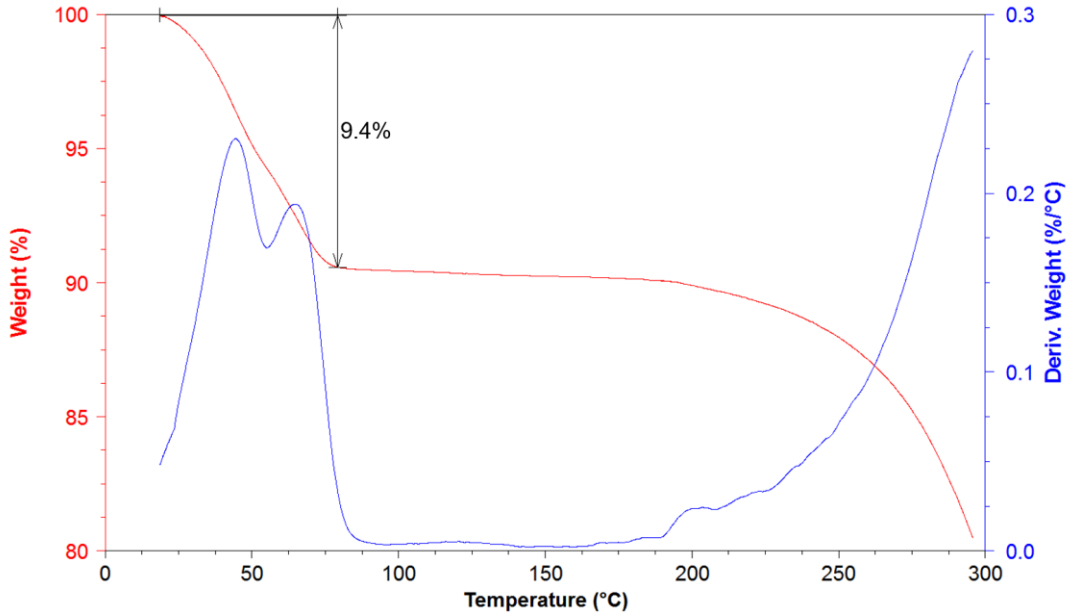

Figure 4.16 Thermogram of **2**·2(ACN) obtained by solvent exchange from **1**·xylene. A weight loss of 9.4% is equivalent to two ACN molecules per metallocycle.

4.6.1. Calculation of Selectivity Coefficient

The selectivity coefficient[43] represents the preference of a host for one of the compounds in a binary mixture. It can be expressed as $K_{A:B}$ and calculated according to the following equation:

$$K_{A:B} = (K_{B:A})^{-1} = \frac{Y_A}{Y_B} \times \frac{X_B}{X_A} \qquad [4.1]$$

where A and B are the two competing guests in the binary mixture, *X* and *Y* represent the mole fractions of the guests in the original liquid mixture and the resulting solid inclusion compound, respectively, and $X_A + X_B = 1$. A selectivity curve for each pairwise competition experiment can also be plotted as the mole fraction of the guests in the inclusion compound (Y_A/Y_B) as a function of the mole fraction of the guests in the original binary mixture (X_A/X_B).

4.7. Results and Discussion

Crystals of **1**·2(DMSO) were prepared and solvent-exchanged for ACN to yield **2**·2(ACN), and the porous apohost phase **3** was then obtained upon activation of **2**·2(ACN). Vapor sorption experiments (Figure 4.17) were carried out for each of the xylene isomers to establish the affinity of **3** for these guests. *px* was absorbed most rapidly, reaching an occupancy of slightly greater than 1:1 (guest:host) in approximately 155 minutes; from this result we infer that each metallocycle can only accommodate a maximum of one molecule of *px*. Based on this assumption, the total guest:host stoichiometry equilibrates to approximately 1.1:1 after 800 minutes, and we attribute the slight guest excess to a small amount of surface adsorption. Over the same timeframe, *mx* and *ox* reached stoichiometries of *ca* 85 and 67%, respectively. During the initial stages of the experiment, *ox* was absorbed most rapidly, followed by *px* and *mx*. However, after a few minutes the uptake of *ox* slowed down considerably. Although we have already shown that initial absorption rates do not necessarily comport with selectivity,[44] the vapor sorption experiments indicate that the uptake of *px* reaches equilibrium most rapidly, followed by *mx* and then *ox*.

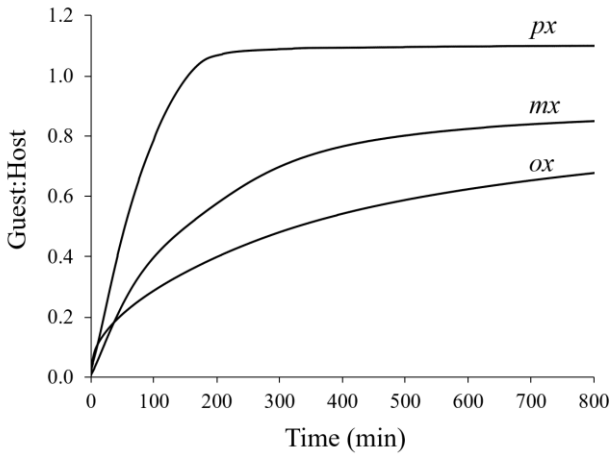

Figure 4.17 Kinetic sorption plots for **3** exposed to pure vapors of *px*, *mx* and *ox*.

A series of experiments was carried out to test the affinity of the host **MC2** for the different isomers of xylene by immersing activated crystals (i.e., form **3**) in binary liquid mixtures of varying composition. Using optical microscopy, we first established that the crystals do not dissolve in xylene (Figure 4.11), and also that guest uptake occurs as a single-crystal to single-crystal transformation. Selectivity studies were carried out by immersing activated **3** in varying molar ratios of binary mixtures of xylene isomers. In each experiment, the crystals were soaked for approximately 24 hours, after which the absorbed xylenes were extracted and subjected to GC analysis (Figure 4.18 and Table 4.2).

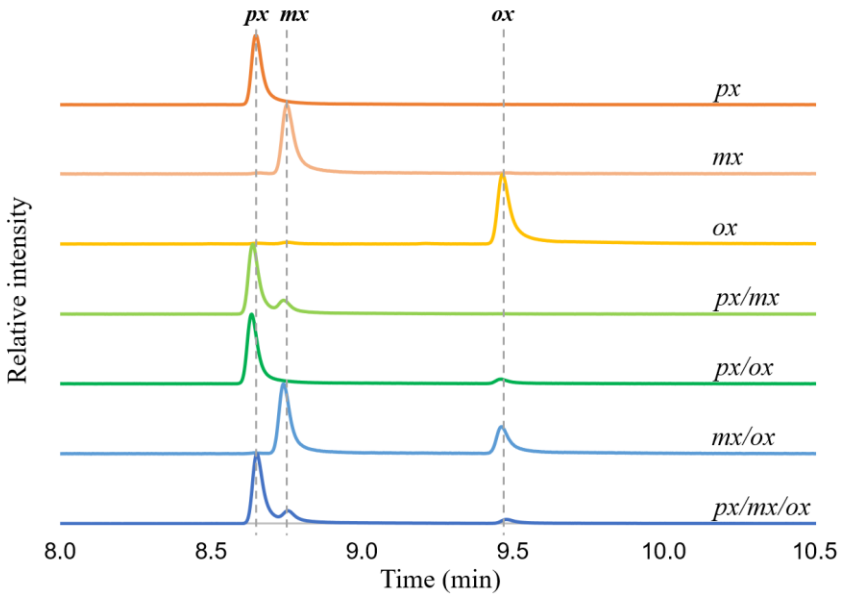

Figure 4.18 GC chromatograms of commercially pure xylenes and equimolar binary and ternary mixtures of xylene extracted from the **MC2**·xylene crystals.

Table 4.2 Selectivity coefficients for liquid binary mixtures A:B of xylene isomers ranging from approximately 1:9 to 9:1.

Composition A:B	Ratio in liquid (X_A:X_B)	Ratio absorbed (Y_A:Y_B)	Selectivity coefficient $K_{A:B}$	Average $K_{A:B}$
px:*mx*	8:92	37:63	6.73	5.12
	17:83	59:41	6.87	
	26:74	69:31	6.14	
	36:64	76:24	5.71	
	45:55	82:18	5.38	
	55:45	86:14	4.87	
	65:35	90:10	4.74	
	75:25	90:10	3.09	
	85:15	93:7	2.55	
px:*ox*	10:90	66:34	17.01	11.40
	19:81	79:21	15.39	
	31:69	87:13	14.12	
	42:58	90:10	12.81	
	53:47	93:7	11.72	
	63:37	94:6	9.85	
	75:25	96:4	7.97	
	83:17	97:3	6.97	
	92:8	99:1	6.79	
mx:*ox*	11:89	20:80	2.15	1.96
	21:79	35:65	2.00	
	33:67	51:49	2.07	
	43:57	62:38	2.12	
	54:46	69:31	1.96	
	65:35	79:21	2.06	
	75:25	85:15	1.84	
	83:17	90:10	1.91	
	92:8	94:6	1.55	

The resulting competition plots shown in Figure 4.19 confirm that **MC2** is most selective for *px* over both *mx* and *ox*. The lower selectivity for *mx* over *ox* is indicated by the flatter curve, which is still above the zero-selectivity line. The average selectivity coefficients for the *px*/*mx*, *px*/*ox*, *mx*/*ox* mixtures are 5.12, 11.40 and 1.96, respectively (Table 4.2). In general, selectivity coefficients above 5 are rarely observed[9] and these selectivity values compare favorably with those reported in the literature (Table 4.3). When **3** was exposed to an approximately equimolar ternary xylene mixture (*px*:*mx*:*ox* = 32:37:31), the composition in the crystals equilibrated to *px*:*mx*:*ox* = 78:17:5 (Figure

4.18). These results are consistent with the selectivity plots, as well as the vapor sorption kinetic plots (which show a preference in the order *px* >> *mx* > *ox* with regard to the time taken to reach equilibrium).

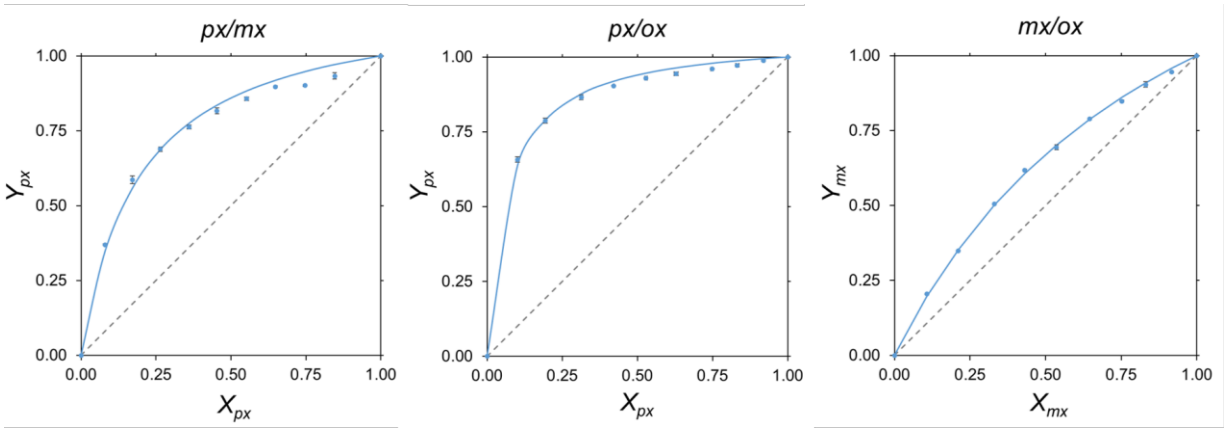

Figure 4.19 Selectivity plots derived from competition experiments carried out with binary mixtures of xylene in the range $X_{A:B}$ = 0 to 1. Error bars are included but may be too small to discern. The diagonal dashed line represents zero selectivity. The solid line represents the best fit to the experimental data, as modeled using Equation 4.1 and empirically selecting a value of $K_{A:B}$ that minimizes the least-squares errors.

Table 4.3 Porous materials and their reported xylene selectivities.

Porous materials	Selectivity coefficients			References
	px/*mx*	*px*/*ox*	*mx*/*ox*	
Metallocycle $[Cu_2L_2Cl_4]$*	65.7	51.6	37.5	[19]
FAU zeolite (K^+-exchanged Y zeolite)	5.25	4.63	1.0	[9]
MIL-125(Ti)	1.5	1.6	a	[13,45]
MIL-125(Ti)-NH_2	3.0	2.2	1.03	[13,46,47]
Ce(HTCPB)	4.5	5.6	1.22	[48]
Cu(CDC)	7.0	10.0	3.0	[49]
	mx/*px*	*mx*/*ox*	*ox*/*px*	
$Ni(NCS)_2$(isoquinoline)$_2$(4-phenylpyridine)$_2$	4.7	2.6	1.8	[50]
HKUST-1	1.1	2.4	0.7	[51]
POP-1 $[(C_{39}H_{27}NO)_n]$	2.04	2.28	0.89	[52]

	ox/*px*	*ox*/*mx*	*mx*/*px*	
UiO-66	2.4	1.8	-	[53]
CD-MOF	17.9	6.73	2.67	[15]
CAU-13	1.7	2.1	0.8	[54]
CPO-27-Ni	3.3	1.7	2	[55]
MIL-53(Fe)	2.53	1.58	1.83	[56]
$Ni(NCS)_2(ppp)_4$	40.5	34.2	12.7	[44]
$Zn(BDC)(Dabco)_{0.5}$	1.83	1.64	a	[57]
Co_2(dobdc)	3.9 ± 0.5	2.5 ± 0.1	1.6 ± 0.2	[7]
MIL-53(Cr)	13.75	8.01	1.72	[58]
Sql-1-Co-NCS	9.6	7.5	1.3	[59]

*L=1,3-Bis(imidazol-1-ylmethyl)-2,4,6-trimethylbenzene; [a]Two isomers could not be separated.

In order to gain structural insight into the mechanism for guest inclusion, and to explain why the metallocycle prefers *px*, we used SCD to determine the crystal structures of the xylene inclusion compounds. In our efforts to obtain single crystals of the xylene-included forms, similar results were obtained for all three isomers. Therefore, in the discussion that follows the reader can suppose relevance to any of the three isomers where reference is made to “xylene”. Crystals of the brown activated phase **3** were immersed in xylene for at least 24 hours, during which time they gradually became orange. SCD analysis of one of these crystals showed that the metallocycle reverts to host structure type **1** upon inclusion of the xylene. Owing to poor data quality (likely due to the crystals having experienced three phase transitions, each involving significant changes in the conformation of the metallocycle), we have deemed this structural analysis unsuitable for publication. However, PXRD analysis (Figures 4.20–4.21) of a bulk sample of the orange crystals confirm the phase transition from host form **3** to structure type **1**.

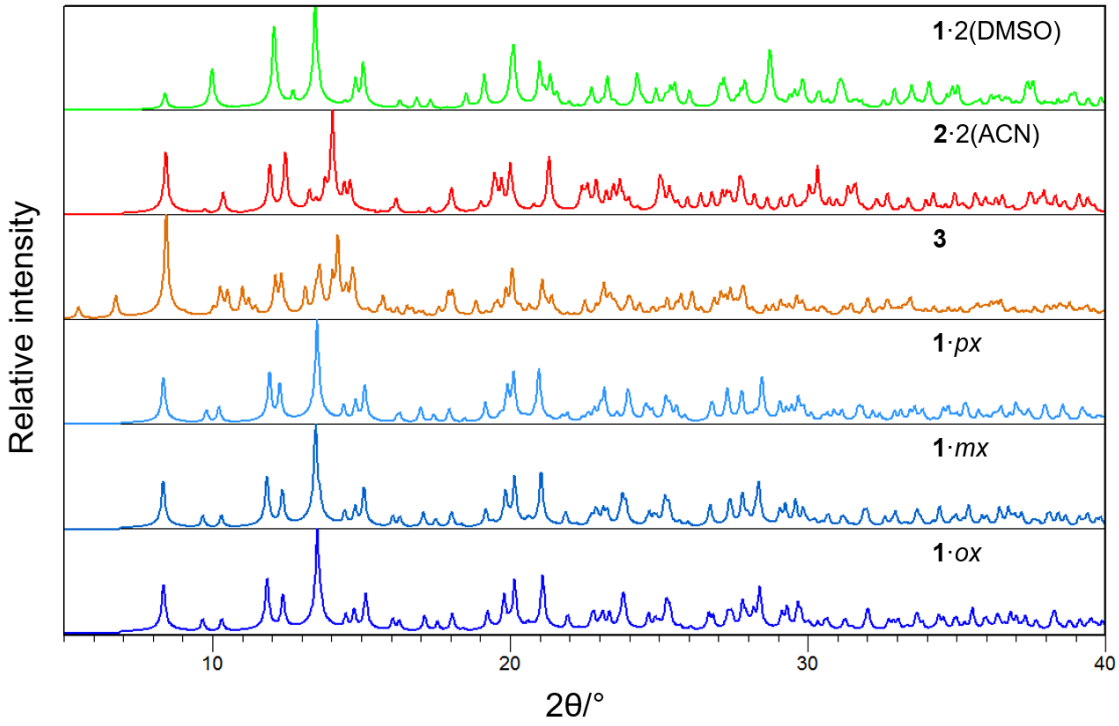

Figure 4.20 Diffractograms calculated from single-crystal structures; **1**·xylene crystals were obtained by solvent exchange (immersing **2**·2(ACN) in xylene for at least 3 days).

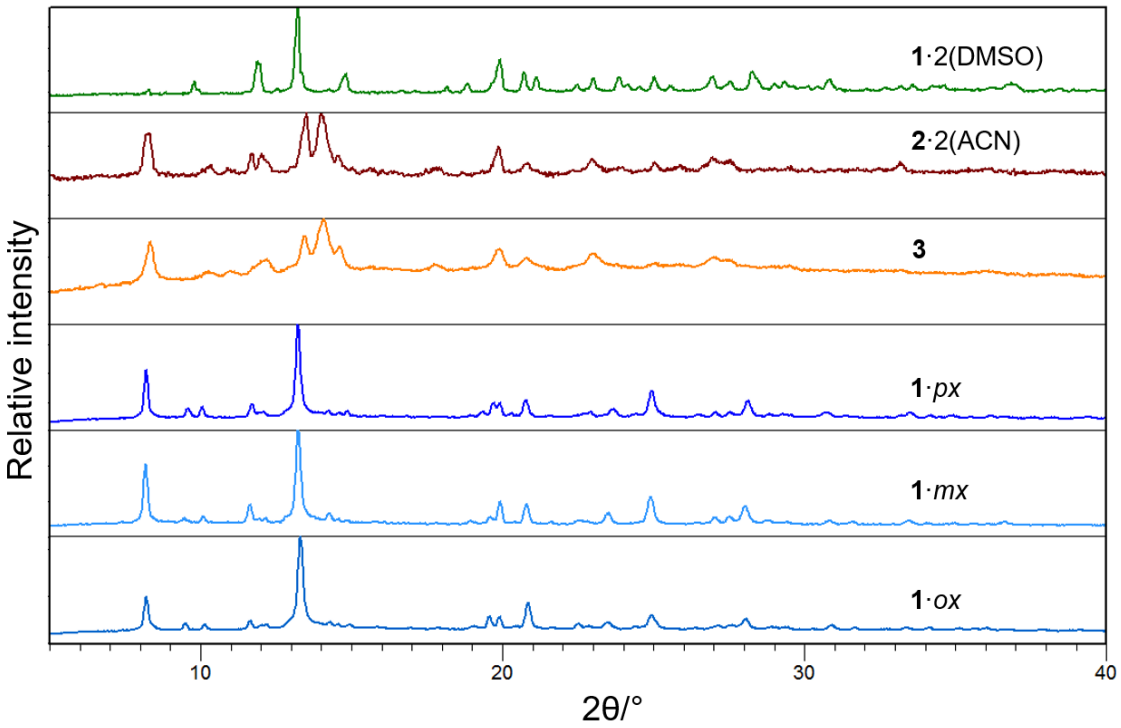

Figure 4.21 Experimental powder patterns. The **1**·xylene forms were obtained by immersing **3** in xylene for at least 24 hours.

We next attempted to obtain the xylene-included forms by means of solvent exchange. Crystals of **1**·2(DMSO) were immersed in xylene over a period of 3 days, during which time the solvent was refreshed 4 times. However, the crystals remained green, from which we inferred that no solvent exchange of DMSO for xylene had occurred. This observation can be rationalized by considering that the DMSO molecules are coordinated to the Cu ions of the metallocycle and are thus not easy to displace without an energetic incentive such as a phase transition (Scheme 1). Immersion of **2**·2(ACN) in xylene resulted in a change in color from red to orange over a period of 3 days, and PXRD analysis (Figures 4.22–4.24) of the bulk sample indicated that exchange of ACN for xylene in this manner yields the same form as that obtained by exposing form **3** to xylene. The guest-exchange process occurred as a SC-SC transition to yield crystals suitable for SCD analysis, which confirmed that exposure of **2**·2(ACN) to any of the three isomers of xylene results in reversion to host structure type **1**, with concomitant inclusion of one molecule of xylene per metallocycle. We note that xylene vapor sorption also yields structure type **1** (Figures 4.22–4.24).

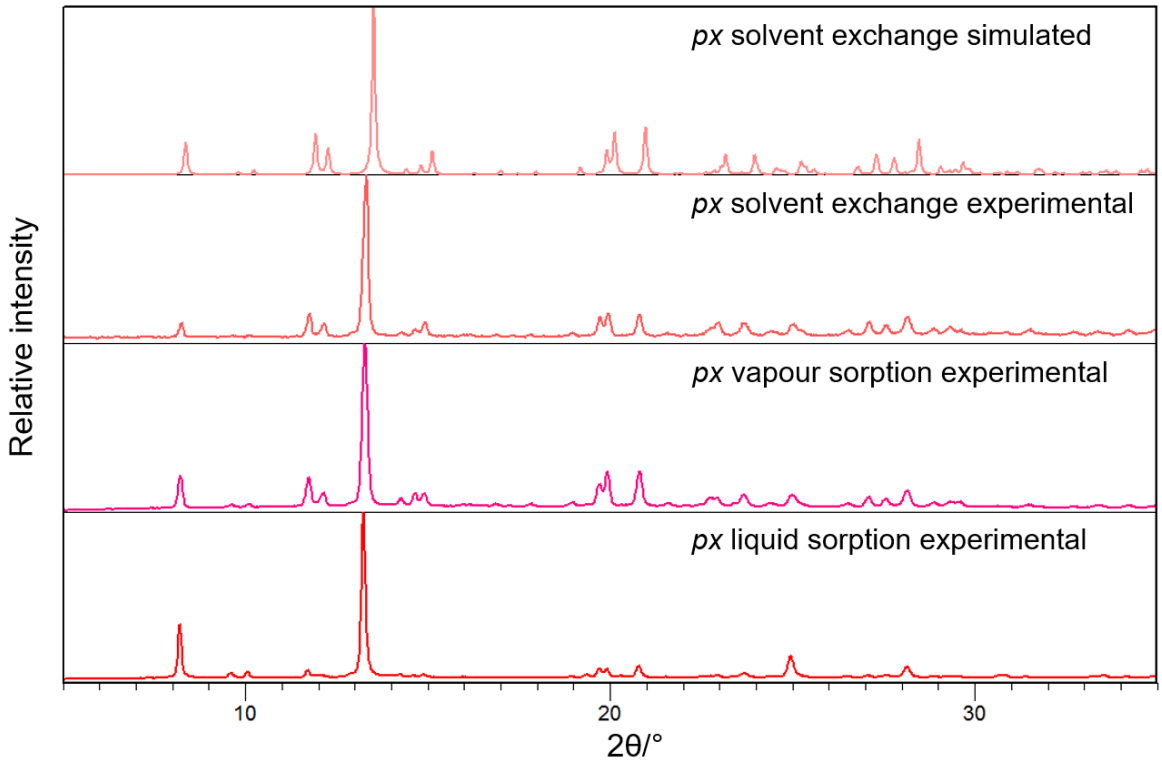

Figure 4.22 Powder patterns of the inclusion compound **1**·*px* obtained via different methods.

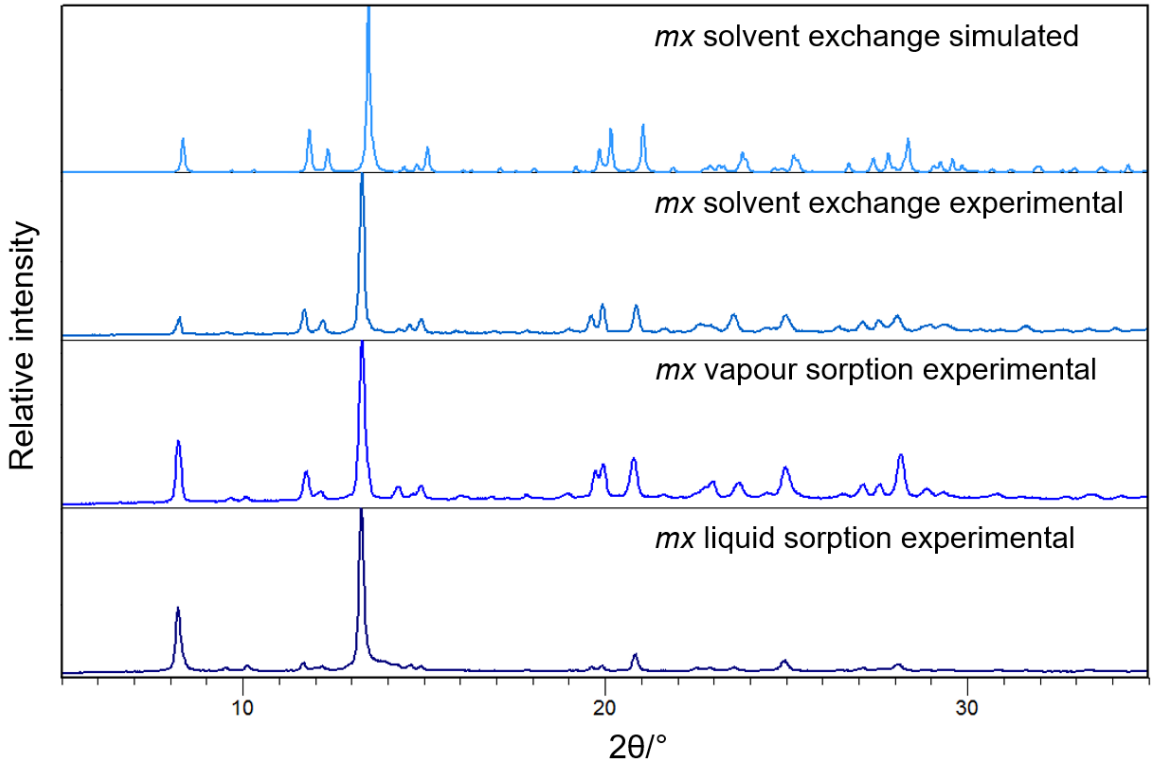

Figure 4.23 Powder patterns of the inclusion compound **1**·*mx* obtained via different methods.

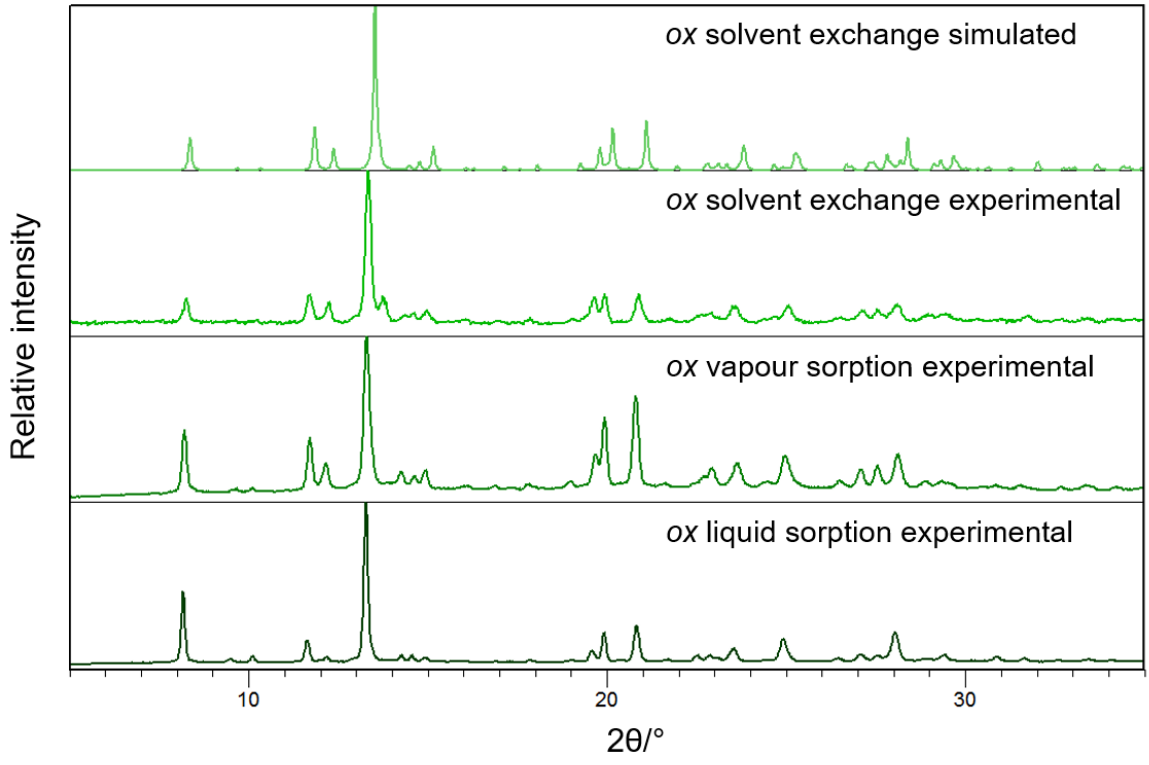

Figure 4.24 Powder patterns of the inclusion compound **1**·*ox* obtained via different methods.

SCD analyses of **1**·*px*, **1**·*mx* and **1**·*ox* confirm that the conformation of **MC2** reverts to UUDD in all three cases, with intrinsic inclusion of the guest molecules within the metallocycles as observed for **1**·2(DMSO) and **1**·2(acetone).[21] Owing to -1 site symmetry at the centroid of each host molecule, the guest molecules in **1**·*px* are ordered (Figure 4.25a), while those in **1**·*mx* and **1**·*ox* are each required to be disordered over two positions of equal site occupancy (Figure 4.25b and 4.25c, respectively). The xylene molecules are aligned parallel to the methyl groups of the host in order to minimize steric hindrance, and they interact with the host via relatively weak C—H···π contacts (Figure 4.26 and Table 4.4).

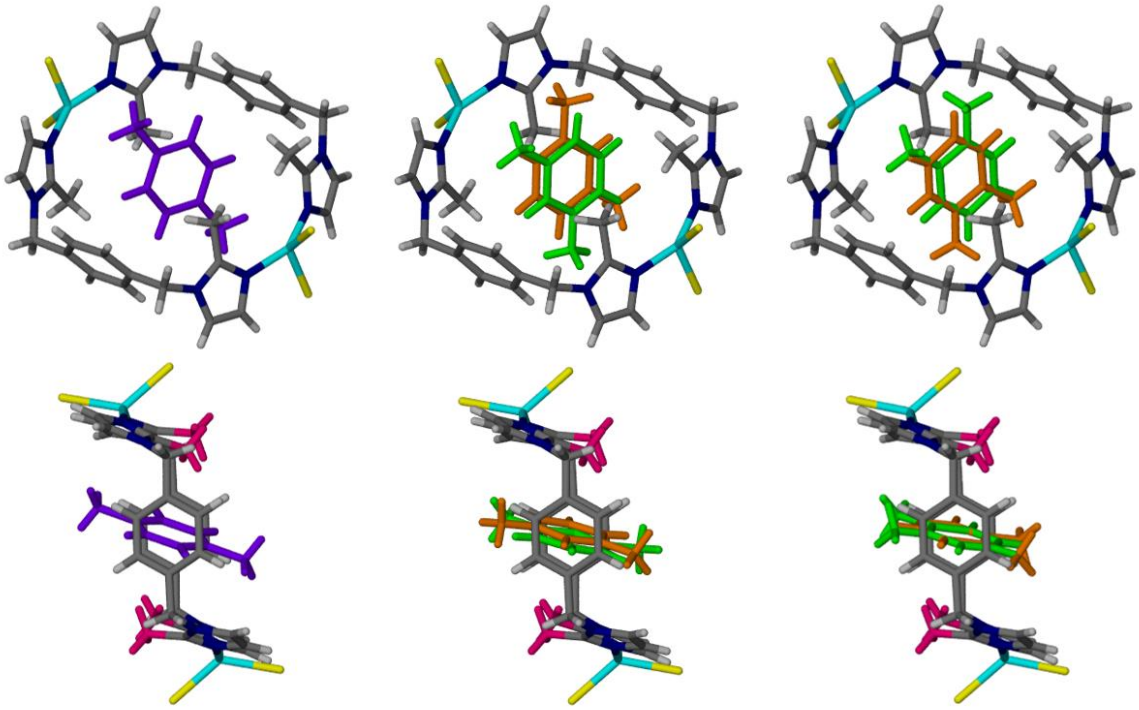

Figure 4.25 Perspective views showing the inclusion compounds (a) **1**·*px*, (b) **1**·*mx* and (c) **1**·*ox* projected along [9 5 -2] (top) and [-9 -6 -5] (bottom). In (a) the ordered *px* guest molecule is colored purple and in (b) and (c) the two disordered components are colored orange and green. In the projections at the bottom, the methyl groups of the host are highlighted in pink to show their almost parallel orientation with respect to the guest molecules.

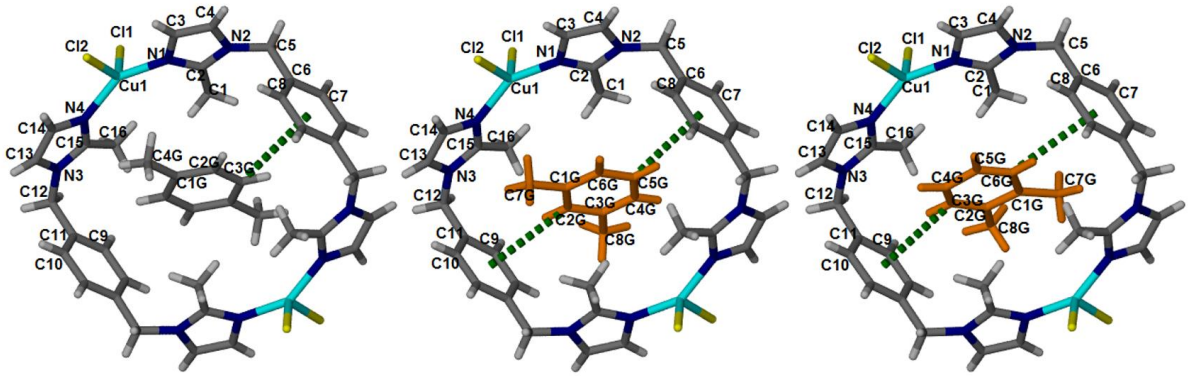

1·*px* **1·*mx*** **1·*ox***

Figure 4.26 Close contacts between the host and guest as indicated by the dashed green lines. Only one of the disordered components for each of **1**·*mx* and **1**·*ox* are shown for clarity.

Table 4.4 Close contacts between the host and guest.

Inclusion compounds	H···π distance (Å)	C – H···π distance (Å)
1·*px*	2.98	3.71
1·*mx*	2.68	3.57
	2.84	3.71
1·*ox*	2.71	3.57
	3.03	3.88

By considering the guest-accessible volumes of the three open-form structure types **1**–**3**, we can rationalize why inclusion of any of the three xylene isomers by either of the structure types **2** or **3** requires the host to transform to type **1**. As shown in Figure 4.27a, pairs of acetonitrile guest molecules in **2**·2(ACN) occupy 0D pockets (i.e., there are no permanent channels in the crystal structure that lead to the guest-accessible spaces).

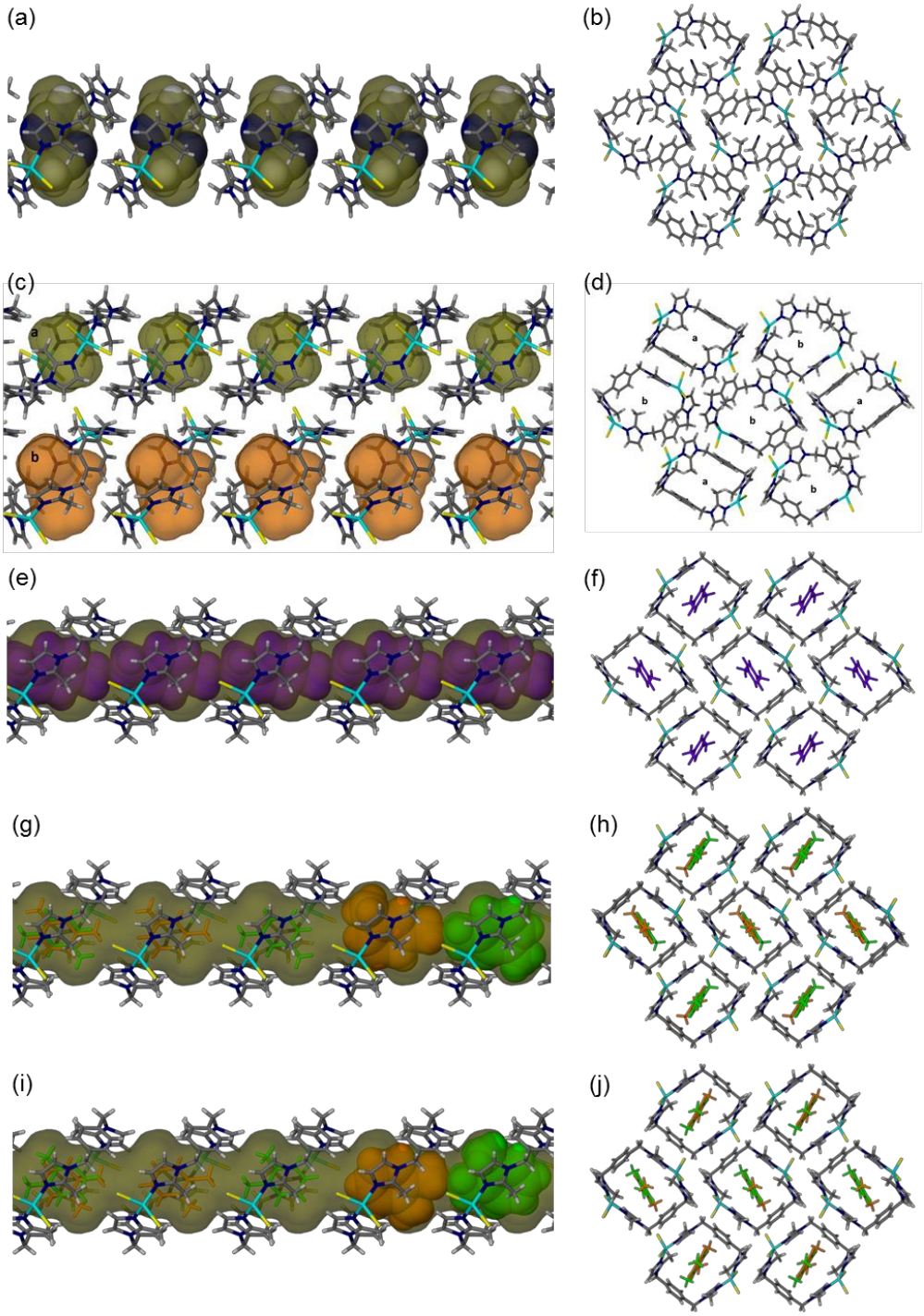

Figure 4.27 Crystal structures of **2**·2(ACN) (a and b), apohost form **3** (c and d), and the three xylene inclusion compounds **1**·*px* (e and f), **1**·*mx* (g and h) and **1**·*ox* (i and j). Left: views along [010] showing the guest-accessible pockets or channels. Right: corresponding views along [100]. Host molecules are shown in capped-stick representation. In (a) and (e) the guest molecules are shown in spacefilling representation. In (g) and (i) the guest molecules are shown in mixed representations, with the two disordered components colored orange and green.

Each metallocycle encircles one of these pockets, and the volume of each pocket is approximately 171 Å^3.[60–64] According to the "rule-of-thumb" reported by van Heerden and Barbour[65] for predicting guest occupancy, a guest molecule occupies approximately double its van der Waals volume when accommodated within a host structure. Each of the three isomers of xylene has a van der Waals volume of ca 110 Å^3 (determined by MSRoll[37–39] via X-Seed,[35,36] using a probe of radius 0 Å). Therefore, it appears that each of the pockets available to guests in the **2**·2(ACN) structure type is too small to accommodate a molecule of xylene. The two crystallographically unique intrinsic pockets of hosts **3a** and **3b** in the apohost form **3** have volumes of 111 and 178 Å^3, respectively (Figure 4.27c). Therefore, we can also predict that structure type **3** cannot accommodate xylene. However, in **1**·2(DMSO) and **1**·2(acetone) the conformation of the host allows merging of the guest-accessible voids to form channels that propagate along [100]. Consequently, the guest-accessible volumes in these forms are approximately 230 and 216 Å^3 per host molecule, respectively. It therefore appears that, of the known host structure types, only type **1** is suitable for the inclusion of any of the isomers of xylene in a host:guest ratio of 1:1 (Figures 4.27e, 4.27g and 4.27i). Indeed, these ratios were confirmed by TGA (Figures 4.12–4.14), and the guest-accessible volumes of 221, 222 and 220 Å^3 per host molecule for the structures **1** ·*px*, **1** ·*mx* and **1** ·*ox* are highly consistent with our ca 50% occupancy rule of thumb.[65] Table 4.5 shows the calculated void volume per unit cell using 1.5 Å probe radius and 0.2 Å gliding space. Table 4.6 are the single-crystal data for the three xylene included compounds.

Table 4.5 Guest-accessible volume per unit cell of the host.

Inclusion compound	Void volume (Å^3) per unit cell	% of unit-cell volume
1·*px*	443	21.6%
1·*mx*	445	21.7%
1·*ox*	440	21.5%

Table 4.6 Crystallographic parameters for individual xylene inclusion compounds.

Identification code	**1**·*px*	**1**·*mx*	**1**·*ox*
Empirical formula	$C_{40}H_{46}Cl_4Cu_2N_8$	$C_{40}H_{46}Cl_4Cu_2N_8$	$C_{40}H_{46}Cl_4Cu_2N_8$
Formula weight (g mol^{-1})	907.73	907.73	907.73
Temperature (K)	100(2)	100(2)	100(2)
Wavelength (Å)	0.71073	0.71073	0.71073
Crystal system	Monoclinic	Monoclinic	Monoclinic
Space group	$P2_1/c$	$P2_1/c$	$P2_1/c$
***a* (Å)**	8.6906(13)	8.6295(9)	8.6077(5)
***b* (Å)**	13.0701(19)	13.0176(13)	12.9782(7)
***c* (Å)**	18.123(3)	18.3619(18)	18.3576(10)
***α* (°)**	90	90	90
***β* (°)**	95.231(2)	95.392(1)	95.020(1)
***γ* (°)**	90	90	90
Volume (Å^3)	2049.9(5)	2053.6(4)	2042.9(2)
Z	2	2	2
Calculated density (g cm^{-3})	1.471	1.468	1.476
Absorption coefficient (mm^{-1})	1.338	1.336	1.343
F_{000}	936	936	936
θ range for data collection (°)	1.924 – 27.533	1.921 – 25.710	1.924 – 26.401
Miller index ranges	$-11 \le h \le 11$ $-16 \le k \le 16$ $-23 \le l \le 23$	$-10 \le h \le 10$ $-15 \le k \le 15$ $-22 \le l \le 22$	$-10 \le h \le 10$ $-16 \le k \le 16$ $-22 \le l \le 22$
Reflections collected	44846	38980	41475
Independent reflections	4718	3912	4184
Completeness to θ_{max} (%)	100	99.8	99.8
Max. and min. transmission	0.883, 1.000	0.914, 1.000	0.932, 1.000
Refinement method	Full-matrix least-squares on F^2	Full-matrix least-squares on F^2	Full-matrix least-squares on F^2
Data / restraints / parameters	4718 / 0 / 247	3912 / 102 / 284	4184 / 126 / 284
Goodness-of-fit on F^2	1.107	1.204	1.117
Final *R* indices [$I > 2\sigma(I)$]	$R1$ = 0.0282 $wR2$ = 0.0671	$R1$ = 0.0345 $wR2$ = 0.0823	$R1$ = 0.0365 $wR2$ = 0.0833

4.8. Recyclability

As the **1**·xylene can be solvent exchanged to **2**·2(ACN), the metallocycle **MC2** might be recyclable. Figure 4.28 shows a comparison of powder patterns of a xylene-inclusion compound **1**·xylene obtained by immersing **3** in equimolar ternary xylene mixtures for at least 24 hours, a **2**·2(ACN) obtained by solvent exchange of **1**·xylene with acetonitrile, form **3** obtained after activation of **2**, as well as a powder pattern of freshly activated **3**, which confirms its recyclability.

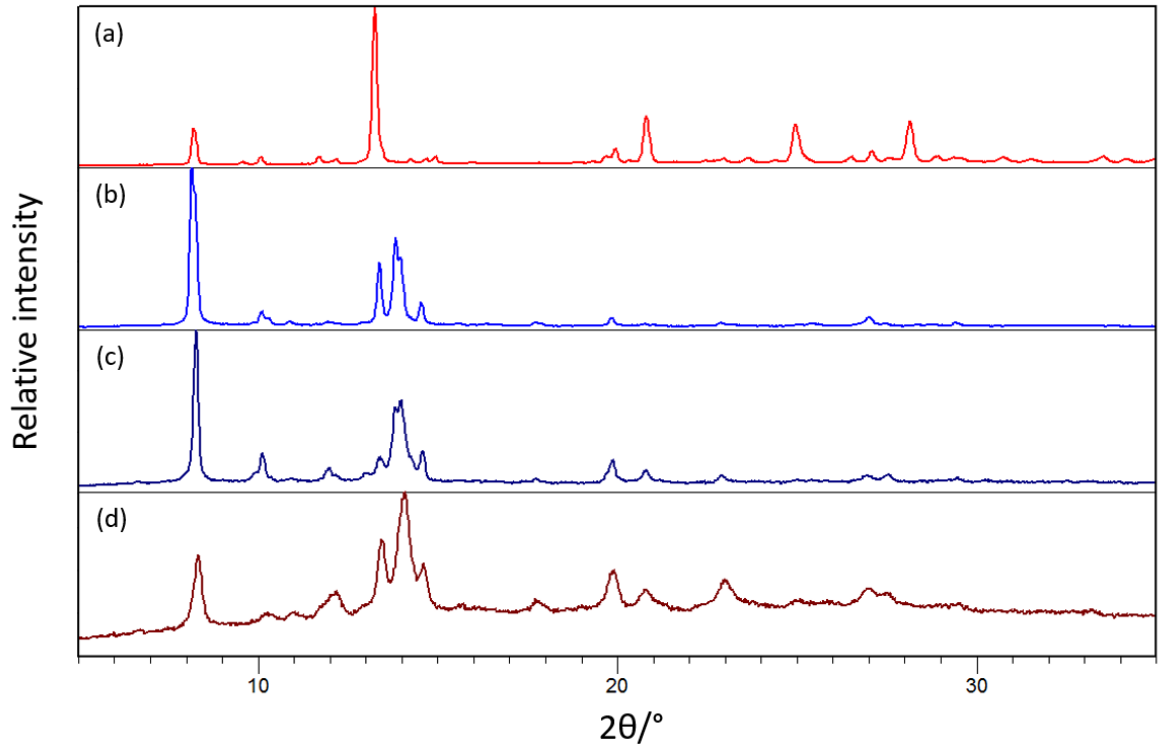

Figure 4.28 Powder patterns of (a) the xylene-inclusion compound **1**·xylene obtained by immersing **3** in equimolar ternary xylene mixtures for at least 24 hours, (b) solvent exchange of **1**·xylene with acetonitrile to obtain **2**·2(ACN) and (c) form **3** obtained after activation of **2**. The PXRD pattern of freshly activated **3** is shown in (d) to confirm its recyclability.

4.9. Conclusion

This study exploits our existing knowledge of the phase-change landscape of **MC2** in order to prepare the appropriate active host phase in a stepwise manner, and to then explore the separation of xylene isomers by using the readily interconvertible phase transformations between different host structural types. The selectivity of **MC2** for xylenes in the order *px* >> *mx* > *ox* follows the trend of increasing kinetic diameter, for which the accepted values are 0.58, 0.64 and 0.65 nm for *px*, *mx* and *ox*, respectively.[46] When crystals of **3** are exposed to xylene in liquid or vapor form, the metallocycle changes its conformation and reverts to its as-synthesized structure type **1** in order to absorb the xylene molecules. Indeed, according to the ~50% "rule of thumb", **1** is the only known structural type capable of accommodating xylene guests. Diffusion of xylene through the crystals occurs despite the absence of permanent channels. Moreover, the xylene-included forms can be obtained as SC-SC transformations[20] by solvent exchange starting with **2** · 2(ACN); although such transitions are not relevant to separation applications, they allow us to determine the crystal structures of the relevant crystal forms, and to thus rationalize the guest-inclusion process. Furthermore, by resolving the problem of obtaining and maintaining phase-pure **3**, new avenues of research are now possible with this material.

4.10. References

1 G. Zhang, Y. Ding, A. Hashem, A. Fakim and N. M. Khashab, *Cell Reports Phys. Sci.*, 2021, **2**, 100470.

2 J. Fabri, U. Graeser and T. A. Simo, *Ullmann's Encycl. Ind. Chem.*, 2012, 39, 643−663.

3 M. Minceva and A. E. Rodrigues, *AIChE J.*, 2007, **53**, 138–149.

4 J. L. Pellegrino, *U.S. Dep. Energy Off. Ind. Technol.*, 2000, 1–225.

5 W. Qi, X. Wang, Z. Liu, K. Liu, Y. Long, W. Zhi, C. Ma, Y. Yan and J. Huang, *J. Colloid Interface Sci.*, 2021, **597**, 325–333.

6 N. Smolarski, *Frost & Sullivan*, 2012, 1–15.

7 M. I. Gonzalez, M. T. Kapelewski, E. D. Bloch, P. J. Milner, D. A. Reed, M. R. Hudson, J. A. Mason, G. Barin, C. M. Brown and J. R. Long, *J. Am. Chem. Soc.*, 2018, **140**, 3412–3422.

8 D. S. Sholl and R. P. Lively, *Nature*, 2016, **532**, 435–437.

9 Y. Yang, P. Bai and X. Guo, *Ind. Eng. Chem. Res.*, 2017, **56**, 14725–14753.

10 X. Li, J. Wang, N. Bai, X. Zhang, X. Han, I. da Silva, C. G. Morris, S. Xu, D. M. Wilary, Y. Sun, Y. Cheng, C. A. Murray, C. C. Tang, M. D. Frogley, G. Cinque, T. Lowe, H. Zhang, A. J. Ramirez-Cuesta, K. M. Thomas, L. W. Bolton, S. Yang and M. Schröder, *Nat. Commun.*, 2020, **11**, 1–10.

11 X. Wu, W. Wei, J. Jiang, J. Caro and A. Huang, *Angew. Chem., Int. Ed.*, 2018, **57**, 15354–15358.

12 X. Cui, Z. Niu, C. Shan, L. Yang, J. Hu, Q. Wang, P. C. Lan, Y. Li, L. Wojtas, S. Ma and H. Xing, *Nat. Commun.*, 2020, **11**, 1–8.

13 A. Torres-Knoop, R. Krishna and D. Dubbeldam, *Angew. Chem., Int. Ed.*, 2014, **53**, 7774–7778.

14 J. A. Gee, K. Zhang, S. Bhattacharyya, J. Bentley, M. Rungta, J. S. Abichandani, D. S. Sholl and S. Nair, *J. Phys. Chem. C*, 2016, **120**, 12075–12082.

15 J. M. Holcroft, K. J. Hartlieb, P. Z. Moghadam, J. G. Bell, G. Barin, D. P. Ferris, E. D. Bloch, M. M. Algaradah, M. S. Nassar, Y. Y. Botros, K. M. Thomas, J. R. Long, R. Q. Snurr and J. F. Stoddart, *J. Am. Chem. Soc.*, 2015, **137**, 5706–5719.

16 Z. Wu, Y. Yang, B. Tu, P. A. Webley and D. Zhao, *Adsorption*, 2009, **15**, 123–132.

17 M. Rana, R. B. Reddy, B. B. Rath and U. K. Gautam, *Angew. Chem., Int. Ed.*, 2014, **53**, 13523–13527.

18 G. Zhang, B. Hua, A. Dey, M. Ghosh, B. A. Moosa and N. M. Khashab, *Acc. Chem. Res.*, 2021, **54**, 155–168.

19 M. du Plessis, V. I. Nikolayenko and L. J. Barbour, *J. Am. Chem. Soc.*, 2020, **142**, 4529–4533.

20 L. J. Barbour, *Aust. J. Chem.*, 2006, **59**, 595–596.

21 L. Dobrzańska, G. O. Lloyd, C. Esterhuysen and L. J. Barbour, *Angew. Chem., Int. Ed.*, 2006, **45**, 5856–5859.

22 L. Dobrzańska, G. O. Lloyd and L. J. Barbour, *New J. Chem.*, 2007, **31**, 669–676.

23 V. I. Nikolayenko, L. M. Van Wyk, O. Q. Munro and L. J. Barbour, *Chem. Commun.*, 2018, **54**, 6975–6978.

24 M. du Plessis, V. I. Nikolayenko and L. J. Barbour, *Inorg. Chem.*, 2018, **57**, 12331–12337.

25 Note on the use of “type”: The terms “form” and “phase” are synonymous, and refer to a distinct crystal structure of a chemical entity or adduct. However, in some instances it is possible for two or more host-guest adducts to have the same arrangement of host structures (i.e., similar packing and near-isometric lattice parameters), in which case the structures can be referred to as being “isoskeletal”. Isoskeletal structures are different forms because their chemical compositions are different. In the present contribution, we refer to the host structure of each isoskeletal series as host structure type **1** or **2**, while the two different guest-free forms can be referred to as either forms **3** and **4**, or types **3** and **4**. The formula **1**·2(DMSO) refers to an adduct of **MC** and DMSO in a host:guest ratio of 1:2, where the host assumes structure type **1**. Similarly, **2**·2(ACN) refers to a 1:2 adduct of **MC** and acetonitrile, with the host assuming structure type **2**.

26 L. J. Barbour, D. Das, T. Jacobs, G. O. Lloyd and V. J. Smith, in *Supramolecular Chemistry: From Molecules to Nanomaterials*, John Wiley & Sons, Ltd., 2012.

27 G. O. Lloyd, J. Alen, M. W. Bredenkamp, E. J. C. De Vries, C. Esterhuysen and L. J. Barbour, *Angew. Chem., Int. Ed.*, 2006, **45**, 5354–5358.

28 L. J. Barbour, *Chem. Commun.*, 2006, 1163–1168.

29 M. du Plessis, MSc Thesis, Stellenbosch University, 2012.

30 MiTeGen, MicroLoops LD™, https://www.mitegen.com/learn/technotes/microloopsld/, (accessed 20 January

2022)

31 *APEX3, SAINT, and SADABS*; Bruker AXS Inc.: Madison, WI, 2016.

32 G. M. Sheldrick, *Acta Crystallogr.*, 2008, **A64**, 112–122.

33 G. M. Sheldrick, *Acta Crystallogr.*, 2015, **C71**, 3–8.

34 G. M. Sheldrick, *Acta Crystallogr.*, 2015, **A71**, 3–8.

35 J. L. Atwood and L. J. Barbour, *Cryst. Growth Des.*, 2003, **3**, 3–8.

36 L. J. Barbour, *J. Appl. Crystallogr.*, 2020, **53**, 1141–1146.

37 M. L. Connolly, *J. Appl. Crystallogr.*, 1983, **16**, 548–558.

38 M. L. Connolly, *Science.*, 1983, **221**, 709–713.

39 M. L. Connolly, *J. Mol. Graph.*, 1993, **11**, 139–141.

40 *POV-Ray for Windows*, version 3.6.1a.icl8.win32; Persistence of Vision Pty. Ltd., 2003.

41 L. J. Barbour, K. Achleitner and J. R. Greene, *Thermochim. Acta*, 1992, **205**, 171–177.

42 CompassCDS, https://scioninstruments.com/products/compass-cds/, (accessed 20 January 2022).

43 A. M. Pivovar, K. T. Holman and M. D. Ward, *Chem. Mater.*, 2001, **13**, 3018–3031.

44 M. Lusi and L. J. Barbour, *Angew. Chem., Int. Ed.*, 2012, **51**, 3928–3931.

45 M. A. Moreira, J. C. Santos, A. F. P. Ferreira, J. M. Loureiro, F. Ragon, P. Horcajada, P. G. Yot, C. Serre and A. E. Rodrigues, *Langmuir*, 2012, **28**, 3494–3502.

46 F. Vermoortele, M. Maes, P. Z. Moghadam, M. J. Lennox, F. Ragon, M. Boulhout, S. Biswas, K. G. M. Laurier, I. Beurroies, R. Denoyel, M. Roeffaers, N. Stock, T. Düren, C. Serre and D. E. De Vos, *J. Am. Chem. Soc.*, 2011, **133**, 18526–18529.

47 M. A. Moreira, J. C. Santos, A. F. P. Ferreira, J. M. Loureiro, F. Ragon, P. Horcajada, P. G. Yot, C. Serre and A. E. Rodrigues, *Microporous Mesoporous Mater.*, 2012, **158**, 229–234.

48 J. E. Warren, C. G. Perkins, K. E. Jelfs, P. Boldrin, P. A. Chater, G. J. Miller, T. D. Manning, M. E. Briggs, K. C. Stylianou, J. B. Claridge and M. J. Rosseinsky, *Angew. Chem., Int. Ed.*, 2014, **53**, 4592–4596.

49 J. Lannoeye, B. Van De Voorde, B. Bozbiyik, H. Reinsch, J. Denayer and D. De Vos, *Microporous Mesoporous Mater.*, 2016, **226**, 292–298.

50 M. M. Wicht, N. B. Báthori and L. R. Nassimbeni, *Polyhedron*, 2016, **119**, 127–133.

51 L. Alaerts, C. E. A. Kirschhock, M. Maes, M. A. Van Der Veen, V. Finsy, A. Depla, J. A. Martens, G. V. Baron, P. A. Jacobs, J. F. M. Denayer and D. E. De Vos, *Angew. Chem., Int. Ed.*, 2007, **46**, 4293–4297.

52 H. Tan, Q. Chen, T. Chen and H. Liu, *ACS Appl. Mater. Interfaces*, 2018, **10**, 32717–32725.

53 M. A. Moreira, J. C. Santos, A. F. P. Ferreira, J. M. Loureiro, F. Ragon, P. Horcajada, K. E. Shim, Y. K. Hwang, U. H. Lee, J. S. Chang, C. Serre and A. E. Rodrigues, *Langmuir*, 2012, **28**, 5715–5723.

54 F. Niekiel, J. Lannoeye, H. Reinsch, A. S. Munn, A. Heerwig, I. Zizak, S. Kaskel, R. I. Walton, D. De Vos, P. Llewellyn, A. Lieb, G. Maurin and N. Stock, *Inorg. Chem.*, 2014, **53**, 4610–4620.

55 D. Peralta, K. Barthelet, J. Pérez-Pellitero, C. Chizallet, G. Chaplais, A. Simon-Masseron and G. D. Pirngruber, *J. Phys. Chem. C*, 2012, **116**, 21844–21855.

56 R. El Osta, A. Carlin-Sinclair, N. Guillou, R. I. Walton, F. Vermoortele, M. Maes, D. De Vos and F. Millange, *Chem. Mater.*, 2012, **24**, 2781–2791.

57 P. S. Bárcia, M. P. M. Nicolau, J. M. Gallegos, B. Chen, A. E. Rodrigues and J. A. C. Silva, *Microporous Mesoporous Mater.*, 2012, **155**, 220–226.

58 Z. He, Y. Yang, P. Bai and X. Guo, *J. Ind. Eng. Chem.*, 2019, **77**, 262–272.

59 S. Wang, S. Mukherjee, E. Patyk-Kaźmierczak, S. Darwish, A. Bajpai, Q. Yang and M. J. Zaworotko, *Angew. Chemie*, 2019, **131**, 6702–6706.

60 R. Taylor and C. F. Macrae, *Acta Crystallogr. Sect. B Struct. Sci.*, 2001, **B57**, 815–827.

61 I. J. Bruno, J. C. Cole, P. R. Edgington, M. Kessler, C. F. Macrae, P. McCabe,

J. Pearson and R. Taylor, *Acta Crystallogr. Sect. B Struct. Sci.*, 2002, **B58**, 389–397.

62 C. F. Macrae, P. R. Edgington, P. McCabe, E. Pidcock, G. P. Shields, R. Taylor, M. Towler and J. Van De Streek, *J. Appl. Crystallogr.*, 2006, **39**, 453–457.

63 C. F. Macrae, I. J. Bruno, J. A. Chisholm, P. R. Edgington, P. McCabe, E. Pidcock, L. Rodriguez-Monge, R. Taylor, J. Van De Streek and P. A. Wood, *J. Appl. Crystallogr.*, 2008, **41**, 466–470.

64 C. F. MacRae, I. Sovago, S. J. Cottrell, P. T. A. Galek, P. McCabe, E. Pidcock, M. Platings, G. P. Shields, J. S. Stevens, M. Towler and P. A. Wood, *J. Appl. Crystallogr.*, 2020, **53**, 226–235.

65 D. P. van Heerden and L. J. Barbour, *Chem. Soc. Rev.*, 2021, **50**, 735–749.

Chapter 5
Summary, Concluding Remarks and Future Work

5.1. Summary and Concluding Remarks

Porous materials have potential applications in sorption,[1,2] storage,[3–5] sensing[6,7] and separation,[8–10] *etc*. In this work, the xylene sorption ability and selectivity of two porous metallocycles that were previously reported by the Barbour group were investigated. These are **MC1** ([Cd_2Cl_4(**L1**)$_2$]·2(MeOH))[11,12] and **MC2** ([Cu_2Cl_4(**L2**)$_2$]·2(DMSO)).[13–16] Xylenes are a valuable chemical feedstock used in the production of a wide range of consumer products.[17,18] An enormous amount of pure xylene is required worldwide. However, it is always present as a mixture of isomers during production. Here, we aim to separate xylene isomers using porous materials.

In previous studies, **MC1** proved to be permeable to carbon dioxide (CO_2), carbon disulphide (CS_2), methanol (MeOH) and acetylene (C_2H_2).[11,12] The ligand in **MC1** is flexible and has a relatively long spacer, and it was proposed that this might allow the metallocycle to undergo conformational changes to produce a larger void. However, by performing solvent exchange and liquid sorption, single-crystal X-ray diffraction (SCD) and thermogravimetric analysis (TGA) showed that **MC1** is not suitable for xylene separation. After attempting to exchange MeOH with xylene, the TGA thermogram showed a small guest loss, but it was much less than one xylene per metallocycle. In the SCD analysis, no appropriate model of the guest could be generated. Therefore, the unmodelled electron density was determined by the Platon[19]/SQUEEZE[20,21] routine. The calculated electron density is close to the number of electrons per MeOH molecule. However, there is a notable difference between the electron density map of the MeOH-included metallocycle and the metallocycle after solvent exchange. For that reason, it is difficult to conclude whether any xylene was taken up. For xylene separation, in order to avoid effects due to the guest, activated porous materials are preferred. Liquid sorption using activated material (**MC1a**) was performed at different temperatures (25, 80 and 100 °C). The TGA thermograms were

very similar to that of **MC1a**, indicating that **MC1** does not absorb xylenes under the conditions investigated, and that it is therefore not suitable for xylene separation. The host structure after solvent exchange was unchanged from that of the as-synthesized material, which means that the pore size remains retained. By comparing the kinetic diameter of the xylene isomers to those of the guest molecules permeable to **MC1** it is apparent that the xylenes have much larger kinetic diameters. Therefore, it seems reasonable that xylenes are too large to be taken up by the host in the as-synthesized conformation.

MC2 is a Cu-based metallocycle and its permeability to a wide range of guest molecules was previously explored by the Barbour group.[13–16] Furthermore, this Cu-based metallocycle undergoes color changes in response to guest exchange as well as guest uptake and release, which implies its potential use as a sensor. As previously reported, it has two activated forms produced by different activation methods.[13] Form **3** is the brown open apohost form and **4** is the green closed apohost form. Both forms were soaked in xylenes to investigate if they are able to absorb such guests. **3** can take up xylene to an occupancy of one xylene molecule per metallocycle at room temperature (this is true for all three xylene isomers), while **4** cannot take up xylene efficiently (even at 80 °C). In this work, guest exchange, vapor sorption and liquid sorption of xylenes were performed on **3**. Powder X-ray diffraction (PXRD) was used to analyze the resulting inclusion compounds. The powder patterns indicated that the same xylene-included host conformation type was obtained via the different methods for *px*, *mx*, *ox*. Thereafter, liquid sorption of **3** with binary xylene mixtures was carried out. The ratios of the binary mixtures (A:B) were 10:0, 9:1, 8:2…, 1:9, 0:10 and the liquids were mixed by stirring. The results were analyzed by gas chromatography (GC). **3** is suitable for xylene separation and has a preference in the order *px* >> *mx* > *ox*. The selectivity coefficients are 5.12, 11.40 and 1.96 for the approximate equimolar mixtures *px*/*mx*, *px*/*ox*, *mx*/*ox*, respectively. The composition of xylenes in the crystals after exposure of **3** to an approximately equimolar ternary xylene mixture supports this selectivity trend (*px*:*mx*:*ox* = 78:17:5). In addition, xylene uptake by **MC2** follows the rule-of-thumb described by van Heerden and Barbour: the guest-occupiable space of the host should be double that of the guest.[22] In **3**, there are two crystallographically independent metallocycles; the voids consist of two kinds of pockets with volumes[13] of 111 and 178 Å^3. Xylenes have a volume of approximately 110 Å^3, and consequently the pockets of **3** are too small to accommodate them. Hence, the host undergoes conformational changes and the pockets merge to become channels. The guest-

accessible volume is then approximately 220 Å^3 per metallocycle in **1**·xylene, which is sufficient to accommodate any of the xylenes.

5.2. Obstacles

To investigate the sorption and separation abilities of the materials to xylenes, the phase purity of the bulk sample first needs to be confirmed. PXRD analysis is a method commonly used to determine the purity of a bulk sample. However, at the beginning of this work, the purity of the bulk as-synthesized **MC1** was unconfirmed. The experimental powder patterns did not match those simulated from the single-crystal structure. Additional **MC1** was synthesized, and we again attempted to obtain pure bulk sample. Nevertheless, none of the experimentally-determined powder patterns matched those simulated from the SCD data. Therefore, we explored the possibility that there might be different crystal forms present after one synthesis; the ligand used might be impure or the crystal might degrade during the sample preparation process. Since the phase purity of the as-synthesized crystal could not be confirmed, we decided to continue to investigate if the activated material is able to take up xylene. The as-synthesized material was activated under vacuum at ambient temperature for three hours (as confirmed by TGA) to yield **MC1a**. Surprisingly, the experimental powder patterns of the activated material now matched that simulated from the SCD structure of **MC1a**. The purity of the bulk sample of the apohost was confirmed. Furthermore, we noted that the experimental powder patterns of the as-synthesized crystal were similar to that of the activated crystal. The as-synthesized **MC1** has two MeOH guest molecules per metallocycle, and it is possible that the MeOH escaped at ambient temperature while preparing the sample for PXRD analysis. After the as-synthesized material was fully activated the bulk sample was phase-pure, as determined by PXRD.

Previous studies of **MC2** by the Barbour Group showed that **MC2** has two different activated forms, denoted **3** and **4**.[13] When investigating the xylene separation ability of these forms, we speculated that the two distinct phases might provide different selectivity forwards the xylene isomers. However, the first obstacle was obtaining the pure activated phases. The guest for the as-synthesized material is dimethyl sulfoxide (DMSO). DMSO has a high boiling point and is coordinated to the metal center in the metallocycle. Therefore, activation of the as-synthesized form requires excessive

heating and thus the formation of the closed phase **4**. Thus, solvent exchange with acetonitrile (ACN) was performed to yield **2**·2(ACN). Via different activation methods, **2**·2(ACN) can be transformed into either **3** or **4**. Furthermore, **3** can convert to **4**, but **4** cannot revert back to **3**. After several attempts, the activated crystals obtained were mixtures of **3** and **4** (Figure 1). To obtain accurate experimental data, pure bulk sample is required. When bulk **2**·2(ACN) was activated at ambient temperature for 15 minutes, **3** was obtained, but the TGA results indicated some residual guest (weight loss > 1%). In order to minimize the effect of the original guest on sorption, the weight loss of the activated crystal should be less than 1% (close to 0% is ideal). After attempting different methods of activation by variation of both the temperature and time, phase-pure **3** with weight loss < 1 % was achieved by activation at 25 °C for two hours. The color of the crystals of **3**, determined by visual inspection under a microscope, was brown only. When bulk **2**·2(ACN) was activated under vacuum at 80 °C overnight, **4** was obtained (with weight loss < 1%). However, examining the crystals under a microscope, the presence of some brown colored crystals indicates that some of form **3** is still present (Figure 4.2). Therefore, the bulk sample was still impure. Once again, we trialed various activation methods and found that phase-pure **4** can be obtained by heating **3** under reduced pressure at 80 °C overnight. Besides visually inspecting the color, the phase purity was also confirmed by PXRD as there is a notable difference between the powder patterns of **3** and **4**. Form **3** will partially transform to **4** under ambient conditions over several days and therefore becomes a mixture of the two forms. To ensure the accuracy and the reliability of the experimental data, freshly activated **3** is required. Hence, all batches of **MC2** were stored as phase **2**·2(ACN) and only activated directly before each experiment.

5.3. Conclusion

In conclusion, the material **MC1** is not suitable for xylene separation as its activated form cannot take up xylene. Form **3** of **MC2** can potentially be used for xylene separation as it shows a selective preference for *px* in the presence of *mx* and *ox*. In the absence of *px*, it shows a preference for *mx* over *ox*. The selectivity coefficients are 5.12, 11.40 and 1.96 for the approximate equimolar *px*/*mx*, *px*/*ox*, *mx*/*ox* solutions, respectively. These selectivity values compare well with those reported in the literature as selectivity coefficients above 5 are rarely observed.[9]

5.4. Future Work

The metallocycle apohost **MC1a** showed no permeability to xylenes, as the kinetic diameter of xylenes is much larger compared to the guests to which **MC1a** is permeable. However, it may absorb other guests that have kinetic diameters similar to MeOH, CO_2, C_2H_2 and CS_2. Table 5.1 shows some additional examples of such possible guests. Future work on **MC1** could be to investigate the ability of **MC1a** to sorb or selectively sorb molecules with kinetic diameters between 3.3–3.6 Å.

Table 5.1 Molecules with kinetic diameters similar to guests in **MC1**.

	Kinetic diameters (Å)	References
Cl_2	3.2	23
N_2O	3.3	23
Ar	3.4	23
O_2	3.46	23,24
Br_2	3.5	23
H_2S	3.6	23
SO_2	3.6	23
Kr	3.6	23
N_2	3.64	23,24

MC2 shows selectivity to xylenes in the order *px* >> *mx* > *ox*. Furthermore, **1**·xylene can be transformed to **2**·2(ACN). This implies that the material is recyclable. Future work on **MC2** should investigate its recyclability (Scheme 5.1). After xylenes are sorbed by **3**, **1**·xylene is obtained and can then be immersed in acetonitrile to extract the xylenes. The xylenes are then replaced by ACN, and **2**·2(ACN) is again attained. **2**·2(ACN) is filtered through a syringe filter and the filtrate used for GC analysis to generate selectivity plots and to determine selectivity coefficients. The sample of **2**·2(ACN) in the syringe filter can be re-collected. Then the whole selectivity experiment can be repeated by using the re-collected sample of **2**·2(ACN). This process will be repeated five times. Then the selectivity plots and selectivity coefficients will be studied. If the recyclability deteriorates, further work could be carried out to improve the recyclability.

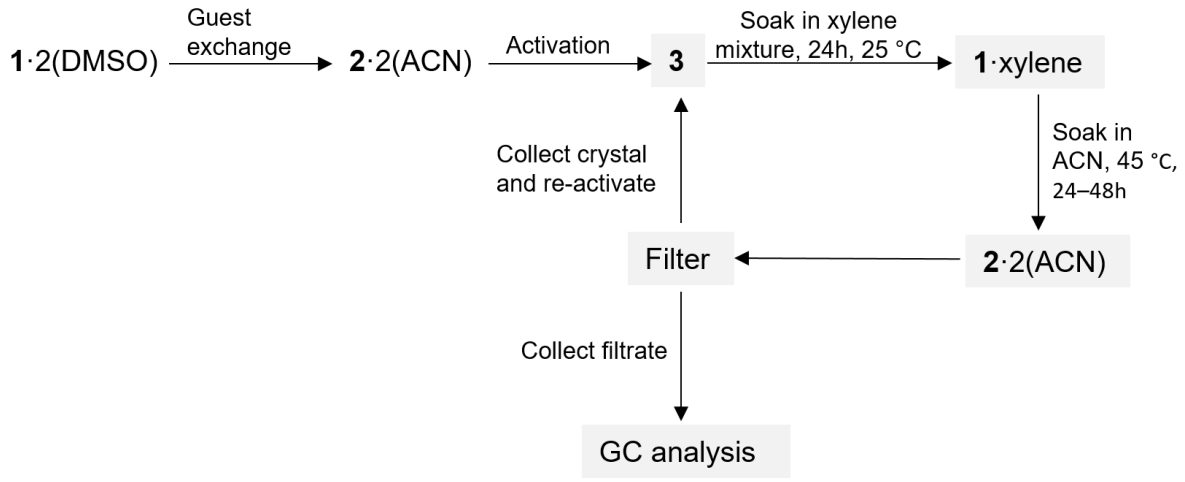

Scheme 5.1 Process of xylene separation by using metallocycle **MC2**. The recyclable processes are highlighted in grey.

Since the obstacle with obtaining phase-pure apohost of **MC2** has been solved, additional exploration can be carried out on it. We are more interested in the porous form **3**. It could be used for gas sorption of climate change gases CO_2, methane (CH_4), nitrous oxide (N_2O), *etc*., using a gas sorption analyzer. Since **MC2** undergoes phase transformations, differential scanning calorimetry (DSC) could be used to investigate the heat evolved during guest uptake. The energy of sorption and the energy of the concomitant phase change could be studied to investigate if the one might offset the other.

5.5. References

1 J. Canivet, J. Bonnefoy, C. Daniel, A. Legrand, B. Coasne and D. Farrusseng, *New J. Chem.*, 2014, **38**, 3102–3111.

2 P. Lama, H. Aggarwal, C. X. Bezuidenhout and L. J. Barbour, *Angew. Chem., Int. Ed.*, 2016, **55**, 13271–13275.

3 K. Sumida, D. L. Rogow, J. A. Mason, T. M. McDonald, E. D. Bloch, Z. R. Herm, T. H. Bae and J. R. Long, *Chem. Rev.*, 2012, **112**, 724–781.

4 L. Jiao, J. Y. R. Seow, W. S. Skinner, Z. U. Wang and H. L. Jiang, *Mater. Today*, 2019, **27**, 43–68.

5 J. A. Mason, M. Veenstra and J. R. Long, *Chem. Sci.*, 2014, **5**, 32–51.

6 W. Qi, X. Wang, Z. Liu, K. Liu, Y. Long, W. Zhi, C. Ma, Y. Yan and J. Huang, *J.*

Colloid Interface Sci., 2021, **597**, 325–333.

7 D. Wang, D. Jana and Y. Zhao, *Acc. Chem. Res.*, 2020, **53**, 1389–1400.

8 M. du Plessis, V. I. Nikolayenko and L. J. Barbour, *J. Am. Chem. Soc.*, 2020, **142**, 4529–4533.

9 L. Liu, H. Y. Zhang, H. J. Wang, S. Chen, J. H. Wang and J. W. Sun, *Eur. J. Inorg. Chem.*, 2019, **2019**, 1839–1846.

10 G. B. Li, B. Q. Song, S. Q. Wang, L. M. Pei, S. G. Liu, J. L. Song and Q. Y. Yang, *ACS Omega*, 2019, **4**, 1995–2000.

11 T. Jacobs, G. O. Lloyd, J. A. Gertenbach, K. K. Müller-Nedebock, C. Esterhuysen and L. J. Barbour, *Angew. Chem., Int. Ed.*, 2012, **51**, 4913–4916.

12 T. Jacobs and L. J. Barbour, *CrystEngComm*, 2013, **15**, 1512–1514.

13 L. Dobrzańska, G. O. Lloyd, C. Esterhuysen and L. J. Barbour, *Angew. Chem., Int. Ed.*, 2006, **45**, 5856–5859.

14 L. Dobrzańska, G. O. Lloyd and L. J. Barbour, *New J. Chem.*, 2007, **31**, 669–676.

15 M. du Plessis, V. I. Nikolayenko and L. J. Barbour, *Inorg. Chem.*, 2018, 57, 12331–12337.

16 V. I. Nikolayenko, L. M. Van Wyk, O. Q. Munro and L. J. Barbour, *Chem. Commun.*, 2018, **54**, 6975–6978.

17 G. Zhang, Y. Ding, A. Hashem, A. Fakim and N. M. Khashab, *Cell Reports Phys. Sci.*, 2021, **2**, 100470.

18 J. Fabri, U. Graeser and T. A. Simo, *Ullmann's Encycl. Ind. Chem.*, 2012, 39, 643−663.

19 P. van der Sluis and A. L. Spek, *Acta Crystallogr. Sect. A*, 1990, **46**, 194–201.

20 O. V. Dolomanov, L. J. Bourhis, R. J. Gildea, J. A. K. Howard and H. Puschmann, *J. Appl. Crystallogr.*, 2009, **42**, 339–341.

21 A. L. Spek, *Acta Crystallogr. Sect. C Struct. Chem.*, 2015, **71**, 9–18.

22 D. P. van Heerden and L. J. Barbour, *Chem. Soc. Rev.*, 2021, **50**, 735–749.

23 E. Albrecht, G. Baum, T. Bellunato, A. Bressan, S. Dalla Torre, C. D'Ambrosio, M. Davenport, M. Dragicevic, S. Duarte Pinto, P. Fauland, S. Ilie, G. Lenzen, P. Pagano, D. Piedigrossi, F. Tessarotto and O. Ullaland, *Nucl. Instruments Methods Phys. Res. Sect. A Accel. Spectrometers, Detect. Assoc. Equip.*, 2003, **510**, 262–272.

24 S. E. Kentish, C. A. Scholes and G. W. Stevens, *Recent Patents Chem. Eng.*, 2008, **1**, 52–66.